United States
Department of
Agriculture

Forest Service

Forest
Products
Laboratory

Research
Paper
FPL–RP–670

Reaction-to-Fire of Wood Products and Other Building Materials: Part II, Cone Calorimeter Tests and Fire Growth Models

Mark A. Dietenberger
Ondrej Grexa
Robert H. White

Abstract

This Part II work evaluated results from the bench-scale cone calorimeter tests (ISO 5660-1) for 11 different untreated wood products, three different fire-retardant-treated (FRT) plywood materials, Type X gypsum board, and FRT polyurethane foam, which were also used in the assessment of reaction-to-fire of common materials using the full-scale room/corner test (ISO 9705) in the Part I report. The evaluation consisted of (1) comparing relative flammability of a variety of wood products and deriving thermophysical and fire properties needed for modeling, (2) developing fire growth models for room/corner fire tests that use the cone calorimeter data to predict heat release rate (HRR) development, and (3) devising reasonable correlations for relating time to flashover to global cone calorimeter data reported as time to ignition (TTI), peak HRR (PHRR), HRR, or peak smoke extinction area (SEA), which provide the link to regulatory test values as described in the Part I report.

Keywords: fire growth, wood, flammability, reaction-to-fire, flashover, heat release rate (HRR), cone calorimeter

Acknowledgments

In the 1990s, the U.S.–Slovak Cooperative Program provided the mechanism and financial support critical for this project and this international cooperation between the national forest products research institutions in Slovakia and the United States. This cooperative project was advantageous to both national institutions. Dr. Marc Janssens was a critical participant in the initiation of this project and was responsible for the modification of Quintiere's model during his tenure at the American Forest & Paper Association. American Forest & Paper Association and Forintek Canada Corp. provided materials for the tests. These room tests would not have been possible without the efforts of Mitch Sweet, former chemist at FPL, and Como Caldwell, head technician for fire research at FPL. This report extends the unpublished report written by Dr. Ondrej Grexa in 1999 to the funding institution at the conclusion of his role in the project.

October 2012

Dietenberger, Mark A.; Grexa, Ondrej; White, Robert H. 2012. Reaction-to-fire of wood products and other building materials: part II, cone calorimeter tests and fire growth models. Research Paper FPL-RP-670. Madison, WI: U.S. Department of Agriculture, Forest Service, Forest Products Laboratory. 58 p.

A limited number of free copies of this publication are available to the public from the Forest Products Laboratory, One Gifford Pinchot Drive, Madison, WI 53726–2398. This publication is also available online at www.fpl.fs.fed.us. Laboratory publications are sent to hundreds of libraries in the United States and elsewhere.

The Forest Products Laboratory is maintained in cooperation with the University of Wisconsin.

The use of trade or firm names in this publication is for reader information and does not imply endorsement by the United States Department of Agriculture (USDA) of any product or service.

The USDA prohibits discrimination in all its programs and activities on the basis of race, color, national origin, age, disability, and where applicable, sex, marital status, familial status, parental status, religion, sexual orientation, genetic information, political beliefs, reprisal, or because all or a part of an individual's income is derived from any public assistance program. (Not all prohibited bases apply to all programs.) Persons with disabilities who require alternative means for communication of program information (Braille, large print, audiotape, etc.) should contact USDA's TARGET Center at (202) 720–2600 (voice and TDD). To file a complaint of discrimination, write to USDA, Director, Office of Civil Rights, 1400 Independence Avenue, S.W., Washington, D.C. 20250–9410, or call (800) 795–3272 (voice) or (202) 720–6382 (TDD). USDA is an equal opportunity provider and employer.

Contents

Executive Summary 1
Introduction 1
Past Work 2
Cone Calorimeter—Equipment and General Procedures 3
Room/Corner Test Materials 3
  Materials and Procedure 3
  Results and Discussion 3
  Thermal Properties Derived from Ignitability Analysis 14
Fire-Retardant-Treated Beech Wood 24
  Sample Preparation and Testing 25
  FRT Beech Wood Results and Discussion 25
Quintiere's Numerical Model 30
  Model Description 30
  Janssens Modifications to Quintiere Model 32
  Input Parameters and Values 32
  Results and Discussion 33
Analytical Flame Spread Model for ISO 9705 36
  Model Formulation 39
  Empirical Relationships to Predict Lateral Flame Spread 46
  Comparison to HRR for FPL Room Tests 47
  Model Sensitivity to Fire Growth Properties 48
Simplified Correlations of the Small-Scale and Full-Scale Tests 49
  Guided Statistical Approach 50
  Acceleration Parameter Approach 50
Conclusion 53
Nomenclature 55
Literature Cited 55

Reaction-to-Fire of Wood Products and Other Building Materials: Part II, Cone Calorimeter Tests and Fire Growth Models

Mark A. Dietenberger, Research General Engineer
Forest Products Laboratory, Madison, Wisconsin

Ondrej Grexa, Wood Protection Department Head & Institute Deputy Director for Research
State Forest Products Research Institute, Bratislava, Slovak Republic

Robert H. White, Research Forest Products Technologist
Forest Products Laboratory, Madison, Wisconsin

Executive Summary

The primary objective of this project was to develop a system to assess the reaction-to-fire of building materials based on the EUREFIC approach developed in the Nordic countries but better able to distinguish between common materials. In Part I, we report on a series of room/corner tests. By using the burner protocol of 100 kW for 10 min, followed by 300 kW for 10 min, and placing the test materials only on the walls in the full-scale room test (ISO 9705), we obtained effective indications of fire performance for 11 different untreated wood products, three different fire-retardant-treated (FRT) plywood products, gypsum wallboard, and a FRT polyurethane foam. In contrast, the protocol option of ISO 9705 with both the walls and ceilings covered (normally used in Europe) and the NFPA 286 option with a less severe burner exposure (normally used in the North America) both resulted in flashover times for the different untreated wood products within a fairly narrow range. The relative performance of the different products tested according to ISO 9705 with walls covered only was consistent with their expected performance in the current North America and Slovak regulatory tests for reaction-to-fire. In addition to the primary flashover time measurements, reaction-to-fire assessments also include measurements relating to intoxicating gases, threatening smoke, radiant heat, and heat release rates needed for comparisons of material fire performances and for validating fire growth models. The assessment methodology proposed in this project provides a more technically sound method that can be tied back to more fundamental fire properties that are determined in the bench-scale cone calorimeter test (ISO 5660).

The second objective of this project was to use the cone calorimeter to evaluate the materials in terms of material properties, and in turn use such properties in mathematical models to predict the full-scale room tests. After considerable work on this second objective, Part II reports on the cone calorimeter evaluation, particularly as needed for alternate fire growth modeling and predictions for the room tests. Materials used in the full-scale room tests were tested with the cone calorimeter. As in the full-scale room test, heat release determination in the cone calorimeter is done by the oxygen consumption method. Using time to ignition data, we obtained the thermal inertia (ρck) and ignition temperature for the different products for within their thermally thick regime. However, the hardboard required a mixed thermally thick/thin analysis that includes the thermal thickness (ρcl) as a material property. We developed a simple correlation between the times for flashover in the room tests and the global fire parameters derived solely from the cone calorimeter. Such simple correlations are limited to the full-scale test protocol used to develop the correlation. To obtain more fundamental predictive capabilities, this project included development and application of physical models for the full-scale room test. Two physical models were part of this research project. One model was a modification of a numerical model developed by Quintiere for fire growth in the ISO 9705 test. The second model is an analytical model of fire growth that includes adaptation for systematic errors in the heat release rate measured by the oxygen consumption method.

Introduction

Two of the major test methods that are available are the ISO 5660—Rate of Heat Release from Building Products (Cone Calorimeter Method) (ISO 1993b) and ISO 9705—Full-Scale Room/Corner Test for Surface Products (ISO 1993a). The former one is a bench-scale test that has as its main measurement the heat release rate (HRR) evolved during the burning of the tested material. The method is based on the oxygen consumption principle, according to which a constant amount of heat is evolved for the constant amount of oxygen consumed in burning (assuming minimal smoke and carbon monoxide are produced). This principle is valid for most common building materials. On average, for 1 kg of oxygen consumed, 13.1 MJ heat is evolved. Recently it was found that wood materials release combustible volatiles having 13.23 MJ per 1 kg of oxygen consumed (Dietenberger

2002). Obviously, there is an adjustment for the combustion of propane from the ignition burner, which generates 12.76 MJ of heat per 1 kg of oxygen used. Application of this principle provides a measurement of the HRR from the burning fuels. The same principle is used in the full-scale room/corner test.

The bench-scale measurements on the cone calorimeter were done at the State Forest Products Research Institute (SDVU), Brastislava, Slovakia. Additional cone calorimeter tests were done at the USDA Forest Service Forest Products Laboratory (FPL) at Madison, Wisconsin, to determine the effect of backing material on the HRR and combustion products profiles. Results of the cone calorimeter tests are reported in this paper (Part II). The cone calorimeter tests were done for the same materials as tested in a series of room/corner tests. Added to the room/corner test materials are pine sapwood and beech wood growing in Slovakia. The beech wood was treated with flame retardant, and several uptakes to wood were investigated. The untreated pine sapwood and fire-retardant-treated (FRT) beech wood were tested only in small-scale cone calorimeter tests.

Three distinct uses of the cone calorimeter data are to (1) compare the fire response of materials to assess their fire performance for materials development or pyrolysis and burning model development, (2) derive the material parameters needed as input to mathematical models for the full-scale room/corner test assessment, and (3) determine for regulatory purposes the characteristic parameters such as peak HRR or total heat evolved (Schartel and Hull 2007). Therefore, the first section of this paper discusses the fire performance of all materials tested in the cone calorimeter for this project. Much attention is given to features of the wood-based materials and fundamental knowledge derivable from comparison testing. Comparisons of their fire response that assess their fire performance are identified. Also, results and discussion on material parameters derived from the cone calorimeter measurement are given. In the second section, using the material properties derived as input, two mathematical models for the room/corner test are evaluated. One of the models was developed as part of this project. The third section of this paper, focusing on regulatory purposes, correlates data obtained in the cone calorimeter with time to flashover measured in the full-scale test. In turn, the time to flashover for the specimen on the wall only was found to be highly correlated with regulatory indices for reaction to fire in at least North America and Slovakia, as reported in Part I of this series of papers (Grexa and others 2012) and in Dietenberger and others (1995).

The main series of tests of this project were the room/corner tests conducted on a number of building materials. The primary objective of the room/corner tests was to evaluate an alternative protocol provided by ISO 9705 (ISO 1993a). Fourteen of the 16 materials were different wood products. Gypsum board and FRT polyurethane foam were also tested. The full-scale tests (ISO 9705) (ISO 1993a) were done at the USDA Forest Products Laboratory. These room/corner tests are reported in Part I of this series of papers (Grexa and others 2012).

Past Work

FPL was one of earliest innovators of bench-scale heat release measurements (Brenden 1973). The first FPL calorimeter used vertically oriented specimens, 0.46 by 0.46 m in size, and was fired with a natural gas burner achieving a maximum heat flux of 35 kW/m^2. The HRR was calculated with the substitution method, whereby an auxiliary propane burner was dynamically metered to reproduce furnace flue-gas thermal response of a material test. The HRR profiles for several materials were obtained (Brenden 1974, 1975, 1977). Composites such as high-density hardboard, particleboard, and polyurethane sandwich panel had the highest HRR values. Materials with medium levels of HRR were Red Oak, rigid insulation board, and Douglas Fir plywood. The lowest HRR profiles were obtained for FRT plywood and the gypsum board assembly. Indeed, this seems to be one of the earliest known indications of flammability of common wood-based materials on the basis of bench-scale HRR that show a correspondence with the flame spread index of Steiner's tunnel test (ASTM E 84). During the 1980s, the FPL calorimeter was replaced by the simpler and more responsive Ohio State University (OSU) calorimeter (based on the enthalpy rise method), which was then modified to include the oxygen consumption method (Tran 1988, 1990). Another series of wood-based materials were tested, including some materials identical to the current test series (Tran 1992). The HRR profiles of wood-based materials by this time could be described as a sharp initial peak at sustained ignition followed by a broad valley profile. A fairly broad second peak was identified for the thinner materials backed by insulation material. The average HRR was found to increase with irradiance and ovendry density and decrease with moisture content. Additional information was obtained on smoke and CO production. The final test series with the modified OSU calorimeter involved correlating HRR with charring rate (Tran and White 1992). Another type of bench-scale HRR measurement was obtained by the enthalpy rise method while measuring and modeling piloted ignition and creeping flame spread on the lateral ignition and flame travel (LIFT) test apparatus (Dietenberger 1995).

To accommodate thermoplastic wood composite materials and to test thin vegetative materials on horizontal surfaces, the OSU calorimeter was replaced by the cone calorimeter in the early 1990s. To justify full reliance on the oxygen consumption HRR method, research on combustion properties indicated that 13.23 kJ of net heat is released for each 1 g of stoichiometric oxygen consumed of cellulosic solids, volatiles, or char, including treated materials (Dietenberger 2002). The use of the heavy backing material from Steiner's

Figure 1. Overall view of FPL cone calorimeter.

Figure 2. Sample burning under cone heater.

tunnel test (ASTM E 84) along with 12.5-mm-thick wood-based materials tested at irradiance of 50 kW/m^2 provided a HRR profile in the cone calorimeter that is reasonably described by a decaying exponential function of time for at least 10 min duration (Dietenberger 2002). It was also reported that backing materials on the average do not affect time to ignition, initial peak HRR, initial peak mass loss rate (MLR), and total heat release (THR) at irradiance values greater than about 25 kW/m^2. However, 10-min averaged HRR, effective heat of combustion (EHC), and overall emissions of smoke, CO, and CO_2 appeared to be affected by the material backings. This result provided an analytical basis for modeling fire growth.

Related works at FPL have concentrated on developing input data, validation data, and model algorithms for compartment fire models. Input data have included heat release data (Tran 1990, 1992; Tran and White 1992), ignition data (Dietenberger 1996), and better characterization of the burner (Tran and Janssens 1993). Previous data from room corner tests were based on the North America exposure program of 40 kW for 5 min and 160 kW for 10 min (Janssens and Tran 1992; Tran and Janssens 1989, 1991).

Cone Calorimeter—Equipment and General Procedures

The cone calorimeter tests were conducted according to the procedure prescribed by ISO 5660-1 (ISO 1993b). The dimensions of the samples were 100 by 100 mm, with the actual thickness. The retainer frame was used to minimize edge effects. The sample was wrapped with aluminum foil on the unexposed sides located on a thick, low-density ceramic fiber blanket backed by a calcium silicate board. The materials were tested in the horizontal orientation in the cone calorimeter at the State Forest Products Research Institute (SDVU), Bratislava, Slovakia, and also in FPL's cone calorimeter (Figs. 1 and 2). In FPL's cone calorimeter (shown in Fig. 1 with the Atlas AutoCal II (Chicago, Illinois) cone calorimeter instrument), the materials were also located directly on Type X gypsum board, which was used as the backing to materials in the room tests.

Room/Corner Test Materials

Materials and Procedure

The materials tested are listed in Table 1. All materials but the gypsum board and FRT polyurethane foam were wood-based products. Materials used in tests 2, 5, 6, and 7 were from the same batch as those tests for the ISR Round Robin (Beitel 1994). Materials used in tests 3 and 4 were obtained from Forintek Canada Corp. Materials for tests 8 to 14 are from a wood industry material bank (MB) for fire research. Some of these materials were tested previously using the 40 kW for 5 min (0 to 300 s), 160 kW for 5 min (300 to 600 s) burner program (Tran and Janssens 1991). The raw cone calorimeter data for these materials are available at www.fpl.fs.fed.us/products/products/cone/fpl_cone_calorimeter.php

The irradiances used were 25, 30, 35, 40, 50, and 65 kW/m^2. For some materials, additional tests were conducted at lower irradiance levels and smaller heat flux increments. Two or three replicate tests were mainly provided at irradiances of 50 kW/m^2. The tests were terminated when the value of mass loss rate over a period of 1 min dropped below 150 g/sm^2. All measured parameters are discussed in the following.

Results and Discussion

Heat Release Rate (HRR)

The HRR is generally considered to be the most important single reaction to fire parameter that characterizes the size of fire. The primary result from the cone calorimeter measurement is HRR. The HRR curves as a function of time for spruce wood are presented in Figure 3. The shape of the curves is typical for wood and wood-based materials that become fully charred and are backed by insulation material (see Dietenberger 1999 and Tran 1992).

Table 1—Characteristics of tested materials

Material	Test no.	Thickness (mm)	Density (kg/m^3)	Moisture content (%)	FPL reference test no.
Type X gypsum board	1	16.5	662	—	49
FRT Douglas Fir plywood	2	11.8	563	9.48	50
Oak veneer plywood	3	13	479	6.85	51
FRT plywood (Forintek)	4	11.5	599	11.17	52
Douglas Fir plywood (ASTM)	5	11.5	537	9.88	53
FRT polyurethane foam	6	23	29	0.0	54
Type X gypsum board	7	16.5	662	—	55
FRT Southern Pine plywood	8	11	606	8.38	56
Douglas Fir plywood (MB)	9	12	549	6.74	57
Southern Pine plywood	10	11	605	7.45	58
Particleboard	11	13	794	6.69	59
Oriented strandboard	12	11	643	5.88	60
Hardboard	13	6	1,026	5.21	61
Redwood lumber	14	19	421	7.05	62
Type X gypsum board	15	16.5	662	—	63
White spruce lumber	16	17	479	7.68	64
Southern Pine boards	17	18	537	7.82	65
Waferboard	18	13	631	5.14	66

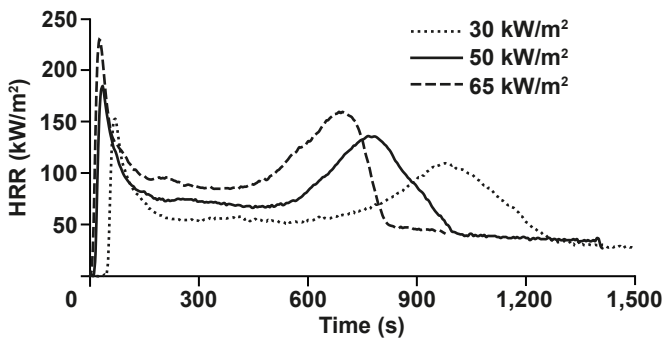

Figure 3. Heat release rate (HRR) as a function of time at three external irradiances for spruce wood (SDVU data).

The first peak of the HRR curve for woody materials corresponds to conditions at ignition and shortly after ignition. The flame occurring after ignition is just volatiles combusting. The forming char layer remains highly reactive for some time because out-flowing volatiles prevent the oxidizing ambient air from reaching the surface. According to Dietenberger (1999, 2002) the initial peak in HRR is the result of unique volatile kinetics of the wood. At high irradiances, the surface temperature rapidly reaches a strong volatization condition at 300 °C (572 °F) or higher at which the wood surface layer is effectively ablated along with its higher heat of combustion than that of the later emitting volatiles. The resulting volatile gases ignite at the electric spark location where fuel and air are optimally mixed. Additional heat flux from the post-ignition flame rapidly increases the wood's surface temperature to yet higher values, leading to higher volatization rates and correspondently higher HRR. Meanwhile, the much lower rate of temperature rise within the virgin porous wood at temperatures between 200 and 300 °C (392 and 572 °F) shifts the wood pyrolysis to interior layers, with more charring and less volatizing (with lowered heat of combustion, as well), thus peaking the HRR profile. With this scenario, the peak HRR obviously can be significantly reduced by (1) lowering surface temperature rise rate, such as with a low-emissivity coating, very high surface heat capacity, or a heat-absorbing dehydration agent in the surface layer, or (2) interfering with ignition during the period of surface ablation, such as with lowered heat of combustion from chemical treatments, flow blockage by impervious intumescences coating, or introduction of inert gases (H_2O or CO_2) to bring the fuel/air mixture beneath the lower flammability limit, even at high temperatures of the ignition source.

After this "ablative" pyrolysis phase, a fairly thin charring layer becomes discernable and the charring rate corresponds to the sliding movement rate of volatization temperature (about 300 °C (572 °F)) into the virgin wood. Because the wood's porous structure is retained at a fairly constant mass fraction after charring (Tran and White 1992), the heat of combustion for wood volatiles becomes constant and thermal diffusivity of char is about the same as that of the virgin wood (Parker 1988). Along with miniscule heat of pyrolysis beyond that of heat capacity alone, the classical heat conduction theory becomes acceptable for predicting the monotonically decreasing sliding movement rate of volatization temperature with time as subjected to constant heat flux from the flame and the heater (Dietenberger 1999). With the charring mass fraction being constant, the volatization mass rate is equal to multiplicative products of wood density, volatile mass fraction, surface area, and charring rate. Finally, the flaming HRR is the heat of combustion times the volatization mass rate. This means that the flaming HRR profile will be monotonically decreasing to a quasi-steady level until the thermal wave has terminated on the

material's backside with the char front just part way through the material. In this quasi-steady scenario, it is obvious we can reduce the HRR profile significantly by (1) reducing the char rate with an inert surface insulation layer, (2) reducing heat of combustion by retaining more carbon in the char, or (3) increasing the char mass fraction with chemical treatment.

In the last phase of wood pyrolysis, the backside temperature begins to rise moderately, perhaps in proportion to the surface heat flux, leading to a thermally thin behavior of the material. This thermal change causes the charring rate to increase, which in turn causes flaming HRR to rise, seemingly proportional to surface heat flux. By this time, glowing combustion is also on the rise in contributing to the second HRR peak because the ambient airflow is now penetrating the charred layer and internal temperatures are very high. The drastic increase in the heat of combustion measured in the cone calorimeter signifies this change from flaming to glowing combustion (typically changing from 12 to 30 kJ/g). The second HRR peak can be significantly reduced by (1) extending the thermal wave period with a very thick material (Tran 1992) or with a heavy backing material (Dietenberger 1999) or (2) preventing wood after-glow by diversion of airflow penetration or chemical treatment of the wood.

For the spruce wood, the first HRR maximum is higher than the second peak for all irradiance levels. The influence of the irradiance on HRR is evident. First and second peaks and the middle part of the curves increases along with irradiance level as expected from the higher responding temperature rise rate (recall that heat of pyrolysis is miniscule). For some of the wood lumbers and composites, the second peak had a much higher value than the first one and it was also subject to greater changes as a function of irradiance. This is not too surprising, given the explanation in the previous paragraph concerning this phase of wood pyrolysis, particularly for relatively thin materials backed by insulation. A typical example is beech wood (Fig. 4). The increase of the first peak measured at irradiance 40 kW/m^2 compared with the peak value measured at 25 kW/m^2 is only 7%. Greater differences were measured at 50 and 65 kW/m^2. Similar relative changes were observed for the middle part of the curve (quasi-steady-state burning) and also for the overall HRR average taken from the flame burning only.

An extreme example of this type of HRR profile is that of hardboard (no. 13). In Figure 5, the first peak of HRR is apparently not present, and the first part of the HRR curve does not increase with increasing irradiance up to 50 kW/m^2. During the test at the SDVU cone calorimeter, deformation occurred on this material. Therefore a retaining grid was used along with the retainer frame to eliminate (or at least minimize) the deformation. However, slight deformation was still observed. As a result the value of the second HRR peak is higher than it would be if the deformation

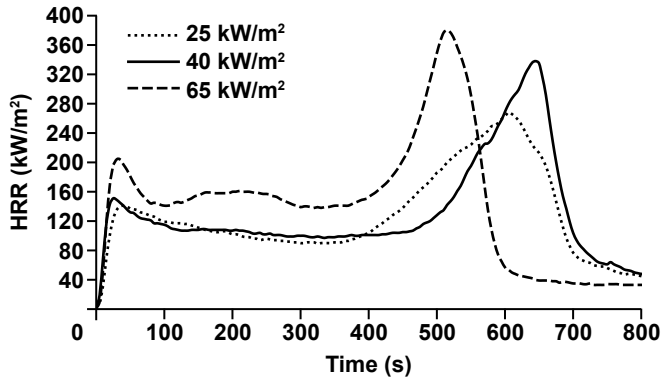

Figure 4. Heat release rate (HRR) as a function of time at three external irradiances for beech wood (SDVU data).

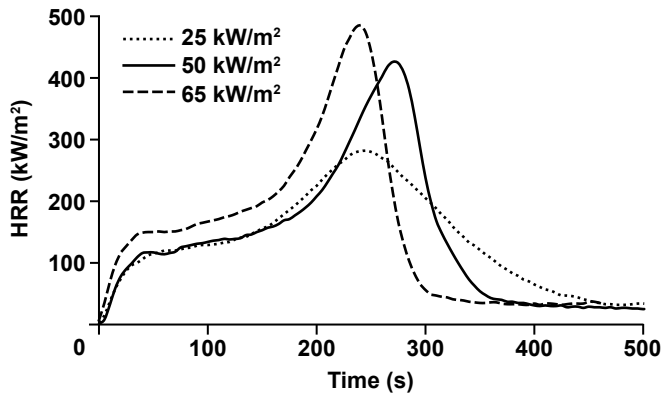

Figure 5. Heat release rate (HRR) as a function of time at three external irradiances for hardboard (test no. 13, SDVU data).

had not occurred. Another complication includes the fact that the hardboard thickness is approximately half that of the other materials. We note that halving the material thickness while keeping other factors unchanged should have the effect of (1) reducing the time period for its quasi-steady charring
(or HRR) by a factor of four and (2) perhaps doubling its charring rate (or HRR) during its thermally thin phase (Dietenberger 1999).

The testing of the hardboard material in FPL's cone calorimeter indicates a narrow initial HRR peak and a much higher second HRR peak, both increasing with heat flux. Interestingly, the first HRR peaks are somewhat higher in FPL's cone calorimeter than they are in the SDVU cone calorimeter, and yet their second HRR peak and THR are generally in agreement between them (this includes several other wood products and irradiances). This difference in performance is readily explained by the different settings for data acquisitions. Data are acquired every 5 s in the SDVU cone calorimeter, whereas in the FPL cone calorimeter, data are acquired every 1 s. Thus FPL's cone calorimeter can better capture narrower peaks than can the

SDVU cone calorimeter. However, explaining the similarities in their second peak HRR values, observable for both cone calorimeters, requires evaluating the gas analysis system. The technical details for a given cone calorimeter are given in appendix C in Part I of this series of papers (Grexa and others 2012). In essence, the mixing time required for gas treatments (removing H_2O, CO_2, CO in three mixing volumes before arrival at the oxygen analyzer and being stirred within the oxygen analyzer) are similar for both cone calorimeters. We verified this by igniting and burning methanol and comparing the time responses between both cone calorimeters, showing a time constant around 9.3 s. The effect of these gas treatments on the HRR profile is as if one applied a low-pass exponential digital filter that not only made the data look less noisy, but also reduced the true peaks and filled in true valleys in the data. Because the first HRR peak is important for predicting initial fire growth for wood products in large-scale tests, it is recommended to use the shortest time intervals for data acquisition and perform numerical deconvolution and time shifting of the various signals to derive the true HRR profiles. This should improve agreements between various cone calorimeters.

The average HRR of the thin hardboard (6 mm) as the function of irradiance is shown in Figure 6. Average HRR is relatively constant up to the irradiance 40 kW/m^2, after which average HRR increases with heat flux. This average HRR would be dominated by the thermally thin phase of material pyrolysis, resulting in high char rate, particularly at high heat fluxes. The HRR would also be especially high because of the low char mass fraction of the composite. For the thick redwood (19 mm), on the other hand, average HRR increases with heat flux at low fluxes (<50 kW/m^2) and becomes relatively constant at high fluxes (Fig. 7). This average HRR (at about 40% that of the hardboard's HRR) would be dominated by the ablating/quasi-steady, thermally thick phase of wood pyrolysis. The high char mass fraction for redwood would make its average HRR more sensitive to the initial peak of wood pyrolysis than that for a typical wood. We note that the largest relative changes in the peak HRR values for redwood were observed at lower irradiances. Similar trends were observed also for some other softwood lumbers (spruce, Southern Pine). With these extreme HRR profiles for wood products one realizes the difficulty of using averaged HRR data for fire growth modeling.

However, when considering the use of simplified fire growth modeling to predict full-scale testing, one realizes that at least for wood-based products, one must be quite selective about bench-scale HRR profiles to prevent contradictory predictions. For either the room/corner or Steiner tunnel tests, we can consider the following constraints. Burn time duration is no more than 10 min. Although the room/corner test has a total test time of 20 min, most flashovers of common materials occur within 10 min after burner ignition, and even with FRT materials, most flashovers occur within 10 min of the increase in the burner output that would

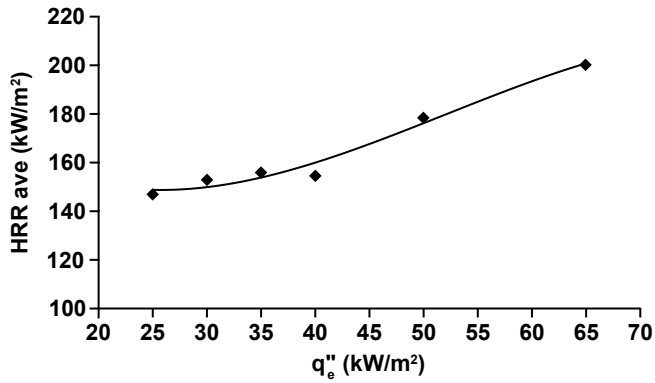

Figure 6. Average heat release rate (HRR ave) as a function of external irradiance for hardboard (test no. 13, SDVU data).

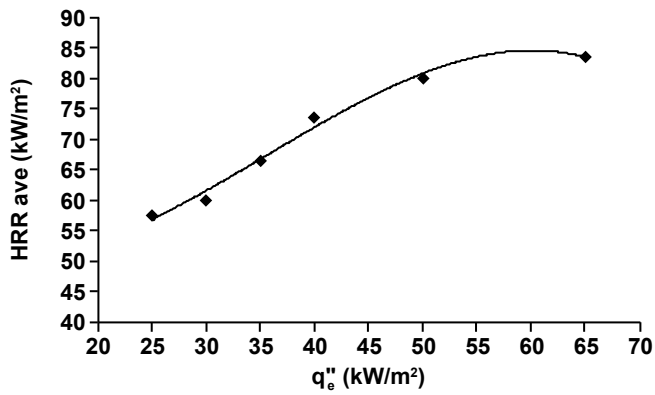

Figure 7. Average heat release rate (HRR average) as a function of external irradiance for redwood lumber (test no. 14, SDVU data).

expose additional "virgin" materials to ignition. The material linings are typically installed on a heavy inert backing material. Finally, direct impingement on the material by the ignition burner flames results in imposed heat fluxes of around 40 to 50 kW/m^2 and prevents fresh air from penetrating the charring surfaces. In the challenging case of the thin hardboard, the second peak HRR was reduced 32% with the use of the Type X gypsum backing board versus the insulation backing when tested at irradiance of 50 kW/m^2 in the FPL cone calorimeter. Preventing glowing as a result of burner's flame impingement on the material would further reduce this peak HRR. If we then also take into account the flashover time of around 225 s for hardboard in our room/corner tests, we find that its burn profile within 225 s is identifiable with the ablation/quasi-steady charring (thermally thick) phase of material pyrolysis.

In a similar manner, all other materials tested are identified with their thermally thick phase of material pyrolysis as being relevant to fire growth modeling in the full-scale tests. This includes the FRT polyurethane foam, a plastic-based material with char forming treatment. We note the constraint identified for the thin hardboard is also applicable

Table 2—Combustion properties for Quintiere's room/corner test model

Material	Test no.	ΔH (MJ/kg)	L (MJ/kg)	Q'' (MJ/m^2)	ϕ[a] (kW^2/m^3)	$T_{s,min}$[a] (°C)
Type X gypsum board	1	9.34	7.49	3.33	0.5	300
FRT Douglas Fir plywood	2	8.19	5.20	28.12	8	180
Oak veneer plywood	3	11.8	3.96	56.40	7.6	73
FRT plywood (Forintek)	4	7.28	13.85	32.88	8	180
Douglas Fir plywood (ASTM)	5	11.80	4.34	58.57	5.7	111
FRT polyurethane foam	6	8.71	5.84	—	3	105
Type X gypsum board	7	9.34	7.49	3.33	0.5	300
FRT Southern Pine plywood	8	8.28	4.80	41.02	8	180
Douglas Fir plywood (MB)	9	11.05	6.25	71.92	5.7	111
Southern Pine plywood	10	12.43	5.81	82.58	7	125
Particleboard	11	11.64	6.10	111.41	8	180
Oriented strandboard	12	12.23	6.49	83.22	2.2	143
Hardboard	13	13.51	4.08	88.67	11	80
Redwood lumber	14	13.19	5.57	101.42	8.8	124
Type X gypsum board	15	9.34	7.49	3.33	0.5	300
White spruce lumber	16	11.60	9.89	92.83	24	155
Southern Pine boards	17	12.06	6.82	125.13	7	125
Waferboard	18	12.83	5.54	104.23	8	180

[a]Values taken from Quintiere (1993) and Janssens (1991).

to untreated plastics that have an HRR profile similar to that of Figure 5. Therefore, we need focus only on (1) the initial peak HRR and the follow-on decrease to a quasi-steady level HRR profile of charring materials or (2) the initial HRR plateau typical of untreated plastics for input to mathematical models. This allows us to ignore the effect of backing materials (and the HRR peak just prior to burnout) when predicting flashover time or flame spread index. For any other fire growth scenarios, such as the post-flashover or extended test duration, such a simplified HRR profile would not be adequate.

Linear correlation of the first HRR peak versus irradiance was used as input to the mathematical models. In Figures 8 to 23, the linear correlations of the peak HRR versus irradiance for tested materials measured in the cone calorimeter are shown. The slope of this linear correlation is the ratio of effective heat of combustion over effective heat of gasification, as defined by Quintiere (1993). The effective heat of gasification is then calculated as the effective heat of combustion divided by the slope of the linear correlation. These values are used for the calculation of the HRR from the material in Quintiere's room/corner test mathematical simulation. The resulting values of effective heats of combustion and gasification (as defined by Quintiere (1993)) are listed in Table 2. This approach was first used successfully with liquid fuels and then extrapolated to solid charring fuels. We note some wood materials already have a high HRR from the flame fluxes alone, so that the addition of external heat flux seems subdued in extracting additional HRR from the material. This implies a changing effective heat of gasification with both time and heat fluxes during wood pyrolysis. This creates a difficulty for Quintiere's model, which requires a single value for the effective heat of gasification.

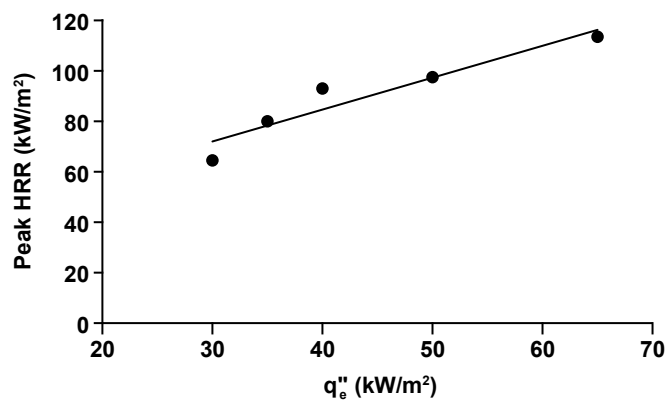

Figure 8. Peak heat release rate (HRR) as a function of external irradiance for Type X gypsum board (test no. 1).

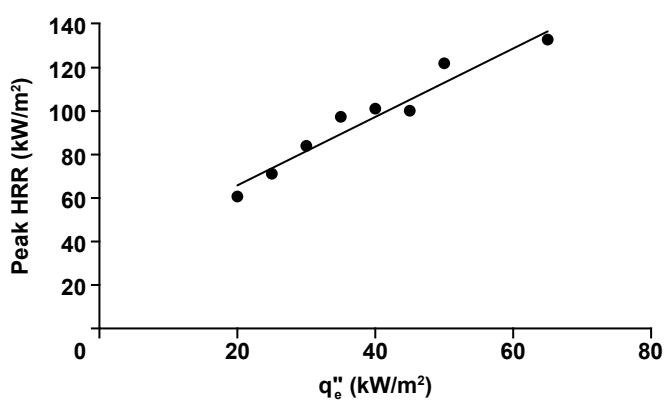

Figure 9. Peak heat release rate (HRR) as a function of external irradiance for FRT Douglas Fir plywood (test no. 2).

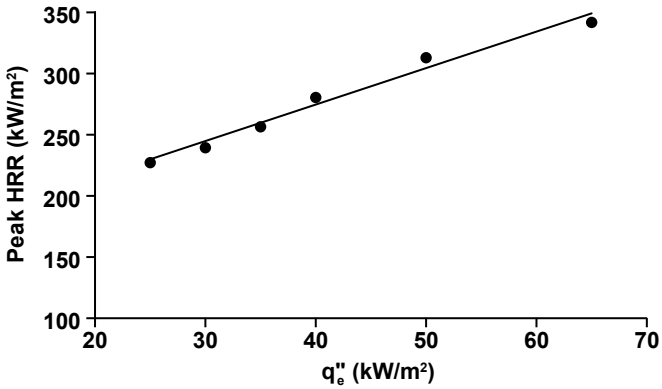

Figure 10. Peak heat release rate (HRR) as a function of external irradiance for oak veneer plywood (test no. 3).

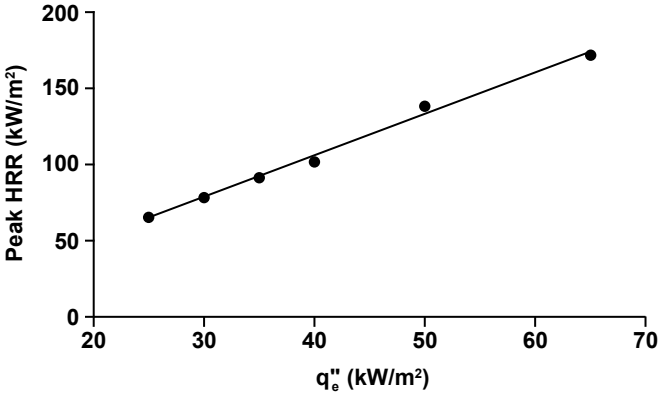

Figure 11. Peak heat release rate (HRR) as a function of external irradiance for FRT plywood from Forintek (test no. 4).

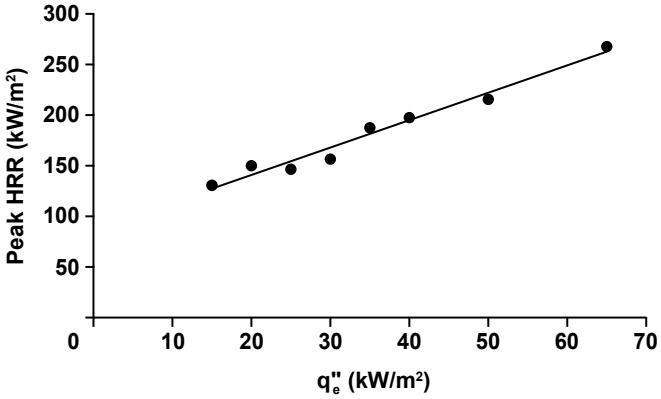

Figure 12. Peak heat release rate (HRR) as a function of external irradiance for Douglas Fir plywood ASTM R.R. (test no. 5).

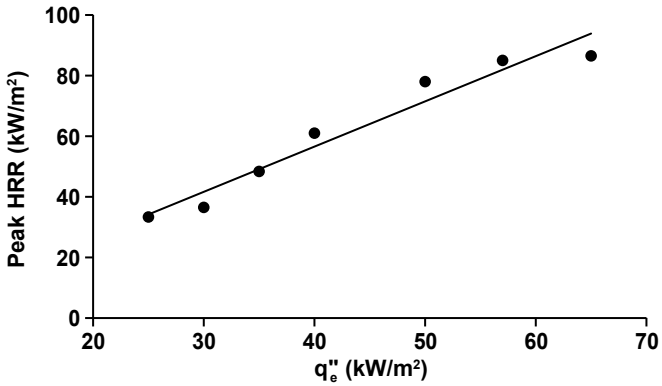

Figure 13. Peak heat release rate (HRR) as a function of external irradiance for FRT rigid polyurethane foam (test no. 6).

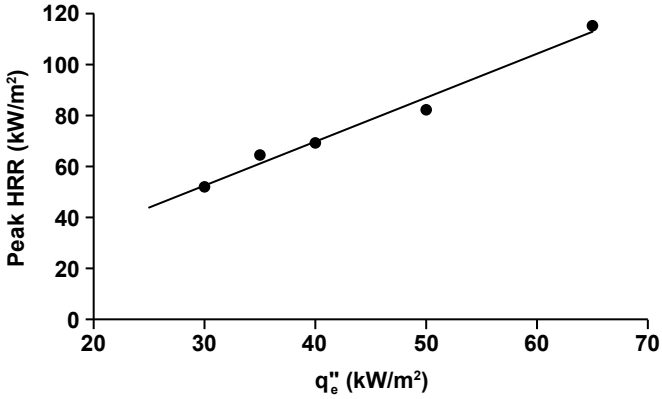

Figure 14. Peak heat release rate (HRR) as a function of external irradiance for FRT Southern Pine plywood (test no. 8).

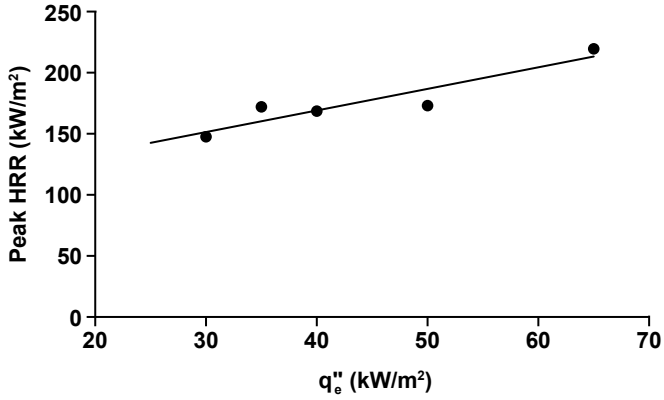

Figure 15. Peak heat release rate (HRR) as a function of external irradiance for Douglas Fir plywood material bank (test no. 9).

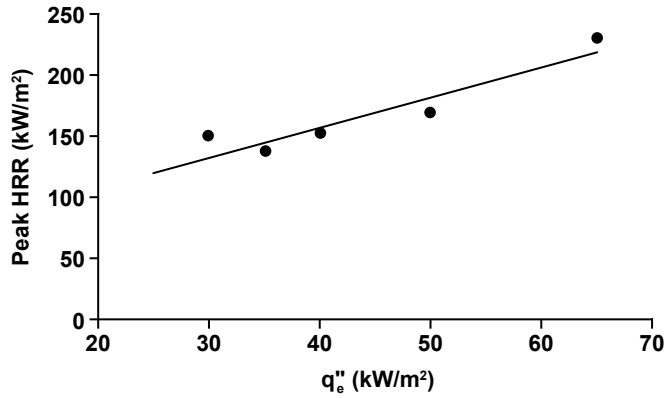

Figure 16. Peak heat release rate (HRR) as a function of external irradiance for Southern Pine plywood (test no. 10).

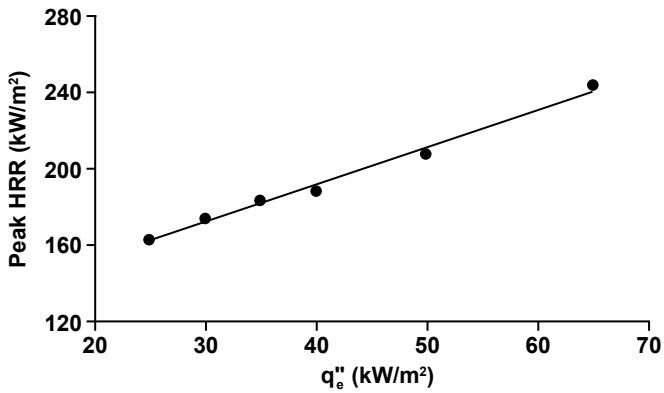

Figure 17. Peak heat release rate (HRR) as a function of external irradiance for particleboard (test no. 11).

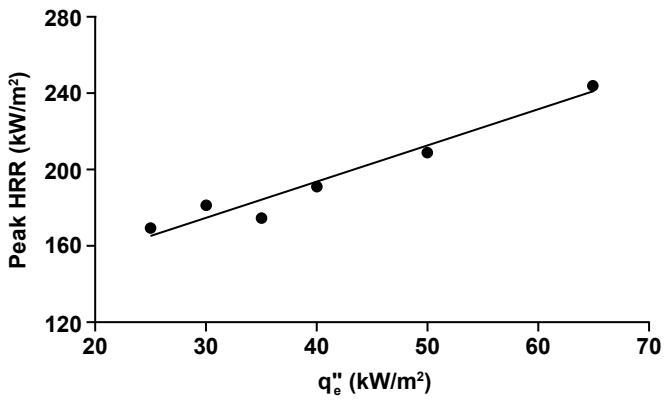

Figure 18. Peak heat release rate (HRR) as a function of external irradiance for oriented strandboard (test no. 12).

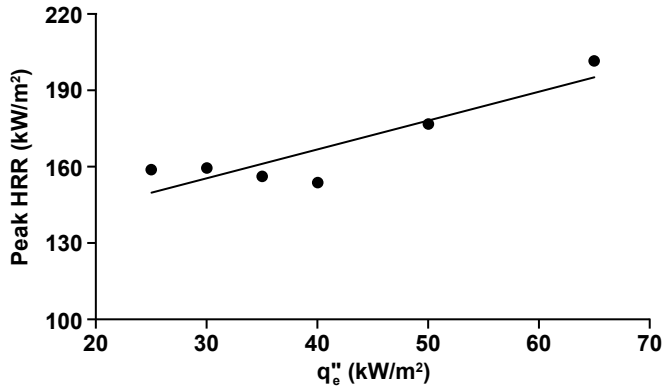

Figure 19. Peak heat release rate (HRR) as a function of external irradiance for hardboard (test no. 13).

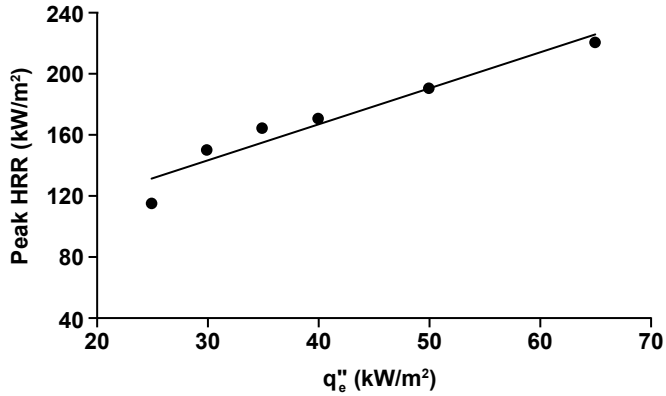

Figure 20. Peak heat release rate (HRR) as a function of external irradiance for redwood lumber (test no. 14).

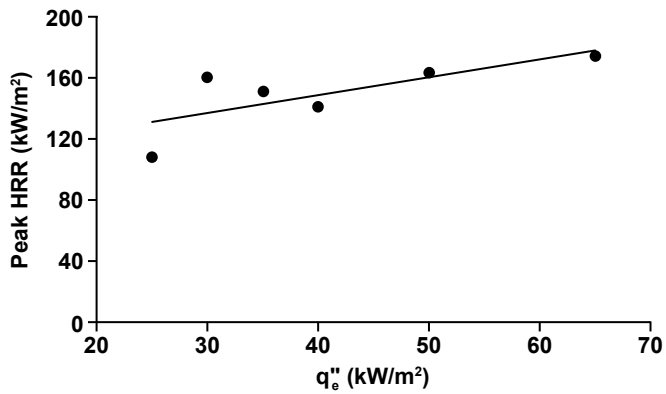

Figure 21. Peak heat release rate (HRR) as a function of external irradiance for white spruce lumber (test no. 16).

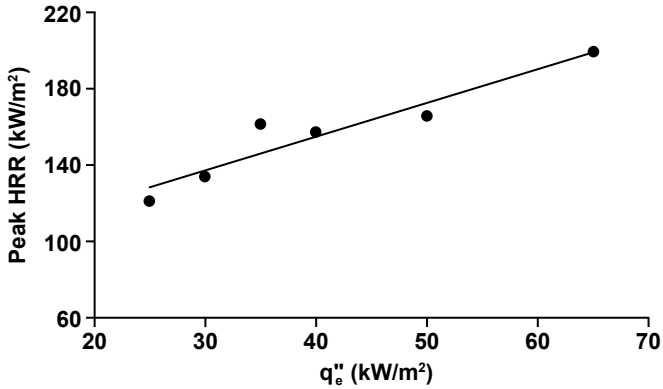

Figure 22. Peak heat release rate (HRR) as a function of external irradiance for Southern Pine boards (test no. 17).

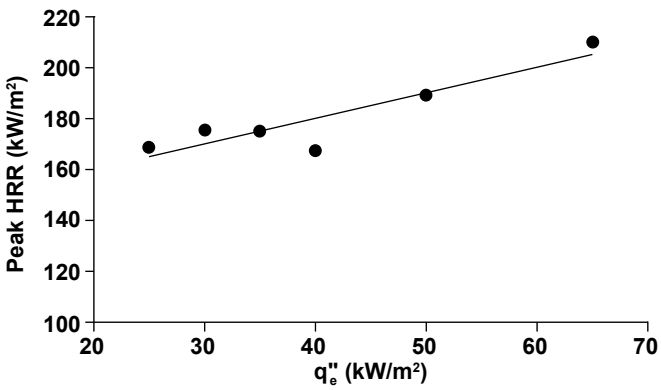

Figure 23. Peak heat release rate (HRR) as a function of external irradiance for waferboard (test no. 18).

The values of slope and constant of the linear correlation of peak HRR versus irradiance for tested materials are listed in Table 3 for use in Dietenberger's analytical model (Dietenberger and Grexa 1999). In this model, the peak HRR is evaluated based on equivalently derived "irradiance" in a fire scenario. It uses the simplification that the burning surface temperature is about the same value in both a fire scenario and the cone calorimeter, making heat losses of surface re-radiation and thermal conduction into the material similar in both scenarios. Therefore, one needs only to equalize the imposed heat fluxes on the tested materials for both scenarios. Imposed heat fluxes in the cone calorimeter are absorption from the heater irradiance and small heat flux from the material flame; whereas in a large-scale fire test, the imposed heat flux has large convective and radiative components from the propane flame. The equivalently derived "irradiance" is then calculated simply as the difference between large heat flux from the propane flame on a burning surface and small flame heat flux on the cone sample. This "irradiance" will vary somewhat among the materials because of unique burning surface temperatures (approximated as surface ignition temperature plus 100 °C (212 °F) recommended by Janssens and others (1995), which is listed in the last column of Table 3).

Total Heat Release and Effective Heat of Combustion

The total heat release (THR) is an important parameter that characterizes the total available energy in the material in a possible fire situation. It is calculated as the area under the HRR curve, measured in the cone calorimeter. The burning time and consequently the burnout area of a material in the

Table 3—Combustion properties for Dietenberger's analytical fire growth model

Material	Test no.	PHRR intercept (kW/m^2)	PHRR slope (–)	THR intercept (kJ/m^2)	THR slope (s)	$T_{s,burn}$ (K)
Type X gypsum board	1,7,15	34.1	1.26	1,481	45.4	708.5
FRT Douglas Fir plywood	2	34.3	1.57	14,740	312.2	746.8
Oak veneer plywood	3	155.4	2.98	38,572	350.9	663
FRT plywood (Forintek)	4	–2.1	2.71	10,509	439.4	750
Douglas Fir plywood (ASTM)	5	86.7	2.71	52,583	170.9	704.6
FRT polyurethane foam	6	3.12	1.49	0.0	271.6	789
FRT Southern Pine plywood	8	43.1	0.935	41,100	0.0	772
Douglas Fir plywood (MB)	9	98.4	1.77	63,900	200	719
Southern Pine plywood	10	57.4	2.49	82,600	0.0	720
Particleboard	11	115.8	1.91	86,529	609.3	663
Oriented strandboard	12	118.2	1.88	73,115	247.4	699
Hardboard	13	121.5	1.134	84,227	108.7	693
Redwood lumber	14	71.9	2.37	85,538	389	738
White spruce lumber	16	101.8	1.17	93,592	–18.8	721
Southern Pine boards	17	84.4	1.77	119,544	137	744
Waferboard	18	139.9	1.00	86,196	442	663

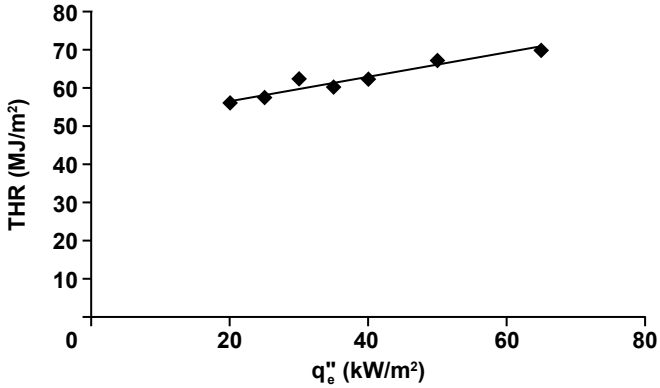

Figure 24. Total heat released for Douglas Fir plywood (test no. 9) as a function of irradiance.

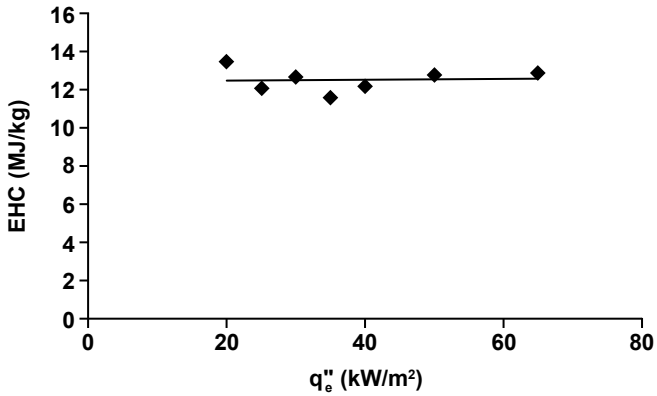

Figure 25. Effective heat of combustion (EHC) for Douglas Fir plywood (test no. 9) as a function of irradiance.

room/corner test can be calculated based on the total heat release (Quintiere 1993). The Quintiere room/corner fire growth model treats the HRR from a unit burning area as a constant and then is set to zero after the THR of the unit burning area is obtained. For wood-based materials, this could result in an overestimation of overall HRR because the HRR from a unit burning area is actually monotonically decreasing (often exponentially) in a large-scale fire test scenario. Indeed, our earlier discussion of bench-scale HRR profile suggested that the second HRR peak typically observed in the cone calorimeter could be ignored for the purposes of predicting time to flashover. The Dietenberger room/corner analytical model, however, explicitly models the bench-scale HRR profile as exponentially decreasing. The THR data in this case are used to define the area under the "modeled" HRR curve, thus also defining how rapidly the HRR decreases with time. Alternatively, one could fit an exponentially decreasing function to the actual HRR profile and derive a "working" THR for input to a model. However, this seemed an unnecessary complication for a simplified fire growth model. Previous work (Dietenberger 2002) showed that the measured THR corresponding to a

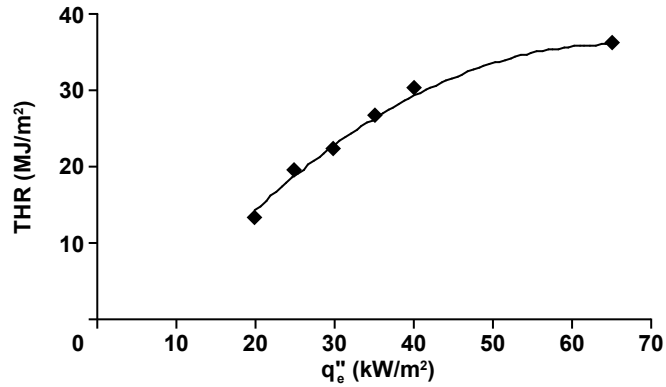

Figure 26. Total heat released for FRT plywood from Forintek (test no. 4) as a function of irradiance.

12.5-mm-thick specimen reasonably represents the relevant HRR profile for the oriented strandboard (OSB), treated and untreated. This means the "working" THR is well approximated by the measured THR multiplied by the thickness ratio of 12.5 mm over measured material thickness (mm) of a specimen that becomes fully charred.

The correlation of THR as a function of irradiance for Douglas Fir plywood is shown in Figure 24. The total heat release slightly increased with increasing irradiance (25% increase in THR over irradiances of 25 to 65 kW/m^2). Similar correlation was found also for other untreated wood products. On the other hand, effective heat of combustion (EHC) did not change with changing irradiance (Fig. 25) within measured exposure levels (>20 kW/m^2) for wood-based products.

The change of THR with increasing irradiance was stronger for the FRT wood products (Fig. 26). The increase of THR evolved at irradiance of 65 kW/m^2 compared with THR evolved at 25 kW/m^2 was around 86%. This THR trend mainly reflects the correspondent trend in peak HRR. However, EHC did not show systematic change as a function of irradiance (Fig. 27). The significant EHC and THR reductions of about 35% and 50%, respectively, for treated wood products are suggestive of relatively higher inert gas dilution of volatiles along with retaining more fuel within the char. Therefore, the chemical retardant primarily affects the quasi-steady phase of wood pyrolysis.

Tested FRT rigid polyurethane foam (material no. 6) showed strong dependence of both THR and EHC on irradiance (Figs. 28 and 29). The burning time for this material was also strongly dependent on the irradiance level and ranged from 0.1 to 100 s. These observations were caused by the presence of flame retardant in the polyurethane foam. At low irradiance levels the effect of flame retardant is the strongest, as shown by EHC vanishing, whereas at high irradiances the FRT becomes ineffective, as shown by the high values of EHC, perhaps close to those of untreated foam.

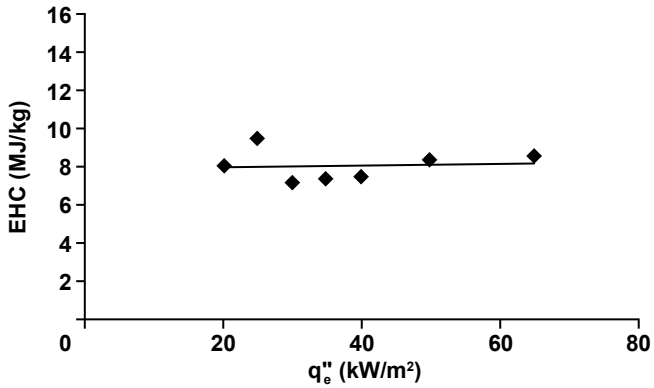

Figure 27. Effective heat of combustion for FRT plywood from Forintek (test no. 4) as a function of irradiance.

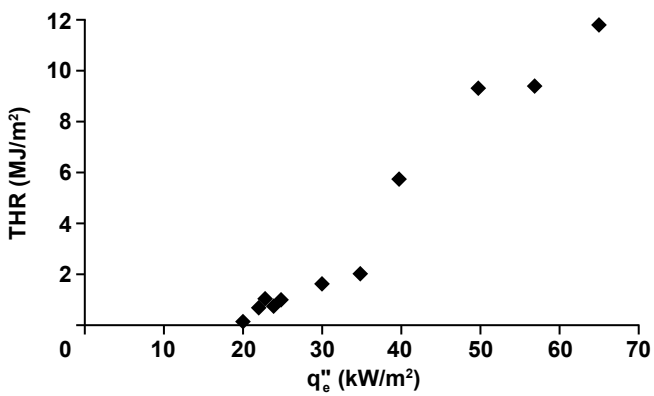

Figure 28. Total heat released for FRT rigid polyurethane foam (test no. 6) as a function of irradiance.

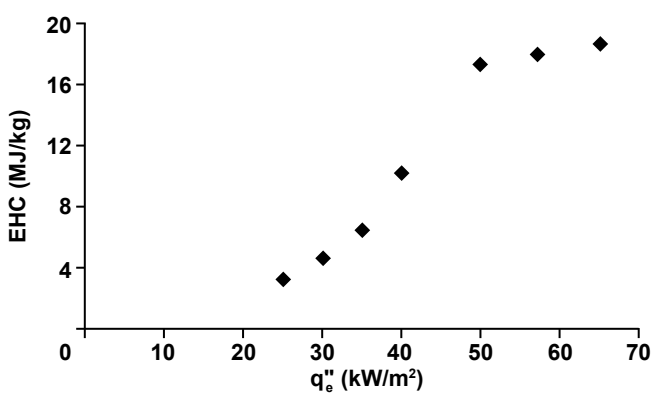

Figure 29. Effective heat of combustion for FRT rigid polyurethane foam (test no. 6) as a function of irradiance.

The resulting average values of THR measured in the cone calorimeter for the tested materials are listed in Table 2 for Quintiere's model. The values of slope and constant of the linear correlation of total heat release versus irradiance are listed in Table 3 for Dietenberger's model.

Combustion Products

In Part I of this series of papers (Grexa and others 2012) that describe the room/corner test results, combustion products were carefully discussed. The most controversial is the production of carbon monoxide, not only because it is very toxic and virtually undetectable to animal senses, but also because wood often is implicated in producing the most CO of the various materials. Soot and water vapor seemed unappreciated as a serious contributors to fire hazard until recent studies began to show their significance, particularly when high thermal radiation from heavily soot-laden and humid hot-gas regions control the progress of fire growth to room flashovers. The influence of CO_2 and total hydrocarbon (THC) production on fire hazard is limited to underventilated fires, as during post-flashovers. Development of excess fuels of CO, soot, and THC in upper hot gas layers can lead to conflagrations under the right conditions.

Given the highly overventilated conditions of the cone calorimeter, serious questions exist as to whether one can expect measured combustion products to be extrapolated to that of the room test fires, particularly if flashovers are routinely observed. In a partial answer to this question, it was determined in appendix C in Part I of this series of papers (Grexa and others 2012) that combustion within the ISO 9705 (ISO 1993a) test room is overventilated as long as the HRR is less than 3.5 MW. This means that even in the post-flashover HRR range of 1 to 3.5 MW, the room's combustion is overventilated. This simplifies the analysis of combustion products to two issues: (1) Are the wood volatile contents similar between the cone calorimeter test and the room test? (2) Is incompleteness of combustion similar between the small-scale and large-scale tests?

According to combustion products development in appendix D of Part I of this series of papers (Grexa and others 2012), the empirical formula, $C_XH_YO_Z$, of the wood volatiles cannot be directly determined for the room tests because the measurements of H_2O and THC are lacking or contaminated by non-wood sources. Therefore, we computed an alternative parameter, the ratio of fuel's molar carbon to fuel's molar stoichiometric oxygen consumption during overventilated combustion (called fuel hydration value), as

$$\frac{\nu_{\mathrm{C,fuel}}}{\Delta\nu_{\mathrm{O2}}} \equiv \frac{X}{X+Y/4-Z/2} \cong \frac{\dfrac{\beta_{\mathrm{CO2}}}{44}+\dfrac{\beta_{\mathrm{s}}}{12}+\dfrac{\beta_{\mathrm{CO}}}{28}}{\dfrac{\beta_{\mathrm{O2}}}{32}+\dfrac{\beta_{\mathrm{s}}}{12}+\dfrac{1}{2}\dfrac{\beta_{\mathrm{CO}}}{28}} \equiv \frac{8\beta_{\mathrm{CO2,st}}}{11} \qquad (1)$$

The various averaged betas are computed from global cone calorimeter test results as

Table 4—Comparison of fuel hydration values computed with Equation (1)

Material	Test no.	Room/ corner tests	Cone test/ insulation (35 kW/m^2)	Cone test/ insulation (50 kW/m^2)	Cone test gypsum (35 kW/m^2)	Cone test gypsum (50 kW/m^2)
Type X gypsum board	1,7,15	1.000	—	0.867	—	—
FRT Douglas Fir plywood	2	1.101	0.736	0.825	0.723	1.131
Oak veneer plywood	3	1.061	0.987	0.948	0.874	0.968
FRT plywood (Forintek)	4	1.080	—	—	—	—
Douglas Fir plywood (ASTM)	5	1.012	0.854	0.778	0.968	1.028
FRT polyurethane foam	6	0.889	0.889	0.783	—	—
FRT Southern Pine plywood	8	1.033	0.836	0.800	0.912	0.835
Douglas Fir plywood (MB)	9	0.863	0.823	0.867	1.069	0.944
Southern Pine plywood	10	0.956	0.804	0.815	1.023	0.881
Particleboard	11	0.992	0.791	0.856	0.896	0.872
Oriented strandboard	12	0.994	0.807	0.816	0.955	1.072
Hardboard	13	0.991	0.835	0.985	1.041	0.910
Redwood lumber	14	0.913	1.027	0.861	0.935	0.844
White spruce lumber	16	0.979	0.841	0.864	1.098	1.114
Southern Pine boards	17	0.965	0.813	0.844	0.918	0.899
Waferboard	18	0.938	0.801	0.847	0.871	0.875

$$\beta_{\mathrm{f}} = 1/r_{\mathrm{o,cone}} = 13.1/\mathrm{EHC}$$
$$\beta_{\mathrm{CO2}} = Y_{\mathrm{CO2}}\beta_{\mathrm{f}}$$
$$\beta_{\mathrm{CO}} = Y_{\mathrm{CO}}\beta_{\mathrm{f}}$$
$$\beta_{\mathrm{O2}} \equiv 1$$
$$\beta_{\mathrm{s}} = (\mathrm{SEA}/8300)\beta_{\mathrm{f}}$$

The fuel hydration value as computed with Equation (1) should agree with that obtained from the room tests if the conditions in the cone calorimeter tests adequately simulate room test conditions. Close examination of the terms in Equation (1) show that the ratio of CO_2 yield to EHC dominates the fuel hydration value, even during incomplete combustion.

We note from earlier discussion that the typical full-scale test duration does not involve the after-glow phenomenon, which is typically observed in a cone calorimeter test for wood materials with an insulated backing. The after-glow usually results in a greater percentage increase in the EHC than the percentage increase in the CO_2 yield, thus lowering the fuel hydration value. To put it in another way, the after-glow drives out the remaining hydrocarbons left in the remaining lignin structure, which lowers the fuel hydration value perhaps to 0.9 or less, so later the char eventually burns out as amorphous carbon, which finally increases fuel hydration value to unity. Indeed, Table 4 shows that a material with insulated backing has a cone fuel hydration value that averages 13% less than the room/corner hydration value. By merely placing gypsum board backing to the specimen, which is known to reduce after-glow considerably, the cone fuel hydration values average only 3.3% and 3.2% less than the room/corner hydration values at irradiances of 35 and 50 kW/m^2, respectively.

Because the specimen mass flow rate was measured in the cone calorimeter along with O_2, CO_2, CO, and soot mass flow rates, equation (D-1) in Part I (Grexa and others 2012) can be rearranged to solve for empirical formula of the "averaged" wood volatiles/water vapor, $C_XH_YO_Z$, as

$$\frac{Y}{X} \cong \frac{[\beta_{\mathrm{f}} + \beta_{\mathrm{O2}} - \beta_{\mathrm{CO2}} - \beta_{\mathrm{CO}} - \beta_{\mathrm{s}}]/9}{\dfrac{\beta_{\mathrm{CO2}}}{44} + \dfrac{\beta_{\mathrm{s}}}{12} + \dfrac{\beta_{\mathrm{CO}}}{28}} \tag{2}$$

$$\frac{Z}{X} = 2 + \frac{Y}{2X} - \frac{11}{4\beta_{\mathrm{CO2,st}}} \tag{3}$$

Table 5 provides the values for the betas and the ratios Y/X and Z/X for the test materials as backed by gypsum board and exposed horizontally to irradiances of 35 and 50 kW/m^2. Whenever possible, the average value over the two irradiances is used because no replicates of tests were performed in the case of gypsum board backing.

We note that soot production yields, despite the high noise level with the cone calorimeter data, are somewhat in agreement with the room/corner test results. However, the CO production in the cone calorimeter tests is typically an order of magnitude less than that in the room tests. Because the soot and CO are mainly produced during thermal cracking of wood volatiles prior to burning, the higher residence time, flame puffing, and higher temperatures possible in the room tests will make combustion of wood volatiles more incomplete than that in the cone calorimeter tests. Therefore, incomplete combustion in the cone calorimeter correlates quite poorly with that in the room tests for wood materials, at least for CO and soot production. However, the empirical formula for wood volatiles/water vapor listed in the last two columns of Table 5 should also be representative of that in the room tests because of the fairly close agreement in their fuel hydration values in Table 4. The gypsum board used as a specimen is the exception, because of its uncertain, but rather large water vapor production from the gypsum

Table 5—Computation of empirical formula for volatiles from FPL cone calorimeter data

Material	Test no.	β_f	β_{Soot}	β_{CO}	β_{CO2}	Y/X	Z/X
Type X gypsum board	1,7,15	29.11	0.0500	0.1488	1.035	97.21	48.30
FRT Douglas Fir plywood	2	2.835	9.57E-05	0.2365	1.393	6.110	3.286
Oak veneer plywood	3	1.358	0.0062	0.0682	1.205	3.950	1.801
FRT plywood (Forintek)	4	—	—	—	—	—	—
Douglas Fir plywood (ASTM)	5	1.264	0.00161	0.0671	1.320	2.991	1.491
FRT polyurethane foam	6	1.747	0.0968	0.1301	1.074	4.329	1.920
FRT Southern Pine plywood	8	1.810	0.00596	0.0880	1.119	6.101	2.759
Douglas Fir plywood (MB)	9	1.080	0.00386	0.0373	1.279	2.748	1.275
Southern Pine plywood	10	1.051	0.00868	0.0210	1.290	2.641	1.219
Particleboard	11	1.081	0.00933	0.00376	1.208	3.371	1.422
Oriented strandboard	12	1.060	0.00659	0.0628	1.347	2.141	1.099
Hardboard	13	0.999	0.00784	0.0602	1.292	2.205	1.052
Redwood lumber	14	0.922	0.00668	0.00193	1.218	2.732	1.116
White spruce lumber	16	1.189	0.00098	0.00774	1.516	2.122	1.253
Southern Pine boards	17	0.981	0.00620	0.00328	1.244	2.799	1.197
Waferboard	18	0.973	0.00755	0.00297	1.195	3.060	1.240

material that considerably dilutes the fuel content, consistent with its quite high values of the ratios Y/X and Z/X and nearly $Y/Z = 2$ ratio in Table 5 for the cone calorimeter tests.

Using the empirical formula of volatiles and the "room" betas of soot, CO, and CO_2 listed in Part I (Grexa and others 2012), the volatile mass flow rate as given by equation (D-1) in Part I can now be calculated for the overventilated room/corner tests. As a result, the average yield of H_2O, CO_2, CO, and soot and averaged stoichiometric heat of combustion (appendix D of Part I) in overventilated conditions of the fire source room can also be calculated. The remaining parameters needed for use in a mathematical model such as the Fire Dynamic Simulator are the mass loss rate (MLR) profile and the thermally cracked volatile yields of soot, CO, CO_2, H_2O, H_2, and THCs prior to incomplete combustion. Because of the nearly constant heat of combustion during the quasi-steady phase of wood pyrolysis, the MLR profile can be approximated by the decreasing exponential MLR ~ HRR/EHC profile for a unit area in full-scale tests. This means that the Dietenberger method of equivalent "irradiance," computed as imposed heat fluxes in a fire scenario minus the cone's flame flux, can be used as input for calculating the MLR decreasing as a function of time via parameters provided in Table 3.

Because component yields of fully thermally cracked volatiles are not experimentally available for room test materials, an idealized set is estimated for input to CFD models such as the Fire Dynamic Simulator. At very high temperatures (>800 °C), major components of volatiles are known to be H_2O, CO, CO_2, and simple THCs (Boroson and others1989). Thus for simplicity, consider the small quantities of soot and H_2 to be part of THCs with an overall empirical formula CH_2. The main sources of H_2O and CO_2 are dehydration and decarboxylation, respectively, of the wood structure at temperatures below that of thermal cracking of the tar. Let $r = 0.1 \pm 0.1$ be a typical ratio of moles of CO_2 to moles of H_2O. Then at higher temperatures, assume the tar primarily cracks into CO and THCs. The result for this idealized set of toxic gases thermally cracked from wood volatiles is

$$\begin{aligned} C_X H_Y O_Z &\Rightarrow n H_2O + rn CO_2 + (Z - n - 2rn) CO \\ &\quad + (Y/2 - n) CH_2 \\ n &= (Z + Y/2 - X)/(2 + r) \end{aligned} \tag{4}$$

Obviously, to get better estimates one would have to sample directly the unburned volatiles coming off the specimen and heat them quickly and anaerobically to at least 800 °C before analyzing the gases. We conclude also that the incomplete combustion production of soot and CO developed in the room test does not correlate well with "averaged" cone calorimeter data, suggesting that a modified cone calorimeter protocol that simulates the room conditions more closely is needed.

Thermal Properties Derived from Ignitability Analysis

Effect of Density on Time to Ignition

A strong correlation was observed between t_{ig} and density (Figs. 30 and 31). As it can be seen in these figures, the materials can be divided into four groups: FRT plywood, lumber, plywood, and other composite materials (waferboard, OSB, hardboard, fiberboard). As will be explained later, for heat fluxes at or above 30 kW/m², a thermally thick response from the materials is expected. That is, the time to ignition is proportional to the thermal inertia (product of density, thermal conductivity, and heat capacity), given that all other factors are constant. At 30 kW/m², large differences were measured only for fire-retardant materials, as shown in Figure 30. The FRT plywood has higher ignition temperature than that of untreated plywood, accounting for

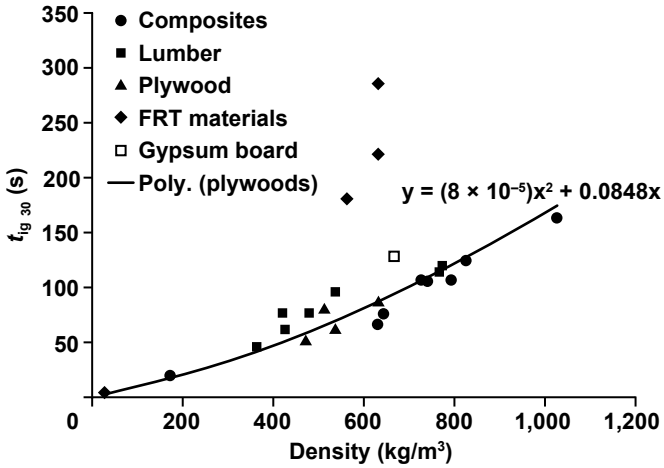

Figure 30. Time to ignition as a function of density of tested materials at 30 kW/m2.

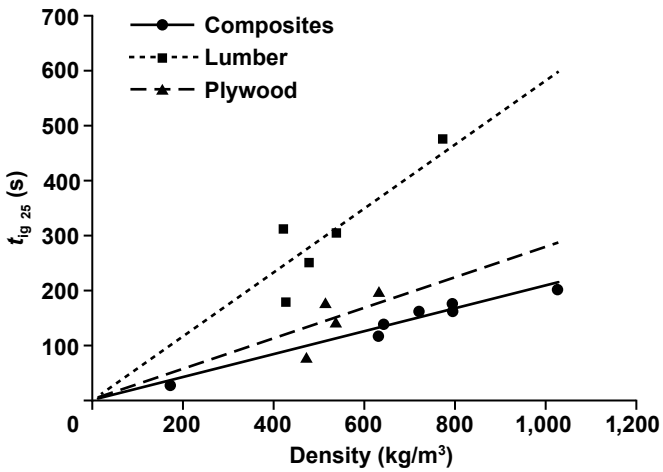

Figure 31. Time to ignition as a function of density of wood products at 25 kW/m2.

their much higher values of time to ignition at similar values of density. Upon close examination, we also observe that the time to ignition for composites is slightly less than that of plywood, which in turn is slightly less than that of lumber, for similar values of density. This would mainly be due to the reductions in thermal conductivity of composite materials compared with the lumber of the same density. This observation is in agreement with the data published by TenWolde and others (1988), who found that thermal conductivity of plywood is about 86% of that for wood with the same density, and for particleboard about 75% of that for wood. Because thermal conductivity is also known to be a linear function of density, we represented the time to ignition as a parabolic function of density in the case of plywood in Figure 30, and it also seems to represent an average for the untreated wood-based materials.

With the higher values of time to ignition shown in Figure 31 at irradiance of 25 kW/m^2, one can expect a significant development of thermally thin response from the materials. That is, in the thermally thin limit, the time to ignition for wood should be proportional to the thermal thickness (product of density, heat capacity, and material thickness), given that all other factors are constant. At this lower irradiance the effect of each type of material is even more evident (Fig. 31). A single functional correlation could not be found that fits the data for all tested wood products (lumber, composites, plywood, FRT wood materials). Rather, the slope of the linear regression for untreated groups decreases significantly in the order of lumber, plywood, and other composites. Because composites have material thickness significantly less than the lumbers, it is also reflected in their significantly less time to ignition at similar density. This is in contrast to the effect of thermal conductivity on the time to ignition shown in Figure 30. Thus, the results in Figures 30 and 31 are suggestive of a heat conduction analysis based on a constant surface temperature at ignition for a given material.

Indeed, Wesson and others (1971) examined similar piloted ignition effects on various lumbers of different oven-dried densities and thickness as exposed to two different types of radiant heat source. Their choice of tungsten lamp and hexane flame as the two radiant heat sources had a significant effect on absorptance values for wood. The radiant energy from the electric heating coils of the cone calorimeter has dominating wavelengths much greater than that of either of Wesson's heat sources, in a region where spectral absorptance has small variations for various wood species (Wesson and others 1971). Therefore, our use of a portable emissionmeter should provide values of emissivity (also equal to long-wavelength average absorptance) suitable for the cone calorimeter tests, but the use of blue flames or solar furnaces in specialized piloted ignition tests will result in a significant reduction in average absorptance for natural wood. Finally, the Wesson and others (1971) correlation for time to ignition is applicable only to imposed heat fluxes significantly greater than the critical flux because they did not explicitly considered re-radiation or convective cooling or even variations in the ignition temperature in the theoretical solution.

In what follows, time to ignition measurement was used to derive the thermal inertia, $k\rho c$, thermal diffusivity, $k/\rho c$, and ignition temperature, T_{ig}. There are several ways for calculating $k\rho c$ and T_{ig} from the time to ignition measurements for thermally thick materials. In this study we used two documented methods, one by Janssens (1991) and the other by Dietenberger (1996). These methods were chosen because the ignition formula was designed to agree with theoretical heat conduction analysis as well as being convenient to use in a spreadsheet application. The Janssens method can be briefly summarized as follows. It was supposed that the tested materials behaved as semi-infinite solids. The boundary condition at the exposed surface and at the ignition time for gray-body materials was expressed by

$$\varepsilon m \dot{q}''_{cr} = h_c (T_{ig} - T_a) + \varepsilon m \sigma (T_{ig}^4 - T_a^4) \equiv h_{ig} (T_{ig} - T_a) \quad (5)$$

The time to ignition was correlated with irradiance by

$$\dot{q}''_e = \dot{q}''_{cr} \left\{ 1 + 0.73 \left[\frac{k\rho c}{h_{ig}^2 t_{ig}} \right]^{0.547} \right\} \quad (6)$$

The critical irradiance level, $\dot{q}''_{cr}$, was found as intercept of the line (fitted to the plot of $(t_{ig})^{-0.547}$ versus q_e) with the abscissa. Ignition temperature T_{ig} was calculated from Equation (5) using the Newtonian iteration method, and subsequently h_{ig} was calculated from Equation (5). The $k\rho c$ parameter was found from the slope of the experimental line and inserting its value into Equation (6). For the ignition temperature calculation, the convective heat transfer coefficient h_c is needed. The value suggested by Janssens (1991) for vertical orientation in cone calorimeter is $h_c = 0.0135$ kW/m²K. Dietenberger (1996) measured the convective heat transfer coefficient in the cone calorimeter in horizontal orientation as a function of external heat flux, which is expressed by the function

$$h_{c,cone} = 0.01433 + 1.33 \times 10^{-4} \dot{q}''_e \quad (7)$$

Because all our measurements were done in horizontal orientation, Equation (7) was used for calculation of the convective heat transfer coefficient. However, this now introduces nonlinearity into Equation (6), causing us to use a different numerical procedure—a nonlinear regression routine, like those available in spreadsheets. The advantage of the Janssens method is that neither ignition temperature nor thermal inertia must be known, and both of these parameters can be obtained only from the ignition time measurements. However, thermal inertia and surface temperature at ignition obtained by the Janssens method are sensitive to small changes in the slope of time to ignition versus irradiance. Also, Equation (6) is sufficiently accurate only for $0.1 \le q_{cr} / q_e \le 0.9$ and $\mathrm{Fo} \le 0.1$, which is satisfied for the room test materials, except for the thin hardboard and FRT polyurethane foam (in its fully melted/collapse condition prior to ignition) and at low irradiances less than or equal to 25 kW/m² for other materials.

Dietenberger's method for calculation of thermophysical parameters is described in detail in Dietenberger (1996). To predict thermal response of material of any thickness, an accurate interpolation formula was developed for finitely thick materials with convective cooling and radiation heating of the exposed side and insulation on the unexposed side. The material is assumed to ignite at a critical surface temperature on the exposed side. The interpolation formula fitted to the finite element solutions of transient heat conduction as a function of Biot and Fourier numbers is

$$\dot{q}''_e = \dot{q}''_{cr} \left\{ 1 + (F_{thick}^n + F_{thin}^n)^{(-1/n)} \right\} \quad (8)$$

where,

$$n = (2.68 + 0.4\mathrm{Bi})/(1 + \mathrm{Bi}) \quad (9)$$

$$F_{thick} = \sqrt{\frac{4}{\pi} \mathrm{Bi}^2 \mathrm{Fo}} \quad (10)$$

$$F_{thin} = \exp\left(\frac{\mathrm{BiFo}}{1 + 0.254\mathrm{Bi}} \right) - 1 \quad (11)$$

$$\mathrm{Bi} = h_{ig} \delta_m / k \quad (12)$$

$$\mathrm{Fo} = (k / \rho c) t_{ig} / \delta_m{}^2 \quad (13)$$

Note that Equation (10) dominates the interpolation and approaches the theoretical formula at low Fourier numbers, whereas Equation (11) dominates the interpolation and approaches the theoretical formula at high Fourier numbers. The empirical Equation (9) provides an accurate transition between Equations (10) and (11) as function of Biot number. Equations (5) and (7) provide definition for critical irradiance and the heat transfer coefficients. Equations (8) to (13) have no heat flux ratios or Fourier number limitations, which is one advantage over Janssens's equation (2) (and also over that of Wesson and others (1971)). Indeed, the results of correlating time to ignition with material density at heat fluxes of 30 and 25 kW/m² can now be explained for Figures 30 and 31. That is, if the irradiance is held constant (thus also making convective heat transfer coefficient a constant), Equation (11) indicates that the product of Biot and Fourier numbers is held constant for thermally thin materials. Upon examining Equations (12) and (13), we find that the time to ignition is proportional to density, heat capacity, and material thickness, just as we deduced for results in Figure 31. In the case of thermally thick materials, Equation (10) indicates the product of Biot number squared and the Fourier number is held constant when all other parameters are held constant. If we again examine Equations (12) and (13), we find that time to ignition is then just proportional to thermal inertia. This explains why the results in Figure 31 appear differently than in Figure 30, even though irradiances decreased only from 30 to 25 kW/m².

Dietenberger (1996) suggests that the volumetric heat capacity, ρc, is known for most materials, and especially in the case of solid woods it is well characterized as functions of moisture content and temperature (TenWolde and others 1988, Janssens 1991, Parker 1988):

$$k_w = \left[(0.1941 + 0.004064 M)(\rho_{od} \times 10^{-3}) + 0.01864 \right] \times \left(T \times 10^{-3} / 297 \right) \quad \mathrm{kW\,m^{-1}\,K^{-1}} \quad (14)$$

$$c_w = 1.25(1 + 0.025M)(T/297) \quad \mathrm{kJ\,kg^{-1}\,K^{-1}} \quad (15)$$

$$\rho_w = \rho_{od}(1 + 0.01\mathrm{M}) \quad \mathrm{kg\,m^{-3}} \quad (16)$$

Table 6—Thermal input parameters to Quintiere's model

Material	Test no.	$k\rho c$ (MJ) (kJ^2/m^4K^2s)	T_{ig} (MJ) (°C)	K_{rc} (MD)[a] (kJ^2/m^4K^2s)	T_{ig} (MD)[b] (°C)
Type X gypsum board	1	0.519	330	0.494	325.645
FRT Douglas Fir plywood	2	0.515	350	0.308	386.81
Oak veneer plywood	3	1.103	204	0.381	295.11
FRT plywood (Forintek)	4	0.412	376	0.373	372.62
Douglas Fir plywood (ASTM)	5	0.282	335	0.242	340
FRT polyurethane foam	6	0.033	272	0.0017	394
Type X gypsum board	7	0.519	330	0.494	325.645
FRT Southern Pine plywood	8	1.209	342	0.408	418.21
Douglas Fir plywood (MB)	9	0.231	361	0.239	347.76
Southern Pine plywood	10	0.256	367	0.335	322.42
Particleboard	11	1.195	251	0.388	324.6
Oriented strandboard	12	0.244	348	0.262	328.42
Hardboard	13	0.4	351	0.545	321.72
Redwood lumber	14	0.165	380	0.129	364.48
Type X gypsum board	15	0.519	330	0.494	325.645
White spruce lumber	16	0.286	342	0.214	357.59
Southern Pine boards	17	0.328	354	0.27	367
Waferboard	18	0.793	236	0.257	338.13

[a]MJ, T_{ig}, and $k\rho c$ derived by Janssens's procedure.
[b]MD, T_{ig}, and $k\rho c$ derived by initial Dietenberger's procedure.

We note Equation (14) for thermal conductivity is correlated for solid wood in the direction perpendicular to the grain. It will also vary with wood grain orientation or if the wood is modified, as it is for composites, but its variation with density, moisture content, and temperature should remain intact. On the other hand, the heat capacity of wood is not dependent on grain orientation or on the reconstitution of the wood into composites and is conveniently measured in a testing apparatus. Equations (14) to (16) can be used to evaluate ignitibility for the solid wood used in the room tests provided the moisture content is evaluated at its initial value and the temperature is evaluated at an average temperature between the room temperature and the ignition temperature.

In justification of this procedure, Janssens (1991) used a finite difference method (FDM) to examine this effect of temperature dependency on the surface temperature prediction using different kinds of boundary conditions. He then showed that when using constant thermo-physical parameters as evaluated at an average temperature between the initial and final values, there was little loss in accuracy in predicting surface temperature. Dietenberger (1995) found that initial moisture content is the best value to use in Equations (14) to (16) and that errors would be small if equilibrium moisture content is used. Because the material thickness, density, moisture content, and surface emissivity are measured independently (see Tables 1, 6 and 7), we are left with the ignition temperature as the sole fitting parameter in the least squares curve-fitting program for solid wood.

For other wood products, the "corrected" thermal conductivity and ignition temperature are the ignitability parameters derived from least squares curve fitting of Equation (8) to the data of irradiance versus time to ignition. For certain composites, however, knowing the volumetric heat capacity in advance may be difficult, or they may have properties that change with increasing levels of irradiance exposure. The ignitability analysis done separately on fire growth modeling via Quintiere's model versus Dietenberger's model may result in somewhat different thermophysical properties because of differing criteria of fitting time to ignition data. The derived values of ignition temperature, thermal inertia, and thermal diffusivity will therefore be listed in two separate tables for the two different models. Our results of ignitibility analysis indicate four major groups of materials. The first group is solid woods and OSB (Figs. 32 to 35), for which Equations (14) to (16) can be directly used in Dietenberger's (and Janssens's) correlation to derive only the ignition temperature. The second group is untreated plywood and waferboard (Figs. 36 to 39), which require thermal conductivity to be derived in addition to the ignition temperature and for which thermal inertia is the main factor determining time to ignition. The third group of materials is the low combustible materials such as Type X gypsum board and FRT plywood (Figs. 40 to 43), which tend to have high values of time to ignition compared to other materials. Finally, the fourth group is materials (Figs. 44 to 47) that show effects of material thickness on derivation of thermophysical properties.

Solid Wood and OSB

The correlation of time to ignition versus irradiance is illustrated in Figures 32 to 35. In the figures, the correlations based on Janssens's method and Dietenberger's method are shown. Of the solid woods, redwood was the first to be evaluated because of the availability of measured surface

Table 7—Thermal input parameters to the Dietenberger's model

Material	Test no.	Material emissivity	k / k_w	T_{ig} (K)	$k/\rho c$ (m^2/s) $\times 10^7$	$k\rho c$ (kJ^2/m^4K^2s)
Type X gypsum board	1,7,15	0.9	NA	608.5	3.74	0.451
FRT Douglas Fir plywood	2	0.9	0.86	646.8	1.37	0.261
Oak veneer plywood	3	0.9	1.11	563	1.77	0.413
FRT plywood (Forintek)	4	0.9	0.86	650	1.31	0.346
Douglas Fir plywood (ASTM)	5	0.85	0.863	604.6	1.37	0.221
FRT polyurethane foam[a]	6	0.68	NA	689	4.91	0.0284
FRT Southern Pine plywood	8	0.9	1.43	672	2.26	0.547
Douglas Fir plywood (MB)	9	0.89	0.86	619	1.38	0.233
Southern Pine plywood	10	0.88	0.86	620	1.38	0.29
Particleboard	11	0.88	1.72	563	2.72	0.763
Oriented strandboard	12	0.88	0.985	599	1.54	0.342
Hardboard	13	0.88	0.604	593	0.904	0.504
Redwood lumber	14	0.86	1.0	638	1.67	0.173
White spruce lumber	16	0.82	1.0	621	1.67	0.201
Southern Pine boards	17	0.88	1.0	644	1.63	0.26
Waferboard	18	0.88	1.62	563	2.69	0.442

[a]Thickness prior to ignition is the melted/shrink thickness.

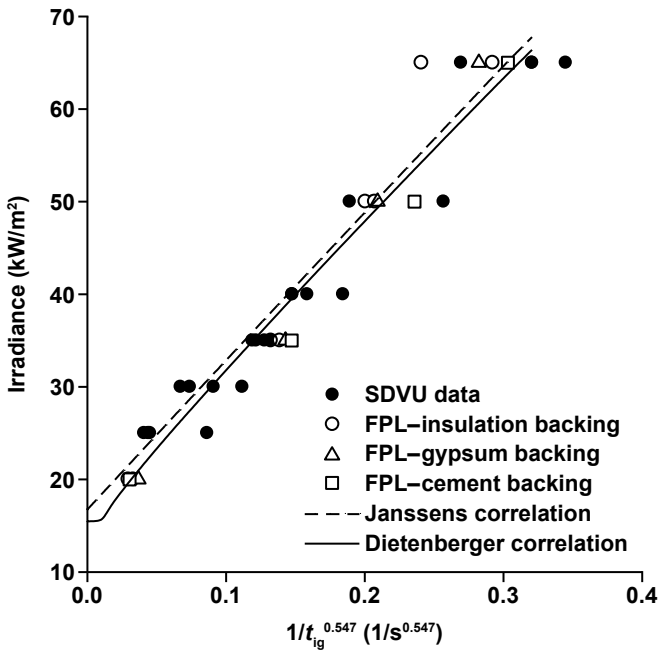

Figure 32. Correlation to piloted ignition data of redwood (test no. 14).

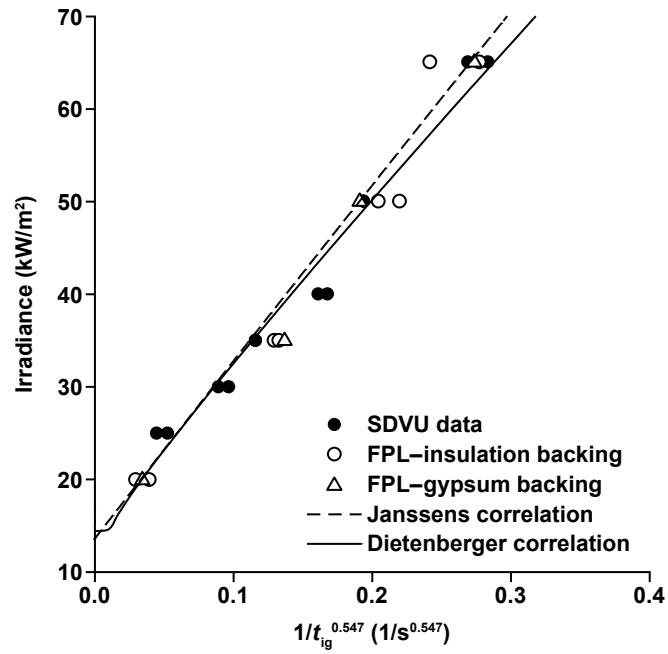

Figure 33. Correlation to piloted ignition data of white spruce lumber (test no. 16).

temperature at ignition (thin thermocouple pressed into wood surface crevice created by a razor blade). Janssens (1991) reported ignition temperatures of 358, 369, and 394 °C for thick redwood at various irradiances. In tests at FPL, the averaged ignition temperatures of 353, 364, and 367 °C for material thickness of 19, 1.8, and 0.9 mm, respectively, were measured. From Janssens's correlation for time to ignition, we derived an ignition temperature of 380 °C; from Dietenberger's correlation (and making use of Eqs. (14) to (16)) we derived 365 °C for ignition temperature. The results are shown in Figure 32, which also shows data on an individual test basis from both SDVU and FPL cone calorimeters. Taking into account the noise level, the two cone calorimeters are essentially in agreement on their measurement of time to ignition. The combined data sets are complementary in the sense that there are more tests overall with the SDVU cone calorimeter, whereas more test data at extreme fluxes of 20 and 65 kWm^2 were obtained with the FPL cone calorimeter (as is also true for the other specimens). If we had used Equations (14) to (16) in Janssens's correlation, an ignition temperature agreeing with Dietenberger's correlation would be obtained. Work is underway

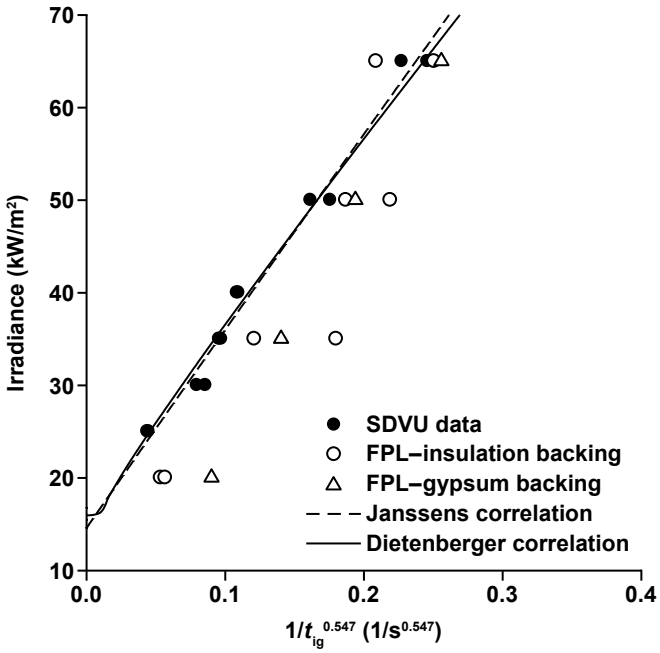

Figure 34. Correlation to piloted ignition data of Southern Pine board (test no. 17).

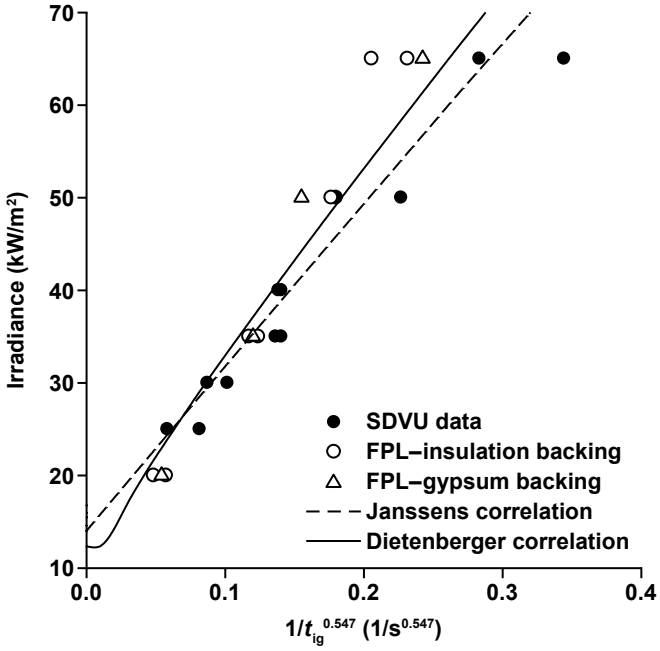

Figure 35. Correlation to piloted ignition data of oriented strandboard (OSB) (test no. 12).

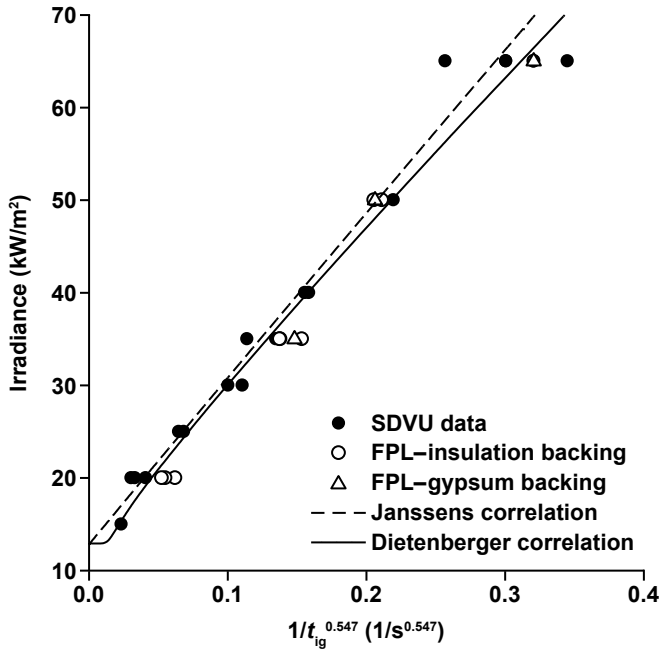

Figure 36. Correlation to piloted ignition data of Douglas Fir plywood (ASTM) (test no. 5).

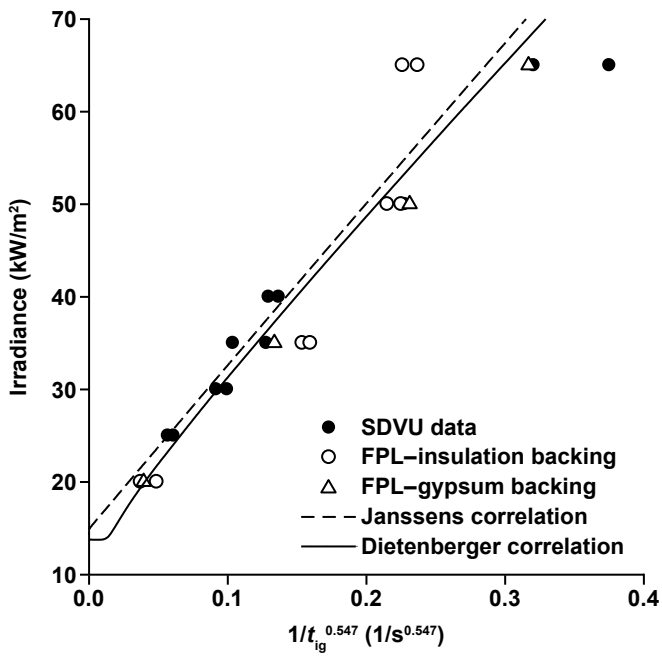

Figure 37. Correlation to piloted ignition data of Douglas Fir plywood (MB) (test no. 9).

to independently measure the thermal conductivity of the redwood sample (and of other specimens) as a check on Equation (14).

Similar correlation was found for white spruce lumber (Fig. 33) and Southern Pine board (Fig. 34). However, we see in Figure 34 that some FPL data are apparently in error. Work is underway to obtain additional Southern Pine board data. The OSB was included in this series of materials because it too was found consistent with the use of Equations (14) to (16). The derived thermophysical constants are shown in Tables 6 and 7. The significance of these parameters for input to computer fire modeling is the flexibility of application to complexity in a thermal conduction model.

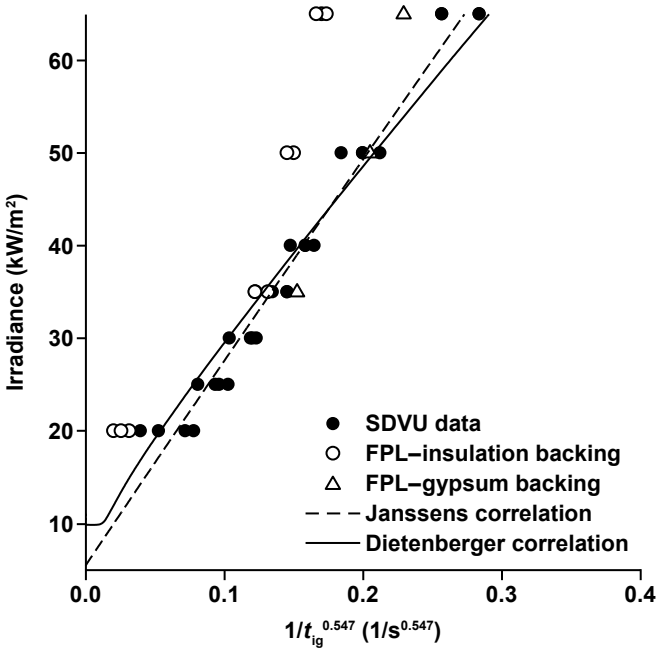

Figure 38. Correlation to piloted ignition data of oak veneer plywood (test no. 3).

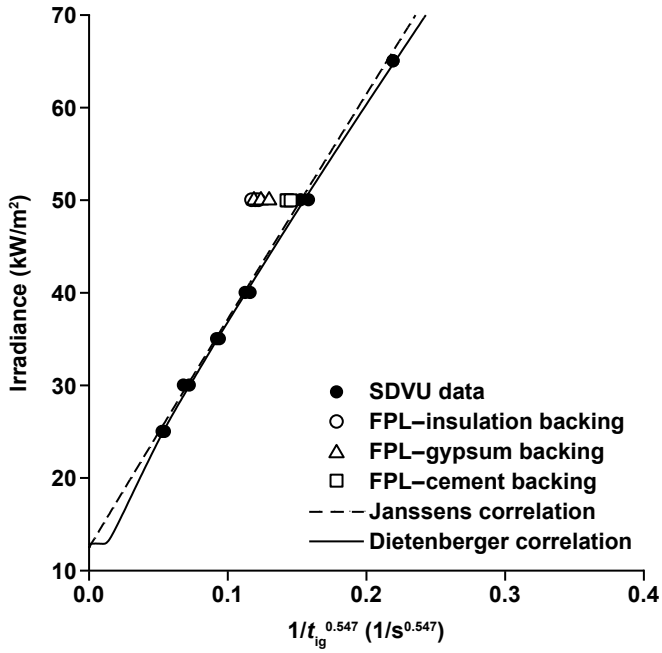

Figure 40. Correlation to piloted ignition data of gypsum X board (test no. 1).

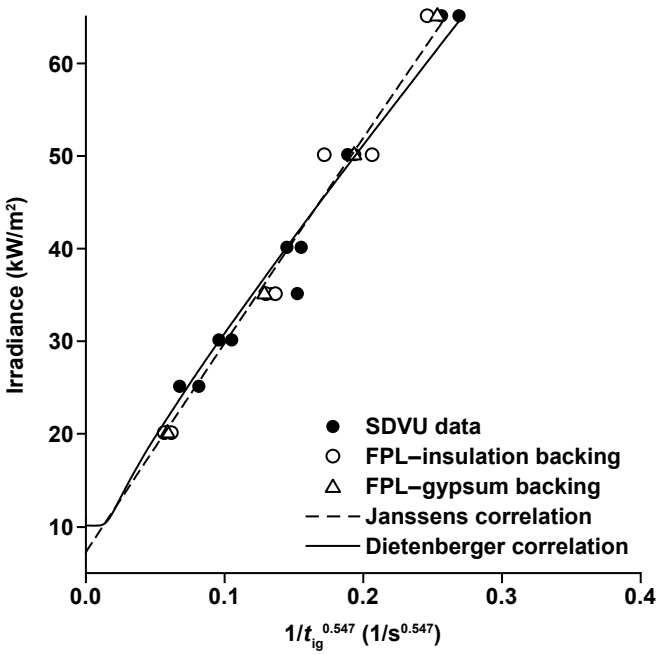

Figure 39. Correlation to piloted ignition data of waferboard (test no. 18).

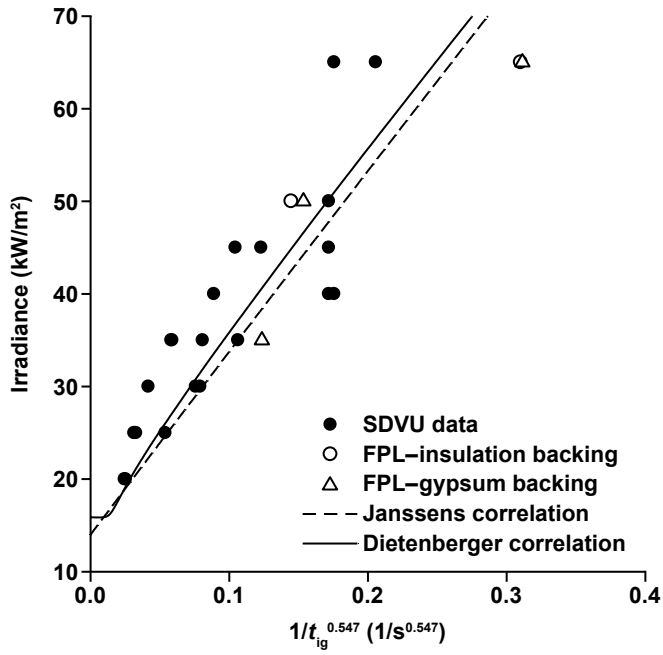

Figure 41. Correlation to piloted ignition data of FRT Douglas Fir plywood (test no. 2).

That is, on the simplest level, a thermal wave solution can be used on a thermally thick material using the thermal inertia and ignition temperature (as well as the other measured properties in other tables) from Table 7. At the next level of complexity, the thermal properties of "averaged" thermal diffusivity, thermal conductivity (derivable using the thermal inertia and thermal diffusivity), and ignition temperature from Table 7 can be used in an efficient finite difference model (FDM) of thermal conduction. At the highest level of complexity, Equations (14) to (16) can be used directly in a mechanistic pyrolysis model in which kinetics of wood pyrolysis is calibrated to obtain ignition temperatures listed in Table 7.

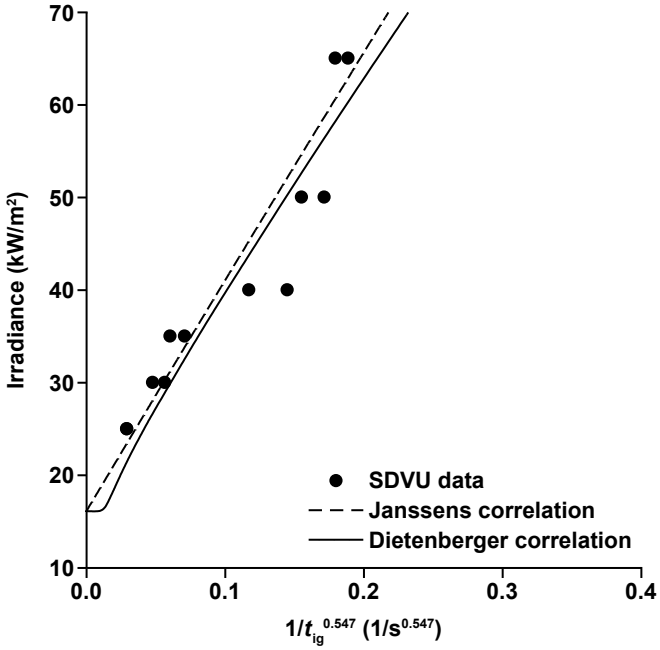

Figure 42. Correlation to piloted ignition data of FRT plywood (Forintek) (test no. 4).

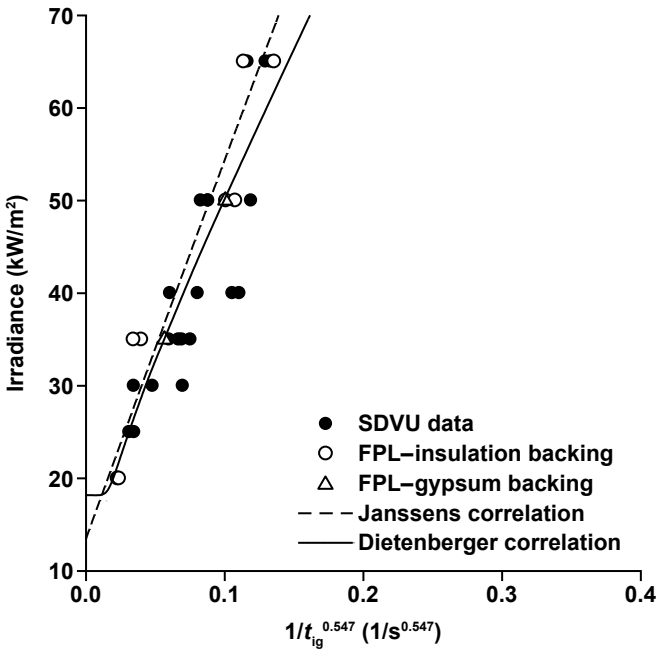

Figure 43. Correlation to piloted ignition data of FRT Southern Pine plywood (test no. 8).

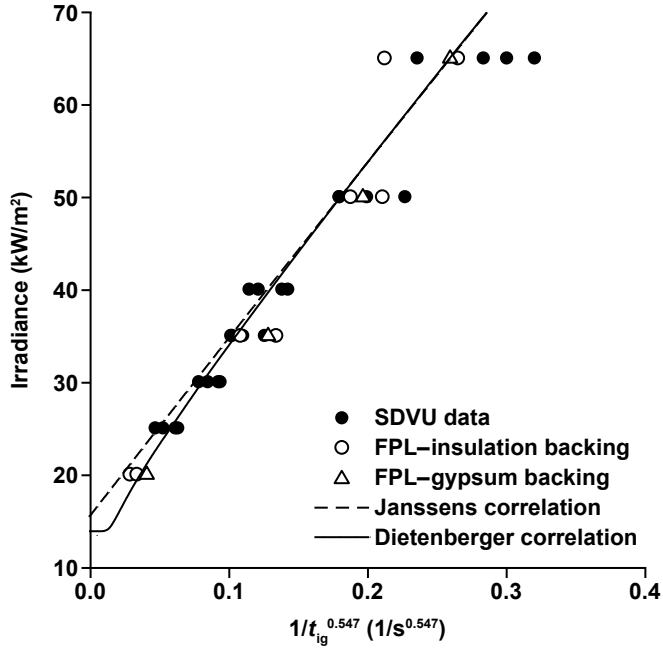

Figure 44. Correlation to piloted ignition data of Southern Pine plywood (test no. 10).

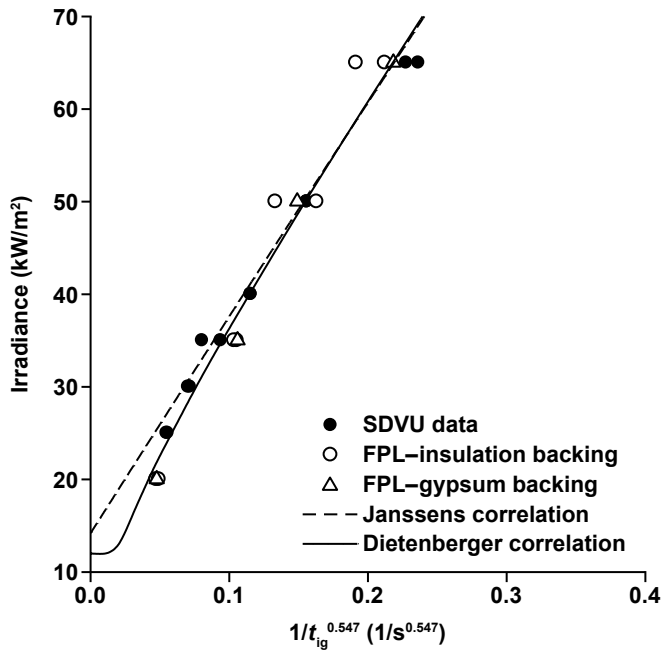

Figure 45. Correlation to piloted ignition data of hardboard (test no. 13).

Untreated Plywood and Waferboard

The next group of materials includes the most easily ignitable wood products because of their low ignition temperatures or low thermal inertia. The most thoroughly tested plywood is Douglas Fir plywood used in the ASTM round robin and corresponding to our room test ISO no. 5.

Figure 36 shows a high correlation coefficient for both the Janssens and Dietenberger correlations ($r^2 > 0.97$). It is noted that at the irradiance of 15 kW/m^2, the Dietenberger correlation captures the long ignition time of around 1,000 s, corresponding to the Fourier number of unity, which is clearly a thermally thin behavior. Even at

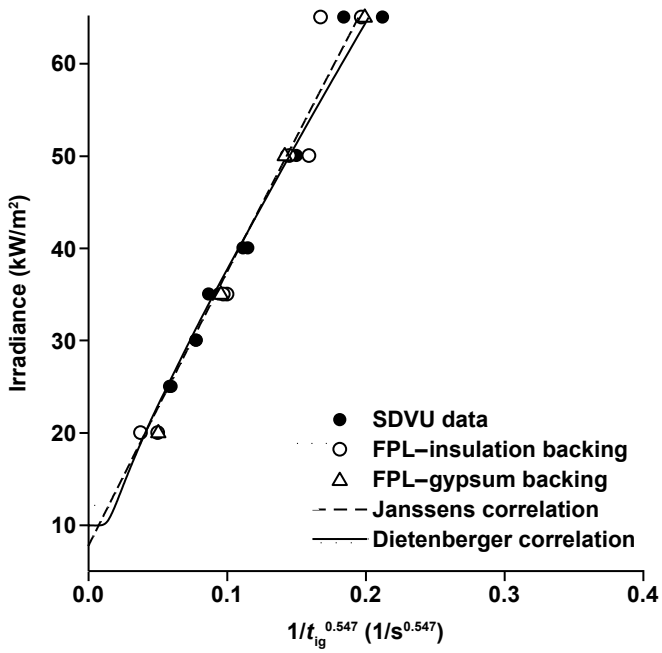

Figure 46. Correlation to piloted ignition data of particleboard (test no. 11).

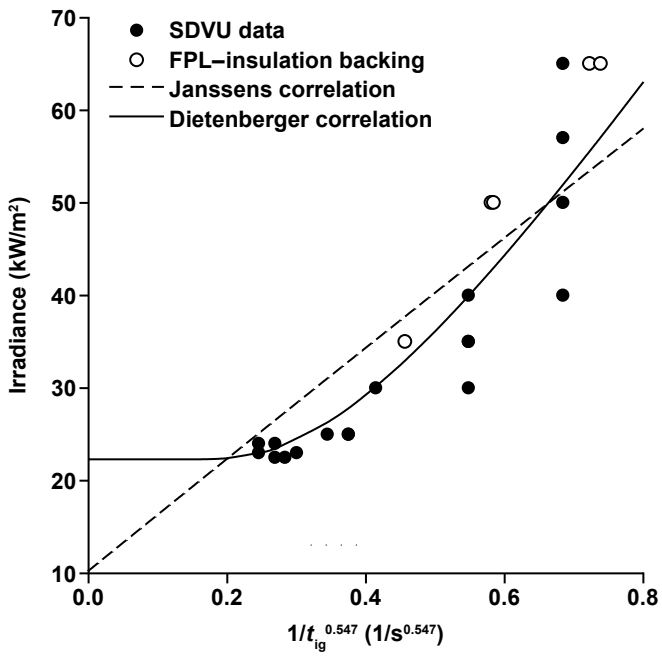

Figure 47. Correlation to piloted ignition data of FRT polyurethane foam (test no. 6).

irradiance of 25 kW/m^2, the corresponding ignition time and its Fourier number are 135 s and 0.13, respectively, indicating that the transition to thermally thin behavior is underway. The derived thermal conductivity was found to be 86.3% of that of the solid wood, in agreement with Ten-Wolde and others (1988) for plywood. The corresponding ignition temperature was a reasonable value of 332 °C. The next material evaluated is another untreated Douglas Fir plywood (Fig. 37), but which has a higher noise level than that in the previous figure. Indeed it is a noise levels that give rise to high tradeoffs between thermal conductivity and ignition temperature in optimally fitting the data. By restricting the thermal conductivity to being 86% that of solid wood, the ignition temperature is a reasonable 346 °C. The unusual features of the next two materials, oak veneer plywood and waferboard (Figs. 38 and 39) result in derived ignition temperatures of 204 and 236 °C using the Janssens correlation. These unreasonably low values of ignition temperature are unavoidable with the Janssens correlation, particularly when one observes the good linearity of the SDVU cone calorimeter data in Figures 38 and 39. Their corresponding derived values of thermal inertias (Table 6) also seemed unreasonably high. If we were to restrict the ignition temperatures to a reasonable lower limiting value of 290 °C, then the Dietenberger correlation results in reasonable derived values of thermal inertia and thermal diffusivity, as given in Table 7 for these materials. The resulting Dietenberger correlation appears to fit the data about as well as the Janssens correlation in Figures 38 and 39 and yet provides a more reasonable critical irradiance of 10 kW/m^2.

Type X Gypsum Board and FRT Plywood

One of the presuppositions in both procedures is that the materials are inert prior to ignition. This means that chemical degradation or dehydration of material is considered negligible prior to ignition. This is a reasonable assumption for untreated wood products. However, chemically treated wood products or Type X gypsum board behave in a significantly different way.

The correlation of ignition time versus irradiance for gypsum board is shown in Figure 40. For gypsum board, the experimentally observed minimum irradiance level, below which no sustained burning occurred, was approximately 20 kW/m^2. The critical irradiance levels derived were 12.5 and 12.9 kW/m^2, respectively, for the Janssens and Dietenberger correlations. Janssens (1993) and Dietenberger (1996) explained the difference between the minimum and critical irradiance for this type of material. At low irradiance levels, fuel volatiles are exhausted or quite diluted with water vapor from dehydration, which keeps the fuel mixture outside the flammability region in the gas phase, even at high temperatures adjacent to the spark plug. At higher irradiance levels, the minimum mass flux of volatiles to create flammable mixture is generated before fuel exhaustion or extreme inert dilution. However, there were no problems in determining the ignition times at irradiances above 20 kW/m^2, and the data showed good linearity in Figure 40. Although ignition temperatures of 330 and 335.5 °C, respectively, for the Janssens and Dietenberger correlations are reasonable, obtaining independent measurements for thermal diffusivity, thermal inertia, or even

ignition temperature will be useful, given the high amount of dehydration occurring in the gypsum substance.

Three FRT wood-based materials were tested in both the cone calorimeter and room/corner test: FRT Douglas Fir plywood (ISO 2), FRT plywood from Forintek (ISO 4), and FRT Southern Pine plywood (ISO 8). The processes occurring in FRT wood depend on the type of fire retardant used, the method of treatment, and the uptake by the material. If an efficient flame retardant is used and the uptake is high, sustained ignition may not occur under realistic exposure levels, despite high mass loss. The change of behavior of chemically treated wood in comparison to untreated wood is greatest at the low irradiance levels.

The Douglas Fir belongs to the class of "hard impregnable" wood. The distribution of impregnating agent is not homogenous in the whole volume, which is caused by its anatomic structure. The non-homogeneity of distribution of impregnating agent in the material can be expected also because the plywood consists of thin veneers connected by water-resistant glue. Furthermore, many fire retardants increase wood hygroscopicity, resulting in higher water content than that of untreated material conditioned in the same atmosphere.

Due to the non-uniformity of the treatment and variance in the uptake, different kinds of burning behavior were observed. In some cases, the specimen was ignited but the flame extinguished shortly after the spark igniter was removed. The flame did not always cover the whole surface of the specimen, mainly under lower irradiance levels. In some cases, the HRR had similar shape as that for untreated wooden materials. In other cases, only a single peak was observed. The variance of the specimen mass of the impregnated plywood materials was much higher than that for the untreated plywood materials. This also suggests that the tested FRT materials were less homogenous than the untreated wood materials.

In spite of these problems, efforts were made to obtain representative ignition parameters from the cone calorimeter measurements. A major problem with evaluation of experimental ignition data for treated wood products was the uncertainty of time to sustained ignition. Visually determined ignition times showed significant scatter. The largest problems of this kind were observed with the FRT Douglas Fir plywood. To overcome the visually observed errors of ignition, the criterion of HRR was chosen for this material and the FRT plywood from Forintek. After some trial and error, HRR = 30 kW/m^2 was chosen as a suitable limit. With a lower value, the flame of some specimens was extinguished shortly after HRR had reached the threshold. It is suspected that pre-flame glowing or smoldering is responsible for HRR < 30 kW/m^2 and provides a heat source added to irradiance to achieve temperatures within the wood for creating volatiles sufficient for flaming ignition. For the FRT Southern Pine plywood, the ignition times were possible to observe visually.

The results for correlating time to ignition for these three FRT wood products are shown in Figures 41 to 43. In examining the derived properties in Table 7, the higher values for time to ignition of FRT Douglas Fir plywood are primarily due to the higher ignition temperatures compared to the untreated Douglas Fir plywood. However, the FRT Southern Pine plywood has the highest values for time to ignition of all the materials due to its high values of both thermal inertia and ignition temperature. Results of Janssens correlations for these materials instead offer primarily derived thermal inertias much higher than that of untreated plywood (Table 6). Because one of the main processes of fire-retardant treatments is to decrease tar production and increase dehydration of the wood substance, the heat of combustion of wood volatiles is significantly reduced for treated wood products. Therefore, to achieve the sufficient ignition criteria of HRR = 30 kW/m^2 will require a corresponding increase in critical volatile mass flow rate only achievable with a higher "true" surface temperature at ignition for treated materials. Effect of smoldering gives an apparent ignition temperature less than this true ignition temperature, but it is often still greater than that of untreated materials, as Table 7 and Figure 30 imply.

Thickness Effects on Wood Composites and FRT Polyurethane Foam

In this section we highlight the effects of material thickness on the derivation of ignition properties. The two thinnest materials, Southern Pine plywood at 11 mm and hardboard at 7 mm, have considerable range of irradiances that should not be considered thermally thick. In the case of Southern Pine plywood (Fig. 44), the irradiances of 30 and 20 kW/m^2 have derived Fourier numbers of about 0.1 and 0.6, respectively, at their times of ignition, whereas for the hardboard (Fig. 45), the irradiances of 40 and 20 kW/m^2 have derived Fourier numbers of about 0.1 and 0.65, respectively, at their times of ignition. We recall that the Janssens correlation is technically limited to Fourier numbers less than 0.1, but it begins to show large errors at Fo > 1/3. We note that the thermal diffusivity is a required parameter of Fourier number (see Eq. (13)), which was used to indicate values of time to ignition for valid use with thermally thick heat conduction solutions. Mere examination of the data presented in Figures 44 and 45 show the linear trend through the noisy data, giving one a false notion that all the data fit within the realm of thermally thick behavior. We note also that the Fourier numbers in the transitional regime between 0.1 and 1.0 would not allow the use of the thermally thin heat conduction solution to correlate time to ignition. This essentially leaves us with the Dietenberger correlation valid with any Fourier or Biot numbers, which is plotted for Figures 44 and 45. It is seen from Tables 6 and 7 that reasonable ignition properties are derived for these wood composites.

Certain materials that are quite thick (FRT polyurethane foam) or have high thermal inertia (particleboard) have

ignition behaviors that are best fitted with a full regime correlation. The particleboard data (Fig. 46) have a highly linear trend so that the Janssens correlation fits the data extremely well ($r^2 = 0.97$). However, the ignition temperature is 251 °C (Table 6), which seems unreasonably low. The use of Dietenberger's correlation provides an equally good fit to the same data, but with a more reasonable ignition temperature of 290 °C and a more reasonable lower value for the thermal inertia (Table 7). The two plywoods, oak veneer plywood and waferboard, discussed in the second group of materials are described similarly. Because of the high tradeoff possible between ignition temperature and thermal properties with either correlation, and because of unexpected problems with the Janssens correlation, it would be useful to obtain independent measurements of thermal conductivity and heat capacity for particleboard, particularly in that the ignition temperature can be better estimated.

The ignition times for the polyurethane foam were very short (between 2 and 12 s) and were subject to significant error (Fig. 47). The experimentally observed minimum irradiance level, below which no burning occurred, was approximately 22 kW/m^2. The thermal properties of polyurethane plastic material available are $\rho = 1201.5$ kg/m^3, $1.68 < c_p < 1.86$ kJ/kg K, $k = 0.0013$ kW/m K, and $T_{ig} = 689$ K (416 °C) (Johnson 1995). We note that this ignition temperature gives a critical flux (see Eq. (5)) of 22.3 kW/m^2, which is comparable to the minimum irradiance for our data. At room temperature, a polyurethane foam of a density $\rho_{foam} = 29$ kg/m^3 has a thermal conductivity approximately $k_{foam} = 0.0239$ W/mK (ASHRAE 2001). Plastics usually melt before igniting and cause an almost instant collapse of the foam to a pure plastic form. In the case of FRT polyurethane foam lying horizontally in a test, its thickness can shrink from 23 mm to a mere 0.56 mm. During this shrinkage, the thermal diffusivity increases only slightly, from 0.49 mm^2/s in the virgin state to 0.64 mm^2/s in the completely shrunk state. This also would make the thermal conductivity approximately proportional to the foam density. The important point is that the Fourier number of completely shrunk foam at the time of ignition is greater than unity for all data shown in Figure 47. At this completely shrunk state, the foam behaves essentially as a thermally thin material. To properly apply a theory of thermal conduction to predict surface temperature leading to ignition, one will need to use "effective shrinkage properties." In the case of FRT polyurethane foam, we found that effective shrunk density three times that of original foam density, effective foam thickness of 0.56 mm, and all other parameters unchanged as used in the Dietenberger correlation fit the data reasonably well. The Janssens correlation, shown as the poorly correlated dashed lines in Figure 47, evidently derives an unreasonably low ignition temperature of 272 °C (or 545 K), which also give a critical irradiance of 10 kW/m^2. The Dietenberger correlation, on the other hand, retains ignition temperature of 689 K (416 °C), with its critical irradiance of 22.3 kW/m^2. The example of the FRT polyurethane foam shows not only the necessity of using a full regime correlation but also that one can also reasonably analyze a seemingly impossible physical phenomena, such as shrinkage of a generic plastic foam.

Fire-Retardant-Treated Beech Wood

The usual way of lowering the flammability of wood is by chemical treatment with flame retardants. Flame retardants are applied as the coatings on the surface of wood or by impregnation into the mass of wood. Composite materials can be also modified by incorporation of flame retardant into the glue system. The use of flame retardant on the surface is usually cheaper, and in most cases it is easy to provide and it can be done after the wood material is installed in its place of use. The disadvantage of surface treatment is that the finishing coating can be damaged and it needs to be renewed after some time. The impregnation of wood by flame-retardant agent protects the whole volume of material, but the cost for the treatment is usually higher. On the other hand, the effect of flame retardant can be very high. Wood is a heterogeneous material and the distribution of impregnating agent after treatment in the mass of wood is not homogeneous. However, for "well treatable" wood species, this heterogeneity of the flame-retardant distribution is lower than that for "hard impregnable" species. Therefore, beech wood (*Fagus silvatica*) was chosen for this study because it is a "well treatable" material. Beech wood was also chosen because it belongs to the industrially used materials.

Monoammonium phosphate (MAP) was chosen as the flame retardant. Ammonium phosphates are well known as effective flame retardants and have been used for the flame retardation of wood for a long time. From the thermoanalytical studies it is known that $(NH_4)H_2PO_4$ decomposes at temperatures of 145 to 165 °C to phosphoric acid and NH_3 (Browne and Tang 1962, Košík and others 1977). At higher temperature, around 216 °C, the phosphoric acid further decomposes. The final products of decomposition are P_2O_5 and H_2O. Ward (1974) found out that the $(NH_4)H_2PO_4$ reacts with cellulose at higher temperatures and an ester is formed that has resistivity to the effects of flame. The phosphates promote the dehydration reactions of wood, with the H_2O as primary volatile product, and increase the char residue (Drews and Barker 1974, Browne and Tang 1962, Shafizadeh 1968). Indeed, by mass spectrometric thermal analysis, Browne and Tang (1962) found that dehydration of pure cellulose is first observed around 220 °C and that depolymerization beginning around 280 °C is from previously unreacted cellulose that volatilizes via an endothermic process competitive with the dehydration. This would make pure cellulose burn predominantly by flaming. However, when dehydration is increased by the effect of inorganic salts (most effectively with ammonium phosphates), there is more solid phase oxidation, or glowing of char, which takes place at the expense of flaming. The decomposition products of lignin are mostly solids in the combustion temperature

Table 8—Characteristics of untreated and treated beech wood

Uptake of MAP (kg/m^3)	Density (kg/m^3)	Content of MAP in wood (%)
0	773	0
5	760	0.7
10	699	1.4
20	702	2.8
40	782	5.1

range, which means it contributes little to flaming but supports the oxidation of solids by glowing (Browne and Tang 1962). The decomposition products of flame retardant itself, which are NH_3 and H_2O, also dilute the flammable pyrolysis gases and thus further lower the flammability of the volatile mixture (Košík and others 1977).

Sample Preparation and Testing

The radial samples of beech wood were prepared with dimensions 100 by 100 by 15 mm. Wood samples were treated with aqueous solutions of monoammonium phosphate (MAP). Four different concentrations of MAP in water were used. The concentrations were chosen so that the uptakes of the flame retardant to the wood samples were 5, 10, 20, and 40 kg/m^3. The impregnation process was done by vacuum–atmospheric technology (vacuum of –93 kPa for 60 min followed by atmospheric pressure for 60 min). After the impregnation, samples were dried in laboratory conditions at 20 °C until the weight reached equilibrium. Prior to testing in the cone calorimeter, the samples were conditioned at relative humidity (RH) of 55% and temperature of 23 °C for 2 weeks. The cone calorimeter tests were done according to ISO 5660 (ISO 1993b) standard. The irradiances used were 25, 30, 35, 40, 50, and 65 kW/m^2. The orientation of samples was horizontal. All other conditions were the same as for other small-scale tests in this project.

FRT Beech Wood Results and Discussion

The characteristics of untreated and treated wood samples are listed in Table 8. The loadings of 5 to 40 kg/m^3 of solution into the wood were used, which amounts to 0.6% to 5% of the flame retardant by weight in the tested beech wood. For some other materials (plastics for example), significantly higher loadings of flame retardant are usually used (40% to 60%). For wood lumber to reach a strong retarding effect, such high loadings are not needed. Indeed, it is possible to use such high loadings of flame retardants that treated wood will contribute only a negligible amount of heat when exposed to the external heat source. In this case ignition and sustained burning may not occur at all. We instead analyze treatment performance by gradually increasing FRT loadings and observe the corresponding effects on the burning characteristics. There are also practical reasons for using

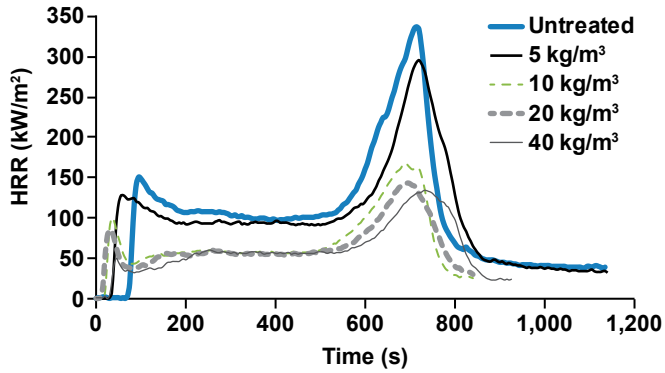

Figure 48. Heat release rate (HRR) as a function of time for untreated and impregnated beech wood at irradiance of 40 kW/m^2 (SDVU data).

this approach. In practice, the minimal required loadings are used to meet the code standards. Also, wood products users may require as little amount of chemicals in the wood as possible. Too much chemical treatment may even change some other physical and aesthetic properties of wood.

Heat Release Evaluations

The main parameter measured in the cone calorimeter is HRR. In Figure 48, time-dependent HRR curves for untreated and FRT beech wood measured with irradiance 40 kW/m^2 are presented. The first maximum in HRR curves decreases with increase in uptake of MAP. Only with the sample having an uptake of 40 kg/m^3 is the first peak almost eliminated. Also, the HRR values after the initial peak HRR are lower than values in the middle part of the HRR curve. The HRR for samples with uptake 10, 20, and 40 kg/m^3 have close values during quasi-steady-state burning (Fig. 48). The forming char layer enhanced by degradation processes of MAP caused this burning behavior. At low irradiances, the volatiles being formed are barely flammable, so transitory flaming is present on the burning surface after ignition. It is seen in the figures that differences of HRR due to various uptakes of flame retardant are less for the higher irradiance (Figs. 48 and 49). At irradiance of 30 kW/m^2, the effect of flame retardant on lowering the HRR was evident even at uptake as low as 5 kg/m^3 (Fig. 49).

The total heat release (THR) as function of irradiance for treated and untreated wood samples is presented in Figure 50. The THR for charring materials tends to have a slight linear increase with irradiance (see Table 3) except for certain FRT materials, such as the strong increases for the FRT polyurethane foam (material no. 6). In the case of MAP-treated beech wood, the highest relative change of THR was measured for the samples with uptake of 40 kg/m^3 (Fig. 50), where the THR increased from 34 MJ/m^2 at irradiance of 25 kW/m^2 to 66 MJ/m^2 at irradiance of 65 kW/m^2 (95% increase). For specimens with uptake of 20 kg/m^3, the increase was less at around 54%. For the remaining samples,

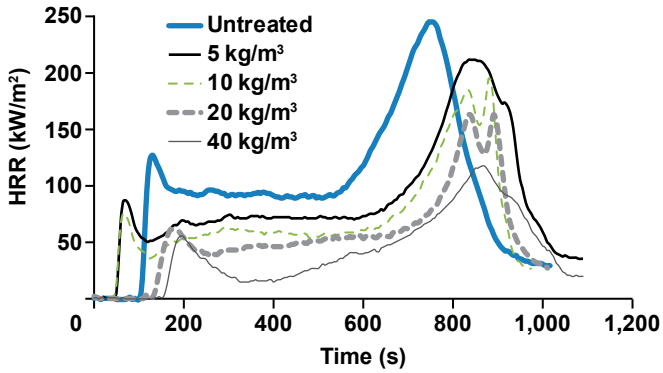

Figure 49. Heat release rate (HRR) as a function of time for untreated and impregnated beech wood at irradiance of 30 kW/m² (SDVU data).

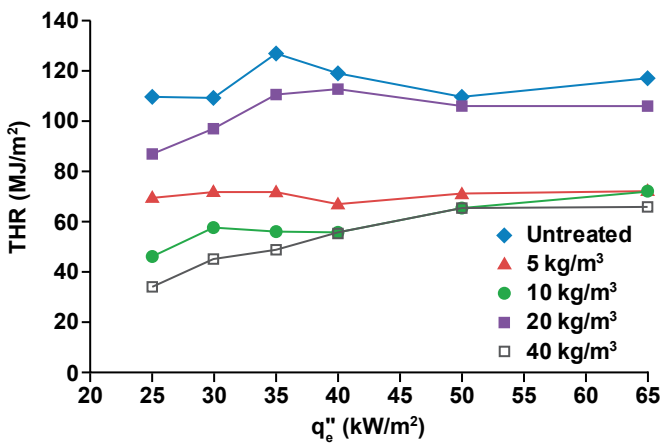

Figure 50. Total heat released as the function of irradiance for untreated and impregnated beech wood (SDVU data).

Table 9—Measured characteristics of untreated and impregnated beech wood

Uptake (kg/m^{-3})	Moisture content (%)	ΔH (MJ/kg^{-1})	Slope (ΔH /L)	THR average (MJ/m^{-2})
0	10.3	10.7	1.53	115.2
5	8.7	10.0	1.44	105.4
10	8.5	7.7	0.90	70.7
20	8.4	7.4	0.57	58.9
40	8.4	6.4	1.04	52.5

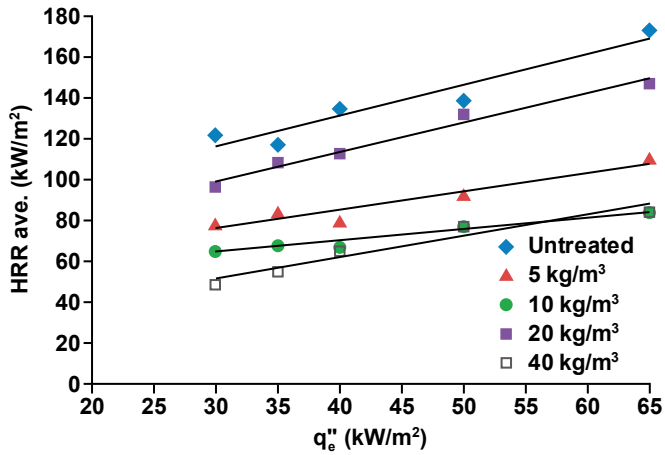

Figure 51. Averaged heat release rate (HRR) as a function of irradiance for untreated and FRT beech wood.

the change of THR with increasing irradiance was relatively small. This means that at low loadings of flame retardant (in this case 0 to 10 kg/m^3), approximately the same amount of energy is released per square meter within external heat fluxes of 25 to 65 kW/m^2. At higher loadings (in this case 20 to 40 kg/m^3), the imposed heat flux has a much stronger effect. On the other hand, the absolute decrease of total heat released in comparison to the untreated wood was growing with increasing flame-retardant loading for all cases (Table 9). For the uptake of 40 kg/m^3, the average THR was 46% of that for untreated beech wood. The measured total evolved heat is also affected by the time of test termination (due to mass loss rate falling below 150 g/sm^2), because had we allowed the afterglow to burn until the ashes remain, the THR would be the same in all cases (providing the combustion is complete (Dietenberger 2002).

The first peak value of HRR is sometimes referred as the parameter representing the HRR of the material. Indeed, Quintiere (1993) suggests using the slope of the linear function fitted to peak HRR versus irradiance for calculating effective heat of gasification (see Tables 2 and 3). However, for the tested FRT beech wood, the beginning of sustained burning did not occur immediately after the initial flashes of flaming combustion as it did for untreated beech wood. In some cases the sustained flaming was present only after the char layer was evidently formed. In the attempt to compensate for this effect, we instead used the average from whole test time to evaluate the linearity of HRR with irradiance (Fig. 51). Although the slope for linear regression of averaged HRR versus irradiance would not represent well the effective heat of gasification (due to greater significance of glowing), it reveals the dynamic aspect of the heat release under changing irradiance.

It can be seen from the Figure 51 and Table 9 that the highest slope of the linear line was found for untreated wood and there was a relatively small difference between the slopes for untreated wood and wood with uptake of 5 kg/m^3. The samples with higher loadings of flame retardant had lower values for the slope. The same order of the slope values was found also for the 1-min average HRR calculated from the time of ignition. Thus the strongest effect of heat flux imposed was observed for untreated wood, whereas at higher loadings this effect was weaker. This is in contrast to the observation for total evolved heat where the strongest effect of imposed flux was found for the highest loading of flame

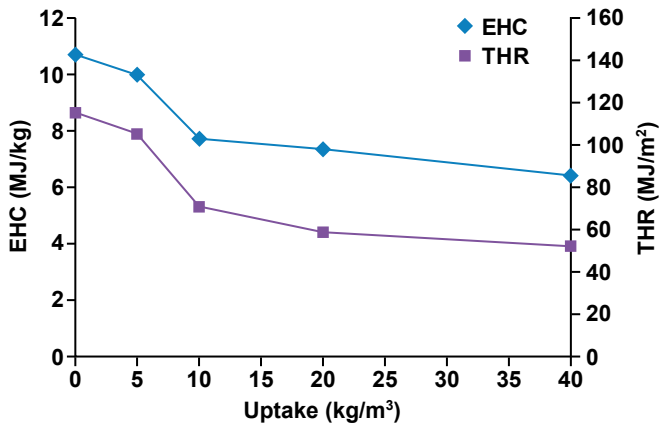

Figure 52. Average effective heat of combustion and average total heat released as the function of flame retardant uptake for beech wood (SDVU data).

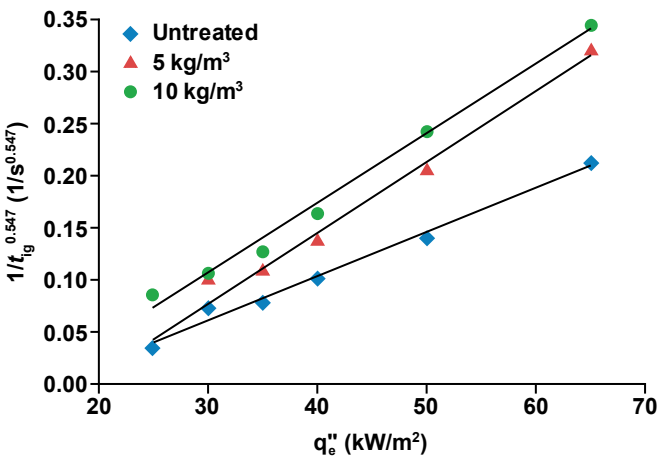

Figure 53. $1/t_{ig}^{0.547}$ as a function of irradiance for untreated and impregnated beech wood (SDVU data).

retardant. This phenomenon is explained by the thermally thin response of the material during the second peak HRR feature. That is, the overall charring rate would then be somewhat proportional to the imposed heat flux (irradiance plus flame flux, otherwise irradiance minus convective heat loss during flameout). This translates directly to overall flaming HRR that will directly increase with irradiance. Also, because of more rapid temperature response at higher irradiance, a greater fraction of wood substance will convert to volatiles, thus increasing flaming HRR. However, the glowing HRR is also becoming significant simultaneously and is not affected as much by irradiance. Thus the untreated wood has most of its total HRR by flaming and therefore is most sensitive to irradiance, whereas the treated wood has more of its total HRR attributed to glowing and is less sensitive to irradiance. Because glowing is a slow combustion process with low HRR, the length of the test time becomes influential in determining the apparent total heat release for treated beech wood.

The net heat of combustion measured in oxygen calorimetric bomb for the beech wood is 18.7 MJ/kg (Babrauskas 1992). The average effective heat of combustion measured for untreated samples in our case was 10.7 MJ/kg. This difference is due to the fact that the effective heat of combustion for wood represents mainly the heat of combustion of volatiles. The average effective heat of combustion of tested samples decreases with the increasing uptake of MAP, down to as far as 6.4 MJ/kg, and reflects the dilution of volatiles by H_2O generated by the increased dehydration of wood structure and decomposition of the MAP (Table 9). This observation is in agreement with the average values of THR for treated samples and confirms that the heat potential was decreasing with the growing loading of flame retardant (Fig. 52). Because the heat of combustion during afterglow is around 30 MJ/kg, it is apparent that glowing is a much slower process than is flaming. Shortly after flameout and when the mass loss rate falls below some detectable level, the test is stopped. In this way the THR is mostly the result of flaming and directly reflects the effective heat of combustion rather than the net heat of combustion for beech wood.

Ignitability Analysis

The MAP influenced the process of ignition of beech wood. After the samples with higher MAP uptake were exposed to irradiance, at first transitory flaming appeared on the exposed surface. The transition from transitory to sustained burning for these samples was gradual. In those cases, the time to sustained burning was determined by the HRR criterion. Time when the HRR reached 30 kW/m² was considered as the beginning of sustained burning. The inverse ignition time ($1/t_{ig}^{0.547}$) plotted as the function of irradiance level for samples with the flame-retardant uptake of 0 to 10 kg/m³ is presented in Figure 53.

The linearity of the correlation of $1/t_{ig}^{0.547}$ versus irradiance was good for the untreated samples up to loading of 10 kg/m³. At higher loadings of flame retardant (20 and 40 kg/m³), the correlation differed from linear relationships, as shown in Figure 54. At these loadings, the time to ignition was changing little at irradiances 50 to 65 kW/m², and the greatest change was observed between the irradiances of 35 to 50 kW/m². Similar effect was also observed for FRT polyurethane foam (material no. 6), although their causes are likely to be dissimilar.

The flame retardant generally shortened the ignition times of treated wood except at the highest MAP uptake or the lowest irradiance. Figure 55 shows the graph of time to ignition (normalized to that of untreated wood) versus MAP loadings for each irradiance condition. It can be seen that at irradiance of 25 kW/m², the ignition times of treated samples were higher than that of untreated wood except for the samples with uptake of 10 kg/m³. The start of the sustained burning was not clear for these samples (Fig. 56). Initially, transitory flaming occurred on the surface and extinguished

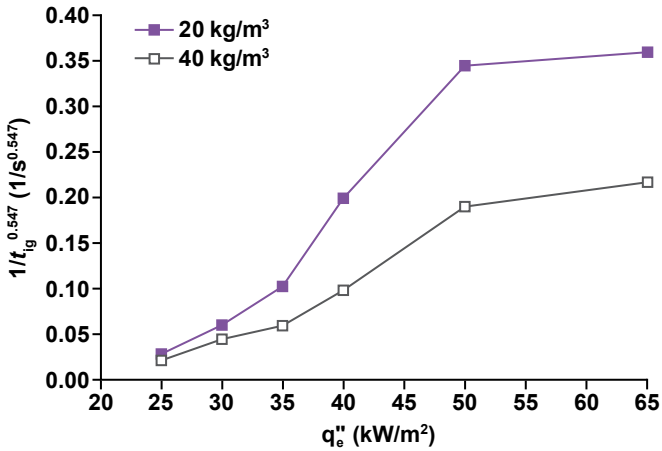

Figure 54. $1/t_{ig}^{0.547}$ as a function of irradiance for beech wood with the loading of flame retardant at 20 and 40 kg/m³ (SDVU data).

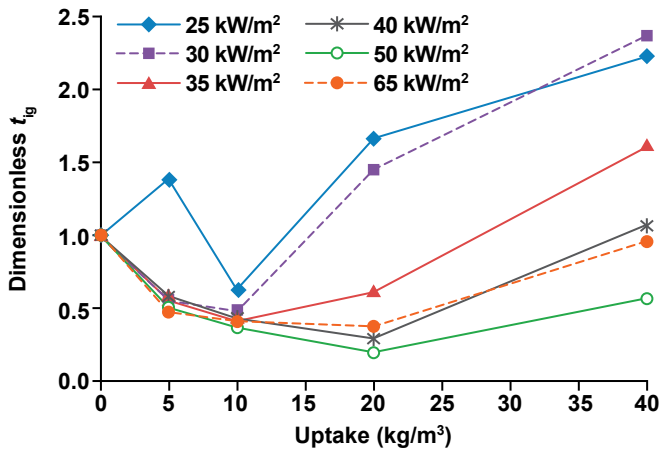

Figure 55. Dimensionless time to ignition as a function of uptake of flame retardant at various irradiances.

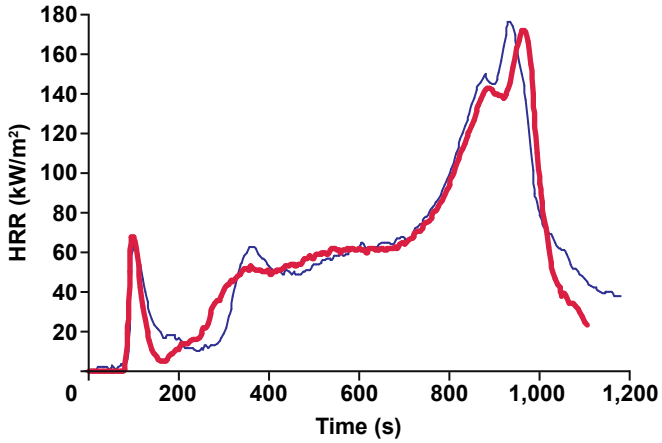

Figure 56. Heat release rate (HRR) as a function of time for wood samples with FR uptake of 10 kg/m³ at irradiance of 25 kW/m².

after a short time. After that, re-ignition was observed but again as transitory flaming, which gradually changed into sustained burning. As a result we found it difficult to assign a precise time for when sustained burning began. The value for ignition time in this case was assigned as the time when HRR of 30 kW/m² was exceeded. By increasing the irradiance to 30 kW/m², the ignition times for the wood with uptakes of 5 and 10 kg/m² became less than that of untreated wood. As irradiance continued to increase, the higher values for MAP uptake corresponded to the ignition time being less than that of untreated wood. Finally, at irradiances of 50 and 65 kW/m², ignition times for all loadings of flame retardant were at least less than that of untreated wood. These relative decreases in the ignition time seemed at first inconsistent with how the MAP reacts within the wood structure and was also contrary to the behavior of FRT plywood versus that of untreated plywood.

Further insights can be gained by examining derived fire properties of ignition. The results of straight-line regressions in Figures 53 and 54 using the Janssens correlation are listed in the second and third columns of Table 10. We note the main decomposition processes of the untreated beech wood take place in the temperature range of 250 to 350 °C (Keylwerth and Christoph 1963). It is obvious from Table 10 that the derived ignition temperatures are too high and derived thermal inertias are too low. Therefore we proceed to Dietenberger's correlation and analyze the data as in the group of solid wood for the room burn materials. This means using the thermophysical properties from Equations (14) to (16), making no adjustment to the thermal conductivity, and deriving the ignition temperature only from a non-linear regression fit. Note that we used density values from Table 8 and moisture contents from Table 9, with emissivity set at 0.88. The results are shown in Figure 57, with derived properties in Table 10. It is seen that the untreated wood is predicted quite well ($r^2 = 0.98$) with a reasonable surface temperature of 332 °C at piloted ignition.

It is known that the main course of degradation of wood treated with MAP begins at the lower temperatures (Košík and others 1977). From actual mass measurements, as shown in Figure 58, the impregnated samples started their decomposition at much lower times than that for untreated wood. At first one would think this is the reason for shorter ignition times for the treated samples. However, at treatment levels at or above 5.1% MAP impregnation, the ignition times actually become equal to or greater than that of untreated samples. Recall that the treatment generally lowers the effective heat of combustion due to dilution of volatiles by water vapor. From this factor alone, piloted ignition temperature of treated wood should be greater than that of untreated wood. Recalling Browne and Tang's (1962) data on the effects of MAP on wood combustion, the tendency to flaming is replaced by the tendency to smoldering at around the degradation temperatures associated with treatment.

Table 10—Thermal parameters of untreated and MAP-treated beech wood

Uptake (kg/m^{-3})	T_{ig} Janssens (K)	$k\rho c$ Janssens (kJ^2/m^{4}K^{2}s)	k / k_w	T_{ig} Dietenberger (K)	$k/\rho c$ (m^2/s) × 10^7	$k\rho c$ (kJ^2/m^{4}K^{2}s)
0	644	0.362	1.0	605	1.514	0.515
5	683	0.123	1.0	557	1.548	0.427
10	623	0.178	1.0	550	1.566	0.357
20	721	0.0495	1.0	534	1.568	0.345
40	711	0.157	1.0	600	1.550	0.494

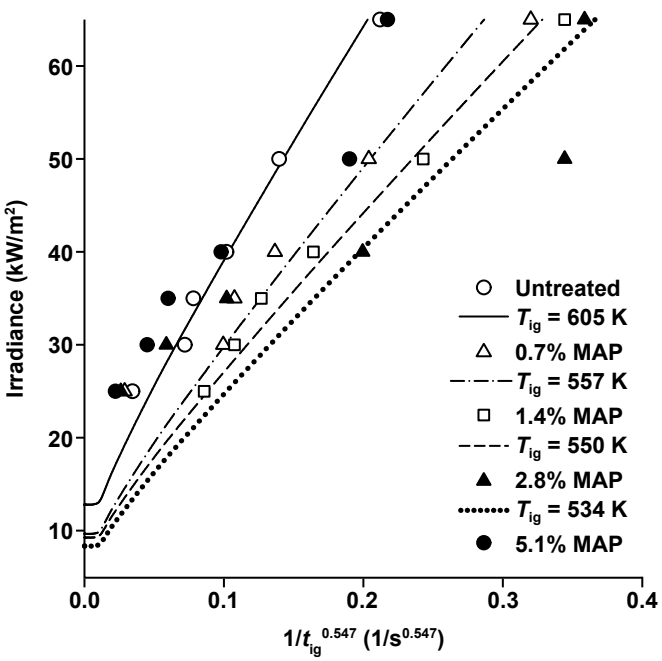

Figure 57. Fire-retardant MAP effects on beech wood piloted ignition.

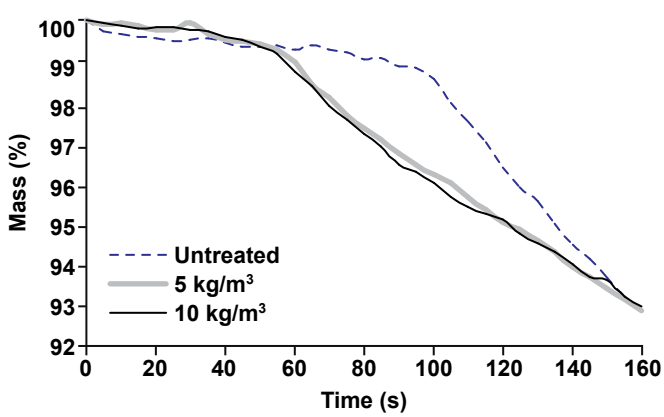

Figure 58. Percentage mass loss as a function of time for impregnated and untreated beech wood at irradiance of 30 kW/m^2.

Smoldering would then provide a localized heat source to further increase material temperatures to the point where the volatile mixture is flammable. The ensuing sustained flame would then suffocate the surface smoldering and cause a dramatic drop in the "white" smoke. To account for the smoldering ignition phenomena in a thermal conduction theory, we postulate an "apparent" ignition temperature that is always less than the "true" ignition temperature. An alternative approach would be to derive an "apparent" heat source that would allow deriving a "true" ignition temperature. However, this alternative approach would add an unnecessary, perhaps confusing, variable. Because of the competition for smoldering versus water vapor dilution of volatiles, the apparent ignition temperature of treated wood can be either less than or greater than the ignition temperature of untreated wood. The success of this approach can be seen in Figure 57, with derived properties listed in Table 10.

Combustion Products Evaluation

The peak specific extinction area of smoke (SEA) for untreated and impregnated samples is shown in Figure 59. Graphs show the peak values of SEA increasing with the increasing irradiance level and decreasing with the uptake of MAP in wood. If one can assume the soot mass fraction and the heat of combustion do not vary with irradiance, then the increase of HRR (and MLR) with irradiance would be directly reflected in the corresponding increase of SEA (Grexa 1999; also see Part I of this series of publications (Grexa and others 2012)). The decreasing SEA with the growing loading of the flame retardant is explained with a known process that water vapor is released into the volatiles at the expense of tars, thereby removing the "airborne" carbon source needed for soot production (Dietenberger and Grexa 2000). This change in volatile mixture also significantly decreases the heat of combustion and is the main cause of the lowering of HRR for impregnating samples.

The MAP promoted the formation of CO (Fig. 60) at the expense of CO_2, which is another factor in the lowering of HRR for impregnating samples. The strongest change of average production rate of CO with the growing flame-retardant loading was observed at low irradiances. The growing irradiance weakened the increase of CO production rate. We theorize that the dilution of combustible volatiles

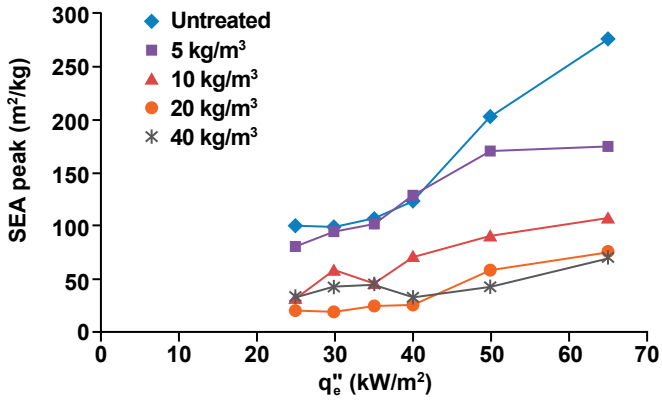

Figure 59. Peak specific extinction area as a function of irradiance of smoke for untreated and impregnated beech wood.

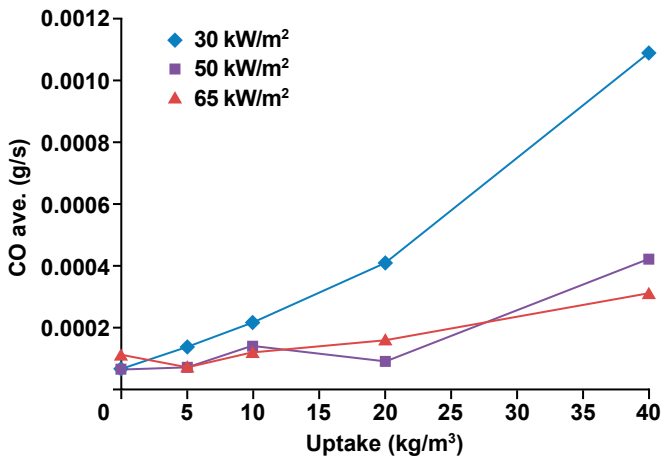

Figure 60. Average CO production for untreated and impregnated beech wood at different irradiances.

with considerable noncombustible gases promotes the localized regions of nonflammability, leading to incomplete combustion in those regions despite the overventilation conditions of the cone calorimeter. The mere thermal cracking of wood-derived volatiles will generate considerable CO, tar, and soot that are then reduced by the presence of combustion (whereas plastic and accelerant volatiles have CO and soot that appears only with the combustion process). This development of "white smoke" for a considerable heated time is consistent also with the difficulty of achieving flaming ignition in the cone calorimeter with treated materials. However, once the flaming combustion process is easily achieved, as at higher irradiances (or with a methane afterburner flare above the cone heater), the CO, tar, and soot will convert to lower levels and will have the properties more consistent with that of untreated wood materials, as Figure 60 seems to show. We note that this two-staging development of CO and soot within wood volatiles is a complication that is not adaptable from material conversion concepts developed for plastic and accelerant materials, and it should be solved for before using the properties in a CFD code.

FRT Beech Wood Summary

Cone calorimeter measurements were performed on untreated and impregnated beech wood. Monoammonium phosphate was used as the flame retardant. The concentrations of impregnating solutions were prepared so that the uptake of flame retardant to wood was 5, 10, 20, and 40 kg/m³. The MAP had a strong effect by lowering the HRR overall. The change of total heat released, as a function of irradiance, was relatively small for untreated wood and for treated samples except for samples with uptakes of 40 kg/m³. The ignition times for treated samples were basically less than the ignition times of untreated beech wood, except for high uptakes of 40 kg/m³. This was caused by the fact that the processes of decomposition for treated wood started at lower temperatures than the decomposition for untreated wood, and likely resulted in smoldering leading to sustained flaming. The actual mass measurements also confirmed that this early mass loss during the exposure to irradiance is higher for treated samples than for untreated wood. However, the ultimate mass loss was less for treated samples than for untreated wood, as a result of lower overall mass loss rate when the wood is treated.

Quintiere's Numerical Model

The first model used in this work was originally suggested by Quintiere (1993) and modified by Janssens and others (1995). Quintiere's numerical model was chosen for the model calculations of the room/corner test results because it has capabilities to be modified for the different burner output protocols, the different installations of the material in the room, and different room dimensions. Input parameters to the model are in the form of thermophysical properties that can be derived from the measurements on cone calorimeter and LIFT apparatuses. The main features of the model are described below.

Model Description

The original Quintiere's model simulates the ignition, flame spread, burn-out, and burning rate of wall and ceiling materials subject to a corner fire ignition source in a room. It is assumed that the ignition burner located in the corner of the room heats a rectangular area of the back and side walls. The width of the area, $x_{p,0}$ (m), is equal to the burner widths, and the height of the area, $y_{p,0}$, is 1.3 and 3.6 m corresponding to the 100- and 300-kW burner output, respectively. This area behind the burner is assumed to ignite when its surface temperature, $T_{s,0}$, reaches the ignition temperature of the material T_{ig}. The surface temperature is calculated using Duhamel's superposition integral

$$T_{s,0} = T_a + \frac{1}{\sqrt{\pi k \rho c}} \int_0^t \frac{\dot{q}''_{bw} + \varepsilon m \sigma \left(T_g^4 - T_{s,0}^4\right)}{\sqrt{t - \varepsilon}} d\varepsilon \qquad (17)$$

where T_a is the ambient temperature, $\dot{q}''_{bw}$ is the heat flux from the flames of the burner, ε_m is the emissivity of the material, and T_g is the room gas temperature. The surface emissivity was set to unity by Quintiere. In the Janssens modification of the model this value was user defined. Heat flux from the flames is assumed constant and uniform. Quintiere's suggested value for $\dot{q}''_{bw}$ was 60 kW/m^2. The value of Janssens and others (1995) for the burner flames heat flux consisted of both the radiative and convective part. The radiative part was 35 kW/m^2, and the convective part was calculated based on the average flame temperature measured by Kokkala (1993) and Tran and Janssens (1993), which equaled 734 °C. Taking the convective heat transfer coefficient as 15 W/m^{2}K and the wall surface temperature as halfway between T_a and T_{ig}, the heat flux values calculated the way suggested by Janssens for wooden materials became 40 kW/m^2.

The upper gas layer temperature T_g calculated with the McCaffrey–Quintiere–Harkleroad equation (McCaffrey and others 1981) was modified for corner fires by Karlsson and Magnusson (1991) as suggested by Quintiere (1993):

$$T_g = T_a \left\{ 1 + C \left[\frac{\dot{Q}}{\rho_a c_p \sqrt{g} T_a A_0 \sqrt{H_0}} \right]^{2/3} \times \left[\frac{\left(\sqrt{k\rho c/t}\right) A_s}{\rho_a c_p \sqrt{g} A_0 \sqrt{H_0}} \right]^{1/3} \right\} \tag{18}$$

where C is the constant, $\dot{Q}$ (kW) is the total energy release rate in the room, A_0 (m^2) is the area of the ventilation opening, H_0 (m) is the height of the opening, A_s (m^2) is the room surface area, and the $\rho_a c_p \sqrt{g}$ = 3.44 kW/m$^{5/2}$K. The constant C, modified coefficient for corner fires, had the value 2.2. The value of C in the original McCaffrey–Quintiere–Harkleroad equation was 1.63, which corresponds to the room-centered fires.

Once the initially heated area is ignited, upward and lateral flame spread will occur. The height of the pyrolyzing area, y_p (m) is computed from

$$\frac{dy_p}{dt} = \frac{y_f - y_p}{t_{ig}} \tag{19}$$

where ignition time t_{ig} for constant flux on thermally thick material is given by

$$t_{ig} = \frac{\pi}{4} k\rho c \left[\frac{T_{ig} - T_s}{\dot{q}''_f} \right]^2 \tag{20}$$

and y_p and y_f correspond to the wind-aided or "upward" flame spread. Wind-aided spread of flame is taking place in the region above the burner and below the ceiling in the ceiling jet. The depth of the ceiling jet is 0.08H. The flame height, y_f is calculated from

$$y_f = 0.067 \left[\dot{Q}'_b + \dot{Q}'' y_p \right]^{2/3} \tag{21}$$

The term $k\rho c$ is a material property that is determined from the analysis of piloted ignition data measured in the cone calorimeter, or a similar apparatus. The flame heat flux, $\dot{q}''_f$ is assumed constant and uniform with a value of 30 kW/m^2. $\dot{Q}'_b$ (kW/m) is equal to the burner HRR divided by two times the burner width. $\dot{Q}''$(kW/m^2) is equal to the HRR per unit area of the wall material and is calculated from

$$\dot{Q}'' = \frac{\Delta H}{L} \left(\dot{q}''_f - \sigma T_{ig}^4 + \sigma T_g^4 \right) \tag{22}$$

where ΔH (MJ/kg) is the heat of combustion of the material, L (MJ/kg) is the heat of gasification of the material, and $\dot{q}''_f$ (kW/m^2) is the flame heat flux to the pyrolyzing region. ΔH and L are material properties that can be calculated from HRR and mass loss rate measurements in the cone calorimeter. Quintiere suggests calculating L from the slope of the linear correlation of peak HRR versus external irradiance. For the steady burning rate of liquid fuels, this slope represent $\Delta H/L$ and L is a thermodynamic material property. For the solid fuels, the derived L represents an effective material property that enables to calculate peak HRR under various external heat flux conditions (Quintiere 1993). Finally, $\dot{q}''_f$ is a user-specified value.

The lateral (or "opposed flow") flame spread is characterized by the pyrolyzing width, x_p (m). It is computed from the following differential equation (which is numerically integrated in the model):

$$\frac{dx_p}{dt} = \frac{\phi}{k\rho c \left(T_{ig} - T_s \right)^2} \quad \text{for } T_s \geq T_{s,min} \tag{23}$$

where ϕ (kW^2/m^3) is the flame heating parameter and $T_{s,min}$ (K) is the minimum surface temperature for lateral flame spread; ϕ and $T_{s,min}$ are material properties that can be derived from the measurements of the lateral flame spread in the LIFT apparatus (ASTM E 1321) (although there are several questions about the LIFT accurately representing the room burn conditions). The downward flame spread is characterized by z_p (m), which is calculated from Equation (23), with z_p substituting x_p. The surface temperature T_s in the Equations (20) and (23) is determined from the equation similar to (17), but with a different integrand,

$$T_s = T_a + \frac{1}{\sqrt{\pi k\rho c}} \int_0^t \frac{\varepsilon_m \sigma \left(T_g^4 - T_s^4 \right) + h_c \left(T_g - T_s \right)}{\sqrt{t - \varepsilon}} d\varepsilon \tag{24}$$

Quintiere suggested value of unity for the emissivity also using this equation. The total HRR in Equation (18) is given by

$$\dot{Q}(t) = \dot{Q}_b + \dot{Q}'' A_p(t) \tag{25}$$

The pyrolyzing area A_p (m^2) is a function of x_p, y_p, and z_p. The term $\dot{Q}_b$ is the burner heat output in kilowatts. After y_p has reached the ceiling, it is assumed that Equation (19) remains valid to determine the location of the leading edge of the pyrolyzing area. Downward flame spread is taking place near the corner at the burner location and under the ceiling down from the ceiling jet region. The lateral flame spread is taking place from the initial pyrolyzing area and flame jet region above the burner. For materials with a short burning time, the burn-out region must also be determined. The burn-out front position for the upward flame spread, y_b (m) is approximated by

$$\frac{dy_b}{dt} \approx \frac{y_p(t) - y_b(t)}{t_b} \tag{26}$$

The burn-out time, t_b (s) is calculated from

$$t_b = \frac{Q''}{\dot{Q}''} \tag{27}$$

where Q''(MJ/m^2) is the total available energy per unit area and is considered constant for a given material. It can be found as the area under the HRR curve in the cone calorimeter. The burn-out front position for the lateral flame spread, x_b (m) is calculated from the equation similar to Equation (26), but y_p and y_b are replaced by x_p and x_b, respectively. A similar equation to Equation (26) is used also for the downward burn-out front position, z_b (m), calculation.

Janssens Modifications to Quintiere Model

Janssens and others (1995) provided several modifications to the original Quintiere model:

- The equations for calculation of rather complex shape of pyrolyzing area suggested by Quintiere were replaced by a set of rectangles.
- The surface temperature in Equation (24) is considered to equal the ignition temperature of the material. Janssens argues that this is underestimation of the heat losses due to reradiation. He suggests a user-specified vaporization temperature, T_v. For charring materials, his suggested value is T_{ig} + 100 (K).
- The surface emissivity of unity in Equations (17) and (24) was replaced by a user-specified value. The value 0.9 was used for all materials except FRT polyurethane foam, for which the measured value 0.68 was used.

The model was also modified so that it computed the burning area only on walls. The ceiling in this project was covered with paper-faced gypsum board for all tests and not covered with the tested material.

Input Parameters and Values

The input parameters to the model as suggested by Quintiere are as follows:

T_{ig}	Ignition temperature (°C)
$k\rho c$	Thermal inertia
ΔH	Effective heat of combustion (MJ/kg)
L	Effective heat of gasification (MJ/kg)
ϕ	Flame spread parameter (kW^2/m^3)
$T_{s,min}$	Minimum temperature for flame spread (K)
Q''	Total heat evolved (MJ/m^2)

In the Janssens modification, the following parameters are also used:

T_v	Vaporization temperature (°C)
ε_m	Emissivity

The input parameters to the model are derived from the measurements with the cone calorimeter (T_{ig}, $k\rho c$, ΔH, L, Q'') and LIFT apparatus (ϕ, $T_{s,min}$) as provided in Tables 2 and 6 (Grexa and others 1995, 1996). Janssens suggested using the vaporization temperature as the sum T_{ig} + 100 °C. In the Janssens modification, the user can input the value for the emissivity of material. As it was described earlier, the T_{ig} and $k\rho c$ were calculated as suggested by Janssens (1991) and Dietenberger (1996). Quintiere suggested using the slope of the peak HRR as the function of external irradiance for the calculation of effective heat of gasification. This way the derived L allows the model user to calculate the peak HRR for all irradiances in the model simulation. Another way to calculate the heat of gasification was suggested by Janssens (1991), in which the calculated values for heat of gasification were much lower than those calculated from the slope of HRR curve. As for the total heat released per area, Q'', the value of the area under the HRR curve measured in the cone calorimeter was used. This parameter changed little as the function of external irradiance. Therefore, the average from whole measurements was used for all materials. The exception was FRT polyurethane foam, for which the total heat evolved has strongly changed with the external irradiance. Therefore, in the simulation calculation instead of the average value, the total available energy was calculated directly in the model as the function of imposed heat flux, based on the experimental function found in the cone calorimeter.

To test the consistency of our results against those using literature values for the fire properties, we used the values from these sources. The values for paper-covered gypsum board, particleboard, polyurethane foam, and spruce lumber were taken from Quintiere (1993). From the same literature

Table 11—Comparison of the experimental and model time to flashover

Material	Test no.	Experimental flashover time (s)	Model flashover time (MJ)[a] (s)	Model flashover time (MD)[b] (s)
Type X gypsum board	1	NFO[c]	NFO	NFO
FRT Douglas Fir plywood	2	906	875	710
Oak veneer plywood	3	174	419	300
FRT plywood (Forintek)	4	879	1,057	977
Douglas Fir plywood (ASTM)	5	474	378	338
FRT polyurethane foam	6	630	437	15
Type X gypsum board	7	NFO	NFO	NFO
FRT Southern Pine plywood[d]	8	621	NFO	647
Douglas Fir plywood (MB)	9	546	530	495
Southern Pine plywood	10	330	563	528
Particleboard	11	264	934	686
Oriented strandboard	12	180	621	615
Hardboard	13	255	383	426
Redwood lumber	14	507	339	236
Type X gypsum board	15	NFO	NFO	NFO
White spruce lumber	16	606	649	623
Southern Pine boards	17	258	637	619
Waferboard	18	174	639	511

[a]MJ, T_{ig}, and $k\rho c$ derived by the Janssens's procedure.
[b]MD, T_{ig}, and $k\rho c$ derived by the Dietenberger's procedure.
[c]NFO indicates no flashover.
[d]Ignition burner at 100 kW was of 300 s duration instead of 600 s duration.

source, the values for MDF and particleboard were used for hardboard and waferboard, respectively. The values for redwood, Douglas Fir plywood, Southern Pine plywood, and oriented strandboard were measured by Janssens (1991). From the same literature source, the values for Southern Pine plywood and Victorian Ash were used for Southern Yellow Pine board and oak plywood, respectively. Finally, for the FRT plywood materials, the values of particleboard were used.

Results and Discussion

With these input parameters, the model calculated the times to 1 MW, and the comparisons to experimentally obtained flashover times are given in Table 11. A special exception must be made for test no. 8, in that the burner at the first 100-kW step was inadvertedly shortened to 300-s duration, rather than the required 600-s duration. Because the FRT plywood in the other tests did not flashover during the 100-kW burner phase, one can add conceptually 300 s to the 621 s in test no. 8 to obtain 921 s TFO, which is more typical for the FRT plywoods.

It can be seen that for some materials the experimental flashover time agrees quite well with the flashover time calculated by Quintiere's model (FRT plywood materials, spruce wood, Douglas Fir plywood). The model was able to differentiate between the FRT wood materials and untreated materials. However, for some materials, the differences of experimental and model flashover times are significant.

One problem was that the model did not differentiate the composite materials (OSB, waferboard, particleboard, hardboard) for which the HRR in the room/corner test increased from the beginning until flashover from those for which the HRR passed through the period when HRR did not increase but had a relatively constant value until shortly prior to flashover (spruce wood, redwood, Douglas Fir plywood). Furthermore, for composite materials (OSB, waferboard, particleboard, hardboard, oak plywood, and Southern Pine) the experimental flashover time was much shorter than the flashover time calculated by the model. For particleboard, OSB, and waferboard, the model failed to predict the burner output at which the flashover took place.

Some of the materials tested in this project were tested by Janssens in cone calorimeter and LIFT, and all parameters needed in the model were reported. For some materials tested in this project, the input parameters were also reported by Quintiere. For these "well characterized" materials, the model calculations were also done. The input parameters and the resulting time to flashover are given in Tables 12 and 13. In Table 13 the hardboard is compared to the MDF from Quintiere (1993).

Particleboard was measured by Quintiere and Janssens and also in this project. Calculated time to flashover using the parameters derived in this project about agrees with the time to flashover calculated using Quintiere's input parameters (see Tables 11 and 13). In both cases the simulated

Table 12—Input parameters to the Quintiere's model for well-characterized materials

Material	Test no.	$k\rho c$ (MJ) (kJ^2/m^4K^2s)	T_{ig} (MJ) (°C)	ΔH (MJ/kg)	L (MJ/kg)	Q'' (MJ/m^2)	ϕ (kW^2/m^3)	$T_{s,min}$ (°C)
Type X gypsum board[a]	1	0.593	388	10	4.8	7.2	0.5	300
Douglas Fir plywood[b]	9	0.335	342	12.3	2.95	62	5.7	111
Southern Pine plywood[b]	10	0.259	344	12.3	2.21	83	7	125
Particleboard[a]	11	0.626	405	14	5.4	120	8	180
Particleboard[b]	11	0.283	346	11.8	2.12	111	1.7	184
OSB[b]	12	0.244	302	13.3	2.39	83	2.2	143
MDF[a]	13	0.732	361	14	4.2	100	11	80
Redwood lumber[b]	14	0.187	383	12.6	3.14	101	8.8	124
Spruce lumber[a]	16	0.569	389	15	6.3	120	24	155

[a]Taken from Quintiere (1993).
[b]Taken from Janssens (1991).

Table 13—Experimental and model flashover times using input data from Table 12

Material	Test no.	Experimental flashover time (s)	Model flashover time (MJ) (s)
Type X gypsum board[b]	1	NFO[a]	NFO
Douglas Fir plywood[c]	9	546	288
Southern Pine plywood[c]	10	330	151
Particleboard[b]	11	264	850
Particleboard[c]	11	264	228
OSB[c]	12	180	133
MDF[b]	13	255	631
Redwood lumber[c]	14	507	214
Spruce lumber[b]	16	606	720

[a]NFO indicates no flashover.
[b]Taken from Quintiere (1993).
[c]Taken from Janssens (1991).

flashover took place under increased burner output, which differs from the experimentally measured flashover time. On the other hand, the value obtained from Janssens's data is significantly lower and agrees well with experimentally measured flashover time. The parameter that caused this change was heat of gasification. The Janssens values of heat of gasification were significantly lower than those derived from the slope of peak HRR versus external heat flux. Thus, HRR in the model calculations significantly increased. This caused the flashover time for the particleboard to be short. Low values of heat of gasification shortened the flashover time for other materials as well. The comparison of the time to flashover for oriented strandboard calculated by use of Janssens's data and data derived in this project also shows the same result. All the parameters calculated in this project and by Janssens for OSB have similar values except for the heat of gasification. Therefore, the difference in calculated flashover time for this material is caused by different heat of gasification used. However, if the Janssens values of heat of gasification are used, the flashover time is short for other materials as well. The time to flashover calculated for the Douglas Fir plywood using Janssens's value of heat of gasification is about half the experimentally measured time to flashover. The same is true for Southern Pine plywood and redwood. Thus the use of the L derived by Janssens in the Quintiere model shifted the flashover times to shorter values but the model still did not differentiate between various untreated wood-based products (Fig. 61).

The possible reason for this poor result is the great uncertainty of the lateral and downward flame spread. In the room/corner tests at which the tested materials were installed on ceiling as well, the most important role was the effect by the wind-aided flame spread. The burning of the material on the ceiling had a very significant role in that fire scenario. In this project the materials were installed on three walls only. The ceiling was covered with paper-faced gypsum board. Therefore, the wind-aided flame spread occurred only in the narrow belt behind the burner flames up to the ceiling and in the narrow region under the ceiling. The beginning and the speed of lateral and downward flame spread

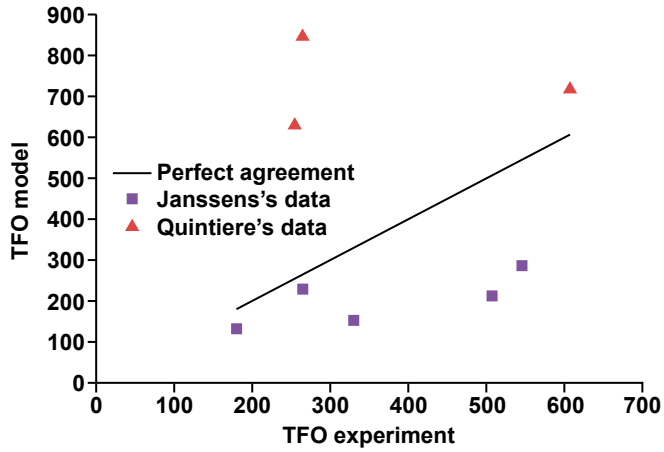

Figure 61. Comparison of the model and experimental time to flashover for input parameters for two references.

played a significant role in our configuration of the room/corner test as well as in the simulation calculations.

In the model, the beginning of the lateral and downward flame spread is defined by the minimum temperature for flame spread $T_{s,min}$, and the "speed" constant is defined by the term $\phi/k\rho c$. The driving force for the lateral and downward spread is $1/(T_{ig} - T_s)$. The values for minimum temperature for opposed-flow flame spread, $T_{s,min}$, for particleboard given by Quintiere (1993) ($T_{s,min}$ = 180 °C) and Janssens (1991) ($T_{s,min}$ = 184 °C) agree well. The value of flame spread parameter ϕ differs. Quintiere's reported value for ϕ is 8 kW^2/m^3, and Janssens's value for ϕ is 1.7 kW^2/m^3. The rate $\phi/k\rho c$ for Janssens's value is 7.1 and for Quintiere's value is 12.8. From the simulations of the room/corner scenario by Quintiere (1993), it is clear that for the particleboard the agreement of experimental and calculated time to flashover was very good. In that case the materials were installed on walls and ceiling. The rate $\Delta H/L$ reported by Quintiere (1993) was 2.6, but better correlation was found for the value of 2.0. This value is in good agreement with the $\Delta H/L$ derived in this project, which is 1.9.

Despite these good characterizations for particleboard, the model failed to predict the experimentally obtained flashover time in the room configuration with the particleboard on walls only. The calculation shows that the flame quickly spreads in the region of wind-aided mode (behind the burner's flames and in the area below ceiling). When the flames reached the front wall, the flame spreading in the model simulation stopped until the average surface temperature reached the value of $T_{s,min}$. Contrarily, in the real room/corner test, the HRR steadily increased until the flashover was reached. Modifying the $T_{s,min}$ in the model simulation did not solve the problem. For example, by changing $T_{s,min}$ to the value 65 °C, the time to 1 MW was 426 s, which is still a very high value. In fact there is no real justification to modify the $T_{s,min}$ for particleboard, because both Janssens's and Quintiere's values of $T_{s,min}$ are almost the same. Because of the described problems and uncertainty of the start and speed of the opposed-flow flame spread by using $T_{s,min}$ and ϕ parameters, respectively, it was decided to modify the model and use an alternative formulation for these parameters.

To predict the flame spread over a solid fuel, two major aspects must be considered: the response of the solid fuel to heat transfer from the flame and/or external heat source and the heat transfer from the flame to the fuel ahead of the pyrolysis front. The former aspect corresponds to the piloted ignition, the latter one to the mechanisms of heat transfer between the flame and the virgin fuel (radiation, gas phase conduction, and solid phase conduction) (Janssens 1991). Material properties, which are often used to characterize the piloted ignition, are ignition temperature and thermal inertia. In practice, however, the time to ignition measurements are used to derive the ignition temperature and/or effective thermal inertia. Concerning the second aspect of the flame spread, some authors used the HRR to correlate the flame spread characteristics (Green 1995). Here the effort was done to correlate the ignition data and HRR derived from the measurements in the cone calorimeter to the "lateral and downward" flame spread as it is defined in the Quintiere model.

With these considerations, it was decided to use Equation (23) for calculation of the "lateral and downward" flame spread. Thus, instead of the rate of flame spread parameter ϕ and thermal inertia in Equation (23), a correlating "flame spread constant", F_s (K^{4}m/s^3), was formulated. The time to ignition, ignition temperature, $\Delta H/L$, and total heat release were used to correlate with F_s. The parameters for the correlation of F_s were chosen so that they would be consistent with the input parameters to the Quintiere model. However, instead of using $k\rho c$, the ignition time measured at 25 kW/m^2 was chosen. The resulting correlation function is

$$\ln(F_s) = a + b\left[T_{ig}^{p} t_{ig}^{q} \left(\frac{\Delta H}{L}\right)^{r} Q''^{s}\right] \tag{28}$$

where a,b are constants and p,q,r,s are exponents. The value of $\Delta H/L$ is the slope of linear correlation to the peak HRR. The best correlation was found for the following values of constants and exponents to Equation (28):

a = 0.23
b = 625.47
p = –1.36
q = –0.40
r = –0.20
s = 0.93

Equation (23) was then changed to

$$\frac{dx_p}{dt} = \frac{F_s}{(T_{ig} - T_s)^2} \quad \text{for } T_s \geq T_{s,min} \tag{29}$$

Table 14—Comparison of the experimental and model time to flashover for tested materials using modified flame spread concept

Material	Test no.	Experimental flashover time (s)	Model flashover time (MJ)[a] (s)	Model flashover time (MD)[b] (s)
Type X gypsum board	1	NFO	NFO	NFO
FRT Douglas Fir plywood	2	906	NFO	851
Oak veneer plywood	3	174	210	217
FRT plywood (Forintek)	4	879	947	875
Douglas Fir plywood (ASTM)	5	474	334	357
FRT polyurethane foam	6	630	612	609
Type X gypsum board	7	NFO	NFO	NFO
FRT Southern Pine plywood	8	621	NFO	851
Douglas Fir plywood (MB)	9	546	464	428
Southern Pine plywood	10	330	469	318
Particleboard	11	264	281	239
Oriented strandboard	12	180	286	269
Hardboard	13	255	300	353
Redwood lumber	14	507	321	240
Type X gypsum board	15	NFO	NFO	NFO
White spruce lumber	16	606	606	604
Southern Pine boards	17	258	377	417
Waferboard	18	174	172	177

[a]MJ, T_{ig}, and $k\rho c$ derived by the Janssens procedure.
[b]MD, T_{ig}, and $k\rho c$ derived by the Dietenberger procedure.
[c]NFO indicates no flashover.

In the calculations, the $T_{s,min}$ was set arbitrarily to the low value 50 °C for all materials. The resulting calculated times to flashover in comparison to experimental times to flashover for tested materials are given in Table 14. As it can be seen from Table 14, the greatest differences between experimental and simulated times to flashover for the Dietenberger ignition parameters were calculated for redwood, whereas for Janssens's ignition parameters the greatest differences in TFO between experiment and model were obtained for FRT Southern Pine plywood and FRT Douglas Fir plywood. For other materials, the simulated time to 1 MW improved in comparison to the values in Table 12 or 13. However, not much improvement was achieved in distinguishing TFOs of composite materials from that of untreated plywoods or solid wood.

Comparison of the predicted room/corner test results using the ignition data derived by Dietenberger's method to that derived by Janssens's method shows that for most wood-based products the accuracy of prediction is about equal. Even though for some materials the T_{ig} and $k\rho c$ derived by these two methods differ significantly, in the simulation calculations they compensate for each other. We note that the modified concept for lateral and downward flame spread calculation was done for $T_{s,min}$ artificially set to a low value and constant for all materials. This simplification clearly does not correspond to the real conditions in the room/corner test and real material properties. It must be also noted that Equation (29) found by correlation has its validity limited to the fire scenario defined in this work. However, the effort here was done to keep the calculation philosophy of the original Quintiere numerical model and use the data measured in the cone calorimeter for the prediction of room/corner test results. Yet the empiricism involved in modeling lateral and downward flame spreading needs to be resolved by a better physical modeling process before general predictions can be asserted.

Analytical Flame Spread Model for ISO 9705

There are various types of flame spread models for the ISO 9705 (ISO 1993a) room that are still in development. Previously, a numerical model (modification of Quintiere's model) to predict a fire growth scenario for use on a personal computer was described. A limited number of first-order differential equations are set up to simulate specific events such as upward, lateral, and downward flame spread while including material burnout, approximated radiation from upper gas layer, and temperature responses of wall lining and upper gas layers. There are also some published papers on the computational fluid dynamics (CFD) modeling of room fire growth. Yan and Holmstedt (1996) have modeled both full- and one-third-scale room corner fire growth on particleboard with a CFD model. Although CFD models are showing some success one still has to contend with many

model parameters and to have access to a supercomputer. It is certain the numerical models will continue to improve as computer technology and fire material properties become better known.

After searching the published literature, we found a dearth of analytical models for room fire growth since two 1992 publications. In the first model (Wickstrom and Goransson 1992), the cone calorimeter data is used as input to a simplified fire growth model. Basically, the burning area growth rate is made proportional to the inverse of the time to ignition measured at the cone's flux of 25 kW/m^2 and is decoupled from the HRR. The total HRR is that from the burner and from each incremental change in burn area as multiplied by the actual heat release flux profile measured in the cone calorimeter for irradiance of 50 kW/m^2. For each step increase in the burner output, a surface temperature criterion is used to decide if flame propagation occurs or not.

The second model (Karlson 1993) reported takes a more physically reasonable approach by extending the model Saito and others (1985) (SQW) for thermal modeling of upward spread on a wall to a flame spread along the ceiling lining. Three stages of fire growth were assumed. The first stage is the HRR from the burner and the wall being heated up to the point of ignition. In the second stage, the time to ignition of the wall area behind the burner's flame is calculated as 1.7 times the time to ignition for cone's flux of 50 kW/m^2. A decaying exponential heat release flux profile is fitted to the cone's profile for exposure to flux of 50 kW/m^2. This profile as a function of time is multiplied by the burning wall area (assuming instantaneous upward flame spread) of twice the burner width times the height from the burner to ceiling to give the material's burning rate. Then another similar time to ignition is modeled for an initial ceiling area (which is related to amount of energy carried by the plume to the ceiling) for the third final stage of fire growth. At this point, the SQW thermal model is applied to the ceiling so that a decaying heat release flux profile coupled with the flame spread rate formula can analytically simulate an accelerating, oscillating, or decaying fire growth behavior.

With a propane burner as ignition source (and as a source of radiation heating), all our room tests and the limited CFD simulation show that there are always four significant stages of fire growth leading to flashover. They are back wall ignition, upward flame spread to the ceiling, lateral/ceiling flame spread nearly to the ends of the room, and finally, a rapid uniform downward flame spread just prior to flashover. In the design of the propane burner HRR profile, it is sometimes stated that 100 kW simulates a wastebasket fire and that 300 kW simulates a sofa fire. However, in rating combustible materials it is more beneficial to look for a burner HRR profile that is sufficient to cause flashover for nearly all combustible materials in a reasonable and gradated amount of time. In the ISO 9705 (ISO 1993a) standard, the specification of four ignition scenarios seemed surely to encompass all possible combustible materials. How to best use these ignition scenarios was yet to be determined.

The use of an appropriate fire growth model that has been validated with a few room/corner fire tests for the fire growth scenarios allowed in ISO 9705 (ISO 1993a) should provide considerable assistance for developing a fire test methodology for rating combustible materials. The complexities of fire growth in a room, as compared to flame spread in the Steiner tunnel (ASTM E 84), or just upward wall flame spread will tend to direct developments toward CFD modeling. Or lacking such a model, much attention will be devoted to doing many room burn tests, often without understanding full aspects of fire growth or the impact of measurement errors. Indeed, the effects of gas analysis time response (for both the ISO 9705 (ISO 1993a) room and the cone calorimeter), time response of the burner's propane flow, and the time response of the room's upper air mixing on calculating HRR are not known to be considered in flame spread modeling. If these time response effects are incorporated within an analytical model that fits the experimental data on fire growth, then it is possible to simulate the effect of different laboratories with their different measurement methods on interpreting HRR during fire growth. One would even suspect an effect on prescribing a value of HRR for indicating flashover that can be a cause for differences in results between laboratories and be easily remedied as well.

Before describing the analytical fire growth model developed for this work, we examined existing models, noted their deficiencies for our application, and suggested ways to generalize the formulation. One immediate deficiency is being able to simulate a fire growth scenario corresponding to the 100/300 kW ISO burner and combustible linings on the walls only. Existing analytical and numerical models were based on combustible material being lined on the ceiling also. It is not as simple as merely removing the ceiling layer from being a contribution to HRR, unless one is working with a CFD model, because the physics of flame spread is changed from that of flame spread across the ceiling to that laterally on the wall. Even if a flame spread formulation remains the same, the coefficients need adjustment to fit the altered flame spread process. In fact, there would be one set of coefficients for upward flame spread, another set for lateral spreading, and finally another set for the downward spreading. Indeed, the modified Quintiere's numerical model covers all four phases, whereas Karlson's model is lacking the lateral and downward flame spread phases. However, with the gypsum board as a back board to testing materials, recent cone calorimeter tests show that the secondary peak HRR often noted for wood-based materials is significantly reduced and extends for longer period of time (even up to 20 min) due to heat losses into the back board. Thus, the use of an exponentially decaying HRR profile in Karlson's model would be more realistic than the modified Quintiere's model with its constant HRR and a sharp drop at burnout

time. Finally, the simplicity of the Wickstrom and Goransson (1992) model would probably preclude a more general application, but its relative success for one particular type of fire growth provides impetus to seek simplicity in the general analytical model.

Closer evaluation of published experimental data suggests some simple formulations of sub-models for the room fire growth model. Perhaps the most important characterization is that of the ignition burner. In our facility and in other laboratories, measurements have been made of surface total heat flux distribution, visible flame height, flame temperature, air velocities, and flame extinction coefficients. For relevance to fire growth modeling, we formulated empirical relationships for wall heat flux distribution and the visible flame region as related to total HRR. The average surface heat flux within the initial ignition area at slightly above the burner's height has been measured with fluxmeters at around 55 kW/m^2 for the burner's HRR from 40 to 300 kW for both ISO and ASTM burner (Kokkala and Heinila 1991, Williamson and others 1991, and also our facility). At the flame height (which varies fairly directly with HRR), the total heat flux already decreases to about 25 kW/m^2 and continues to decrease similarly to a decaying exponential function. Using a combustible material instead of an inert board would have even lower surface heat flux because a surface temperature approaching the pyrolysis temperature would lower flame heat flux and increase the surface's re-radiating cooling flux. Similar adjustments to surface heat flux will also be required in the cone calorimeter test conditions.

In any case, the imposed heat flux distribution that should be used in a model of pyrolysis front velocity is a high constant heat flux followed by a decaying exponential profile ahead of the pyrolysis front. Indeed, in detailed measurements (Kulkarni and others 1994) of upward flame propagation on finitely thick materials exposed to external flux, the flame flux profile follows a decaying exponential form immediately at the pyrolysis front. We could use a constant external radiant flux to calculate the preheat temperature as a function of time and then use the flame flux profile to calculate the pyrolysis front velocity by increasing the preheated surface temperature to the ignition point (Dietenberger 1991, Saito and others 1985). Note that the ignition burner's flame serves a double role in fire growth. The first role is to heat and ignite an initial burning region on the combustible material. In its second consequential role, the burner's flame combines with combustible material's flame to create a surface heat flux profile for the flame spread rate, even up to the flashover point. One can imagine the complexity in fire growth modeling that uses preheat temperatures in the computations, which for good predictive accuracy will require use of many surface elements. This is a potential serious weakness in some models, such as that of Quintiere, but is not a problem with CFD models that include detailed localized meshing at boundaries of burning zones. Therefore, in the analytical model, all of the surface heat fluxes are incorporated into the "flame flux profile" in order to completely avoid calculation of preheat temperatures and thus maintain the simplicity of the model for the ISO 9705 (ISO 1993a) test conditions. One might assert that preheat temperatures due to radiation from the upper hot gas layer need to be calculated just prior to flashover in order to create an accelerating HRR profile typically observed. However, an actual HRR that uniformly increases with time in the room will be observed as an accelerating profile because the HRR measurements are affected significantly by the "dead air" time responses in the gas train and in the room's upper gas layer. Second, it is possible to evaluate radiation view factors from the bottom surface of the hot smoky gas layer to the walls so that a "flame flux profile" is formulated for the downward flame spread. The analytical model developed for this work will actually demonstrate these effects and their importance can be assessed.

Other laboratory variations include the time response of the burner itself, which affects the initial time to ignition. This phenomenon is simulated with an analytical solution to the Duhamel's integral of material surface temperature response to an instant flux with the actual time response of the burner surface heat flux. The reduction of peak HRR and its time shift in the cone calorimeter due to the "dead air" response in the gas train is an often-overlooked experimental factor in the use of small-scale data. The effect is particularly severe with materials with low values of THR, such that a simple correction to the peak HRR and its time shift is formulated for inclusion to the fire growth model.

The construction of the analytical fire growth model for the ISO 9705 (ISO 1993a) room is as follows. The properties of ignitability measured and derived with the cone calorimeter are used to calculate time to ignition on the wall behind the pilot burner after making adjustments for surface heat flux levels and time responses. Next, a rate of propagation of pyrolysis fronts is formulated for a finitely thick material responding to a flame flux profile that provides for all of surface heating to the virgin material (that is, modeling of surface preheating is not needed). The length scale of the flame flux profile is then linearly related to the extended flame length using experimental data for upward/lateral flame spread, and to the ceiling flame sheet dimensions for downward flame spread. By converting to the geometrics of burning and flame areas instead of their lengths, a greater simplicity and generality was achieved by relating extended flame area linearly to the HRR even for different burner dimensions and HRR outputs shifting with time. The HRR computed for the material is a Duhamel integral of increasing pyrolysis area with the heat release flux characteristic of the material, as in the SQW method. The Laplace transform provides an analytic solution (with complex variables) to the fire growth. The decaying exponential profile assumed for the heat release flux contributes to the simplicity of the

model by noting that all burning areas will decay at the same rate irrespective of when they began burning. This means every time the model coefficients are changed or when new materials are instantly ignited, the general Laplace solution is restarted with an ignited area equal to the total existing burning area and an adjusted burn time that maintains continuity with the solution prior to the restart. The resulting solution has pyrolysis area increasing monotonically while the HRR (and extended flame area) will show acceleration, oscillation, or deceleration depending on the phase of flame spread and properties of the material. To simulate "dead air" response in the room ceiling and in the gas analysis train, the general Laplace solution is combined with the respective response functions in a Duhamel integral. With this flexibility in an analytical model it may be possible to fit the data with a lesser number of empirical constants. Different physical phenomena and reasonableness of the model are then investigated by varying the material, room, burner, or measurement properties.

Model Formulation

Ignition of the Wall Formulation

For the first phase in fire growth—ignition of the wall—the time to ignition needs to be predicted. The initial burning area needs to be predicted also, and its value is derived later within the formulation of flame area as a function of HRR. In the analysis for ignition, the intent is to use the ignitability parameters derived from the cone calorimeter data. Because the imposed heat flux is from the propane burner rather than the cone heater, the 55 kW/m^2 measured with the fluxmeters is modified as follows. The equation for surface heat flux being absorbed into the surface (fluxmeter or material) is

$$\dot{q}''_{\mathrm{w}} = \varepsilon_{\mathrm{m}}\sigma\left(\varepsilon_{\mathrm{f}}T_{\mathrm{f}}^{4} - T_{\mathrm{m}}^{4}\right) + h_{\mathrm{c}}\left(T_{\mathrm{f}} - T_{\mathrm{m}}\right) \tag{30}$$

The parameters that are known in the case of fluxmeters are $\dot{q}''_{\mathrm{w}}$ = 55 kW/m^2, T_{m} = 298 K, and ε_{m} = 0.97. Three remaining parameters are properties of the propane flame only. The temperature rise above ambient of the propane flame above the ignition area has been measured at about 880 °C by Hasemi and Tokunaga (1984) , 959 °C by Kokkala and Heinila (1991), and 754 °C by Tran and Janssens (1993). Most revealing are the contour plots of flame temperatures at 30 mm above the surface by Kokkala and Heinila (1991) in which the contour of 900 °C covers a reasonably sized ignition area for various burner sizes and output. With these considerations and using the flame temperature T_{f} = 1,173 K, we obtain the high but still reasonable values of flame emissivity and convective coefficient as ε_{f} = 0.395 and h_{c} = 0.0165 kW/m^{2}K to match the heat flux observed with the fluxmeters. Our test materials typically have the surface emissivity, ε_{m} = 0.99, and using the above values for other parameters the imposed heat flux becomes 51 kW/m^2. Therefore we would expect the time to ignition on the wall to correlate best with the cone heater flux of 50 kW/m^2, as found by Karlson (1993) and taken advantage of in his fire growth model. However, a multiplication factor of 1.7 times the time to ignition from the cone calorimeter was used to obtain the actual time to ignition for the room test. A possible explanation for this could be the slow response of the propane mass flow due to a slow valve opening to ensure a 100-kW level or to a large dead air volume from the opening valve to the flames. Although our electronic mass flow controllers are located close to the test room, the propane must pass through the laminar flow device after the control valve. We estimate this effect to give a time response of 1 s or 2.2 s to the 90% level. Using a manual valve to ensure a 100-kW level could mean a time response of 5 s or 11 s to 90% level. This can have a significant effect on time to ignition, as demonstrated later.

To predict time to ignition using derived properties, one must decide if the thermal response is thermally thick or thin and use a simple formula when appropriate. As a first step, we determine the imposed flux when the equilibrium surface temperature is decreased to the ignition temperature (by imagining the flame emissivity to decrease in some way). An equivalent statement is to calculate the heat loss flux to the ambient in which the steady state surface temperature is the ignition temperature as given by

$$\dot{q}''_{\mathrm{ig}} = \varepsilon_{\mathrm{m}}\sigma\left(T_{\mathrm{ig}}^{4} - T_{\mathrm{m}}^{4}\right) + h_{\mathrm{c}}\left(T_{\mathrm{ig}} - T_{\mathrm{m}}\right) = h_{\mathrm{ig}}\left(T_{\mathrm{ig}} - T_{\mathrm{m}}\right) \tag{31}$$

This defines the imposed heat flux level that results in infinite time to ignition and is described as the critical ignition flux. Note that a convective heat loss term is needed to compensate for the reduction of convective heat flux from the flame due to the increase in material temperature. Taking a typical ignition temperature of around 600K and other parameters given above, the critical ignition flux is calculated as 11 kW/m^2. For typical wood thicknesses and time to ignitions for our room tests, the ratio of imposed flux to critical flux of about 5 clearly implies the thermally thick regime but at the same time is not above the ratio of 10 that would allow us to use the classical solution of the material exposed to constant flux. However, Janssens's correlation has good accuracy for the heat flux ratios from 1 to 10 and Fourier numbers less than 0.33. Inverting Equation (6), the analytic expression for time to ignition is

$$\bar{t}_{\mathrm{ig}} = \frac{k\rho c}{h_{\mathrm{ig}}^{2}}\left(\frac{0.73}{q_{\mathrm{w}}/q_{\mathrm{ig}} - 1}\right)^{\frac{1}{0.547}} \tag{32}$$

This correlation was a functional fit to a finite difference solution of a material thermal response to an instant imposed flux. That is, Equation (32) was originally in the form of the temperature rise, $T_{\mathrm{s}} - T_{\mathrm{m}}$, as a function of time t. At very low values of heating times, the rise in surface temperature is proportional to the square root of time. Whereas using

Table 15—Time to ignition for different levels of burner sluggishness room test materials

Material	Test no.	For zero burner time constant t_{ig} (s)	For burner time constant of 1 s t_{ig} (s)	For burner time constant of 6 s t_{ig} (s)
Type X gypsum board	1	18.4	19.5	25.1
FRT Douglas Fir plywood	2	19.3	20.4	26.0
Oak veneer plywood	3	8.4	9.4	15.1
FRT plywood (Forintek)	4	20.8	21.8	27.4
Douglas Fir plywood (ASTM)	5	10.5	11.5	17.2
FRT polyurethane foam	6	2.4	3.5	8.0
Type X gypsum board	7	18.4	19.5	25.1
Douglas Fir plywood (MB)	9	9.8	10.8	16.5
Southern Pine plywood	10	12.7	13.8	19.5
Particleboard	11	23.1	24.1	29.7
Oriented strandboard	12	10.2	11.2	17.0
Hardboard	13	20.2	21.2	26.8
Redwood lumber	14	7.3	8.3	13.9
Type X gypsum board	15	18.4	19.5	25.1
White spruce lumber	16	10.9	11.9	17.7
Southern Pine boards	17	14.9	15.9	21.6
Waferboard	18	11.6	12.6	18.3

Equation (6), the rise in surface temperature is approximately proportional to square root of time for the typical times to ignition for the room tests. In any case, suppose the imposed flux from the burner has the sluggish response as in (and showing the Duhamel's convolution integral equivalent)

$$\begin{aligned}\dot{q}''_{\mathrm{b}}(t) &\equiv \dot{q}''_{\mathrm{w}} S_{\mathrm{b}}(t) \equiv \dot{q}''_{\mathrm{w}}\left(1-\exp\left(-t/\tau_{\mathrm{b}}\right)\right) \\ &= \int_0^t \frac{\dot{q}''_{\mathrm{w}}}{\tau_{\mathrm{b}}} \exp\left(-\left(t-\xi\right)/\tau_{\mathrm{b}}\right) d\xi \equiv \dot{q}''_{\mathrm{w}} \otimes \dot{S}_{\mathrm{b}}\end{aligned} \tag{33}$$

The effect on the surface temperature rise (as proportional to square root of time) is analyzed with the Duhamel supposition integral and solved by the Laplace transform method with the result

$$\begin{aligned}\sqrt{\pi k \rho c}\,\frac{T_{\mathrm{s}}-T_{\mathrm{m}}}{2\dot{q}''_{\mathrm{w}}} &= \frac{1}{2\sqrt{t}} \otimes S_{\mathrm{b}}(t) = \sqrt{t} \otimes \dot{S}_{\mathrm{b}} \\ &= \sqrt{t} - \sqrt{\tau_{\mathrm{b}}} \exp\left(\frac{-t}{\tau_{\mathrm{b}}}\right) \int_0^{\sqrt{t/\tau_{\mathrm{b}}}} \exp\left(\lambda^2\right) d\lambda\end{aligned} \tag{34}$$

The result is the appearance of Dawson function as the exponential/integral term, and its evaluation is available in the literature as an accurate functional relationship. Therefore, the adjustment to the time to ignition is as follows. Taking the square root of Equation (32), the resulting right side of the equation is approximately proportional to the temperature rise to the ignition temperature for the typical time to ignition values. Therefore, the effect of a slow burner response with time constant τ_{b} is to increase the time to ignition from instant burner response through the Dawson function, as in

$$\sqrt{\bar{t}_{\mathrm{ig}}} = \sqrt{t_{\mathrm{ig}}} - \sqrt{\tau_{\mathrm{b}}}\,\mathrm{Dawson}\left(t_{\mathrm{ig}}/\tau_{\mathrm{b}}\right) \tag{35}$$

This nonlinear function was solved by an interval-halving method rather than the standard Newton–Raphson method to ensure rapid and correct convergence. The input data to evaluate Equations (32) to (34) were derived for cone calorimeter data of ignitability shown earlier, and their values are listed in Table 7. The results of Equation (35) for the room test materials are shown in Table 15. The range of time to ignitions in the case of instant burner response, $\tau_{\mathrm{b}} = 0$, is from 8.4 s for the oak-veneer plywood to 23 s for the particleboard. Setting the burner time constant to 1 and 6 s, respectively, generally increases the time to ignition by 1.03 and 6.7 s, respectively. A burner's time constant of 6 s is enough to account for the increase in time to ignition indicated earlier by Karlson. Even if this may not be a problem with the data used by Karlson, the effect of not knowing the propane burner response can be a significant source of confusion and error concerning ignitability in room tests between laboratories or even within a laboratory if a certain quality control is not maintained. Because of our use of the electronic mass flow controller, we expect only a 1-s delay in the time to ignition.

Generic Flame Spread Formulation

The next three phases of fire growth are similar in that they involve the flame spreading process. Thus the flame spread formulation is the same for these phases but with the intention of changing the particular coefficients and the initial conditions as each phase of fire growth is entered. The solution is done in such a way to maintain continuity between phases of fire growth. In what follows, one may note similarities with the SQW model (even the generalized version reported by Hasemi and others (1997)) because of the Volterra-type integral used. However, in other parts of the

formulation the differences are pronounced relative to SQW modeling such that the formulation will be given in some detail. The first step is the description of the extended flame flux profile as an imposed flux applied over the distance y_c followed by an exponential decay with characteristic length δ_f, as in

$$\dot{q}''_{wf}(y) = \dot{q}''_{w}\left[H(y) + \left(\exp\left\{\frac{-(y-y_c)}{\delta_f}\right\} - 1\right)H(y-y_c)\right] \quad (36)$$

were $H(x)$ is the Heaviside function. In the case where the flame is only from the material burning (by imagining the ignition burner to provide only external radiant flux by being away from the wall) Kulkarni and others (1994) gave the following experimental results. The heat flux is 24.3 kW/m^2 for Douglas Fir particleboard and 34.5 kW/m^2 for cardboard. With the length of constant flux x_c identified with the pyrolysis front x_p, the characteristic length was found to be proportional to the extended flame length and correlated as $\delta_f = (y_f - y_p)/c_f$, with value of c_f as 1.37. However, with the pilot burner flames merging with the material flames in the ISO 9705 (ISO 1993a) test protocol, the more appropriate data to use is reported by Kokkala and Heinila (1991). Using their figures of the flame flux profiles for different burner sizes and outputs, we estimated the values for the ratio of extended flame length over characteristic length to vary from 1.2 to 1.4. The actual values used in connection with the room test data are the following. The imposed heat flux $\dot{q}''_w$ and cooling flux $\dot{q}''_{ig}$ are allowed to be functions of material properties such as ignition temperature and surface emissivity, but the flame properties of flame temperature, flame emissivity, and convection coefficient are kept the same for all tests. This results in a different heat flux for each material during flame spreading and is an advance over some other flame spread models. As to the ratio of extended flame length to characteristic length, the value of $c_f = 1.3$ was the best fit to our room test data during the phase of upward flame spread. Other values for lateral and downward flame spread are given later. Having established a flame heat flux profile, we analyzed for the quasi-steady speed of the pyrolysis front by simply using the equality $y - y_{ig} = v_p(t_{ig} - t)$ in Equation (36) to represent the sliding movement of the imposed heat flux profile over a given spot until ignition is reached. With this substitution, the Duhamel supposition integral is the convolution of the material's thermal response to a constant imposed flux with the time changing imposed flux, as in

$$\begin{aligned} T_{ig} - T_m &= \frac{d(T_s - T_m)}{dt} \otimes \dot{q}''_{wf}\left(v_p(t_{ig} - t) + y_{ig}\right) \\ &= (T_s - T_m) \otimes \frac{d\dot{q}''_{wf}\left(y_{ig} - v_p(t - t_{ig})\right)}{dt} \end{aligned} \quad (37)$$

where the integration is taken from zero to the time of ignition, t_{ig}, to correspond to ignition temperature $T_{ig.}$ During flame spreading, the times to ignition of additional materials become large compared to the time to ignition of the initial ignited area. As a consequence, for some materials the thermal response would become thermally thin or even approach the steady-state condition, which tends to complicate the solution.

The choice of the function for the material's thermal response is crucial to the development of the formula for the pyrolysis front speed. A first thought might be to apply the Duhamel supposition integral in the same manner as Equation (24) for thermally thick materials. But one realizes the surface heat fluxes are decreasing over time and then construct an integral that has no analytical solution. However, if the radiant flux is linearized and the gas temperature is assumed constant, then the analytical solution to Equation (24) is given by the complementary error function solution (Dietenberger 1991),

$$\begin{aligned} T_s &= T_m + (T_{eq} - T_m) \\ &\quad \times \left[1 - \exp\left(\frac{h_{eq}^2(t - t_0)}{k\rho C_p}\right)\operatorname{erfc}\left(\sqrt{\frac{h_{eq}^2(t - t_0)}{k\rho C_p}}\right)\right] \end{aligned} \quad (38)$$

where

$$\begin{aligned} \dot{q}''_{wg} &= \varepsilon_m \sigma\left(T_g^4 - T_a^4\right) + h_c(T_g - T_a) \\ &= \varepsilon_m \sigma\left(T_{eq}^4 - T_a^4\right) + h_c(T_{eq} - T_a) = h_{eq}(T_{eq} - T_a) \end{aligned} \quad (39)$$

In the case of a thermally thin material, the corresponding solution for the surface temperature is

$$T_s = T_m + (T_{eq} - T_m)\left[1 - \exp\left(\frac{-h_{eq}(t - t_0)}{\rho C_p \delta_m}\right)\right] \quad (40)$$

In the evaluation of the Duhamel integral Equation (37), most fire growth models use the first form of Equation (37), where imposed flux is considered to be constant up to x_c and then suddenly drop to zero without an exponential decay type function. It is simple to derive the time derivative of surface temperature when a straightforward analytical function is available for temperature predictions. For example, for surface temperature proportional to the square root of time, Equations (17) and (24) are derived from evaluating Equation (37). However, we use the Laplace transform analytical method to solve Equation (37) instead of a numerical solution approach in Quintiere's model. This involves obtaining the inverse transforms of the temperature response and transient imposed fluxes and multiplying them to result in an overall inverse transform that then can be transformed back to provide a modified surface temperature solution. Because we already have the inverse transform of Equations (38) and (40), it was then simpler to evaluate time derivatives of the heat flux profile and derive the inverse transform of the resulting functions. The transform solution of the second form of Equation (37) using these methods resulted

in an analytical function that is rather complex and is given as equation (45) in Dietenberger (1991). The time to ignition that still appears in the formula is related to the pyrolysis spread rate with the substitutions $(y_0 - y_{ig})/v_p = t_{ig} - t_0$ and $(y_c - y_{ig})/v_p = t_{ig} - t_c$ and $(y_c - y_{ig})/v_p = t_{ig} - t_c$, which then make the formula just an implicit function of the pyrolysis spread rate. The function can be greatly simplified by using the results from Kulkarni and others to observe that $y_p = y_{ig} = y_c$ and $y_0 - y_{ig} >> \delta_f$. The resulting simplified formula from Dietenberger (1991) is

$$v_p = \delta_f / \tau_m \tag{41}$$

where for thermally thick materials, the material time constant is

$$\tau_{m,thick} = k\rho C_p \left(\frac{T_{ig} - T_m}{\dot{q}''_w - \dot{q}''_{ig}} \right)^2 \tag{42}$$

and for thermally thin materials, the material time constant is instead

$$\tau_{m,thin} = \rho C_p \delta_m \left(\frac{T_{ig} - T_m}{\dot{q}''_w - \dot{q}''_{ig}} \right) \tag{43}$$

An accurate, but simple, interpolation formula for the material time constant over the full thermal regime from thick to thin was derived by Dietenberger (1991) with the result

$$\tau_m = \tau_{m,thick} \left(\frac{1}{2} + \sqrt{\frac{1}{4} + \left(\frac{\tau_{m,thick}}{\tau_{m,thin}} \right)^n} \right)^{\left(\frac{-2}{n} \right)} \tag{44}$$

where the value $n = 1.3$ obtained for the PMMA material is assumed to apply for other materials. One then realizes that all the material's parameters for thermal response are contained within the material time constant, τ, applicable to flame spreading. Although Equations (42) and (43) are similar to simple formulas for time to ignition (see Eq. (20) as an example), they are an exact result specifically derived for the flame spreading analysis. Several other flame spread models will call the material time constant as the time to ignition, but in reality that is a misnomer. Indeed, the effect of a sluggish burner on the time to ignition for the first ignited region leads to a different formula that uses the very same material parameters for thermal response. Because of the different ways in which material parameters of thermal response are used in a fire growth model, one may come across a subtle behavior for the flashover phenomena not apparent with a limited number of room burn tests.

The final parameter to model is the characteristic length of flame extension. For upward and lateral flame spread, the flame length, y_f, or as a better alternative, the flame area, A_f, is a direct function of total HRR, $\dot{Q}_t$, and pyrolysis area, A_p. For downward flame spread, the characteristic length is related directly to thermal radiation from the bottom of the upper smoky gas layer. The functional dependency is nonlinear, for which an analytic Laplace transform solution is not possible. A good solution can be obtained, however, by piecewise linear approximations to the flame area relationships and by restarts of solution that maintains continuity as the coefficients are changed. The dependency on the HRR implies the use of the heat release flux data from the cone calorimeter in an analytic approximate functional form. Therefore, in the linear portion of fire growth and by multiplying both sides of Equation (41) by the pyrolysis edge arc length, the controlling equation for fire growth is

$$\frac{dA_p}{dt} = \frac{a + bA_p + c\dot{Q}_t}{\tau_m} \tag{45}$$

where the total HRR is given by

$$\begin{aligned} \dot{Q}_t = \dot{Q}_b + \dot{Q}_m = & \sum_i \Delta\dot{Q}_{b,i} H(t - t_i) + \sum_j A_p(t_j)\dot{Q}''_m(t - t_j) \\ & + \int_0^{t-t_j} \dot{Q}''_m(t - t_j - \xi)\dot{A}_p d\xi \end{aligned} \tag{46}$$

The index i provides tracking of changes in the burner output, which is given as a user input value. The index j provides tracking of changes in the phase of fire growth due to the coefficients a, b, and c changing or to "instantaneous" ignition of newly covered areas for step increases of the burner. The integral in Equation (46) is what turns Equation (45) into a Volterra-type integral and represents the HRR from the increasing pyrolysis area. The next step is to determine the heat release flux profile, $\dot{Q}''_m(t)$, as an analytic approximation to the cone calorimeter data so that a Laplace analytical solution is found for Equation (45). Then the values for the coefficients a, b, and c for upward and downward flame spread will be determined directly from experimental data.

After taking into account several factors related to the material's profile for the heat release flux, the appropriate choice is the step exponential decay function,

$$\dot{Q}''_m(t) = \dot{Q}''_{m,ig} H(t) \exp(-\omega_m t) \tag{47}$$

Substitution of Equation (47) into Equation (46) and setting $t^* = t - t_j > 0$ results in a simplified recursive form suitable for solution restarts as

$$\begin{aligned} \dot{Q}_m = & \left(\dot{Q}''_{m,ig} A_{ig,j} + \dot{Q}_m(t_j) \right) \exp\left(-\omega_m t^* \right) \\ & + \int_0^{t^*} \dot{Q}''_{m,ig} \exp\left(-\omega_m \left(t^* - \xi \right) \right) \dot{A}_p d\xi \end{aligned} \tag{48}$$

and

$$\dot{Q}_b = \dot{Q}_b(t_j) + \sum_{t_i > t_j} \Delta\dot{Q}_{b,i} H\left(t^* - t_i^* \right) \tag{49}$$

The total pyrolysis area in the recursive form is

$$A_{\mathrm{p}} = A_{\mathrm{ig},j} + A_{\mathrm{p}}\left(t_j\right) + \int_0^{t^*} \dot{A}_{\mathrm{p}}\left(\xi + t_j\right) d\xi \tag{50}$$

For brevity we define, $A_{\mathrm{p}j} = A_{\mathrm{ig},j} + A_{\mathrm{p}}\left(t_j\right)$, $\dot{Q}_{\mathrm{b}j} = \dot{Q}_{\mathrm{b}}\left(t_j\right)$, and $\dot{Q}_{\mathrm{m}j} = \dot{Q}''_{\mathrm{m,ig}} A_{\mathrm{ig},j} + \dot{Q}_{\mathrm{m}}\left(t_j\right)$.

The Laplace transform of Equation (45) into the frequency domain, s, is

$$s\widetilde{A}_{\mathrm{p}} - A_{\mathrm{p}j} = \frac{a + c\left(\dot{Q}_{\mathrm{b}j} + \sum \Delta\dot{Q}_{\mathrm{b},i} \exp\left(-t_i^* s\right)\right)}{s\tau_{\mathrm{m}}} + \frac{b\widetilde{A}_{\mathrm{p}}}{\tau_{\mathrm{m}}} + \frac{c\left(\dot{Q}_{\mathrm{m}j} + \left(s\widetilde{A}_{\mathrm{p}} - A_{\mathrm{p}j}\right)\dot{Q}''_{\mathrm{m,ig}}\right)}{\left(s + \omega_{\mathrm{m}}\right)\tau_{\mathrm{m}}} \tag{51}$$

The rearrangement of Equation (51) to solve for the pyrolysis area in frequency domain is given by

$$\widetilde{A}_{\mathrm{p}} = \left[\left(s + \omega_{\mathrm{m}}\right)\left(A_{\mathrm{p}j} + \frac{a + c\left(\dot{Q}_{\mathrm{b}j} + \sum \Delta\dot{Q}_{\mathrm{b},i} \exp\left(-t_i^* s\right)\right)}{s\tau_{\mathrm{m}}}\right) + \frac{c\left(\dot{Q}_{\mathrm{m}j} - A_{\mathrm{p}j}\dot{Q}''_{\mathrm{m,ig}}\right)}{\tau_{\mathrm{m}}}\right] \div \left(\left(s - \frac{b}{\tau_{\mathrm{m}}}\right)\left(s + \omega_{\mathrm{m}}\right) - \frac{cs\dot{Q}''_{\mathrm{m,ig}}}{\tau_{\mathrm{m}}}\right) \tag{52}$$

Zero for the denominator of Equation (52) result in two roots,

$$s_i = \frac{b + c\dot{Q}''_{\mathrm{m,ig}} - \omega_{\mathrm{m}}\tau_{\mathrm{m}}}{2\tau_{\mathrm{m}}} - \left(-1\right)^i \sqrt{\left(\frac{b + c\dot{Q}''_{\mathrm{m,ig}} - \omega_{\mathrm{m}}\tau_{\mathrm{m}}}{2\tau_{\mathrm{m}}}\right)^2 - \frac{b\omega_{\mathrm{m}}}{\tau_{\mathrm{m}}}} \tag{53}$$

which are the same as Karlson and others have derived. It is often asserted that if the roots are positive, then the fire growth is accelerative, whereas negative values for the roots means that the fire is dying out despite flame spreading. Karlson allows that if the square root integrand is also negative, the fire growth has an oscillation behavior. Our interest in Equation (53) would be in a design of a test method that avoids extremes in the test times as well as results in a relatively steady fire growth for a standard representative material, such as the red oak flooring used in ASTM E 84. This means setting the magnitude of roots to a reasonable value for a standard material and solving for the imposed flux (via the material time constant) that the burner should provide. The material time constant that corresponds to a minimum value for the roots is

$$\tau_{\mathrm{m},st} = \frac{b + c\dot{Q}''_{\mathrm{m,ig}}}{\omega_{\mathrm{m}}} \tag{54}$$

Comparing with the actual material time constant provides an indication of the accelerative potential of the fire growth during any phase. With the current room tests, one encounters a real difficulty in application of these simple concepts to describing the room flashover. Not only are there multiple numerator terms in Equation (52) representing different contributions to fire growth, the coefficients of fire growth, a, b, and c, change with each phase of fire growth. The fire growth model has a two-part solution, the pyrolysis area and HRR, as

$$\begin{aligned} A_{\mathrm{p}} = {} & \left(\frac{a + c\left(\dot{Q}_{\mathrm{m}j} - A_{\mathrm{p}j}\dot{Q}''_{\mathrm{m,ig}} + \dot{Q}_{\mathrm{b}j}\right)}{\tau_{\mathrm{m}}} + A_{\mathrm{p}j}\omega_{\mathrm{m}}\right) \times \left(\frac{\exp\left(s_1 t^*\right) - \exp\left(s_2 t^*\right)}{s_1 - s_2}\right) \\ & + \frac{c}{\tau_{\mathrm{m}}} \sum_{t_i > t_j} \Delta\dot{Q}_{\mathrm{b}j} H\left(t^* - t_i^*\right) \times \left(\frac{\exp\left(s_1\left(t^* - t_i^*\right)\right) - \exp\left(s_2\left(t^* - t_i^*\right)\right)}{s_1 - s_2}\right) \\ & + \frac{c}{\tau_{\mathrm{m}}} \sum_{t_i > t_j} \Delta\dot{Q}_{\mathrm{b}j} H\left(t^* - t_i^*\right)\left(\frac{\omega_{\mathrm{m}}}{s_1 - s_2}\right) \times \left(\frac{\exp\left(s_1\left(t^* - t_i^*\right)\right) - 1}{s_1} - \frac{\exp\left(s_2\left(t^* - t_i^*\right)\right) - 1}{s_2}\right) \\ & + \left(\frac{a + c\dot{Q}_{\mathrm{b}j}}{\tau_{\mathrm{m}}}\right)\left(\frac{\omega_{\mathrm{m}}}{s_1 - s_2}\right)\left(\frac{\exp\left(s_1 t^*\right) - 1}{s_1} - \frac{\exp\left(s_2 t^*\right) - 1}{s_2}\right) \\ & + A_{\mathrm{p}j}\left(\frac{s_1 \exp\left(s_1 t^*\right) - s_2 \exp\left(s_2 t^*\right)}{s_1 - s_2}\right) \end{aligned} \tag{55}$$

$$\begin{aligned} \dot{Q}_t = {} & \dot{Q}_{\mathrm{b}j} + \left(\frac{\left(a + c\dot{Q}_{\mathrm{b}j}\right)\dot{Q}''_{\mathrm{m,ig}} - b\left(\dot{Q}_{\mathrm{m}j} - A_{\mathrm{p}j}\dot{Q}''_{\mathrm{m,ig}}\right)}{\tau_{\mathrm{m}}}\right) \times \left(\frac{\exp\left(s_1 t^*\right) - \exp\left(s_2 t^*\right)}{s_1 - s_2}\right) \\ & + \sum_{t_i > t_j} \Delta\dot{Q}_{\mathrm{b}j} H\left(t^* - t_i^*\right) \\ & + \frac{c\dot{Q}''_{\mathrm{m,ig}}}{\tau_{\mathrm{m}}} \sum_{t_i > t_j} \Delta\dot{Q}_{\mathrm{b}j} H\left(t^* - t_i^*\right)\left(\frac{\exp\left(s_1\left(t^* - t_i^*\right)\right) - \exp\left(s_2\left(t^* - t_i^*\right)\right)}{s_1 - s_2}\right) \\ & + \dot{Q}_{\mathrm{p}j}\left(\frac{s_1 \exp\left(s_1 t^*\right) - s_2 \exp\left(s_2 t^*\right)}{s_1 - s_2}\right) \end{aligned} \tag{56}$$

The roots are considered complex numbers, which means the above solutions are considered to be in the complex

variable domain. Specialized computer algorithms were developed for complex variable evaluations so that the above functions could be programmed directly (and found to be very efficient compared with numerical solutions such as Quintiere's model).

It is well known that the gas mixing in recirculation zones of the gas flow train causes a significant reduction of the peak HRR as calculated for some materials, particularly those with low total HRR. It is not as well known that the same gas mixing in recirculation zones of the gas flow will cause an instant step increase in HRR to appear as a ramping HRR up to the peak value. A typical time constant, $\tau_c = 9.3$ s, was measured for the methanol flame used in the cone calorimeter with the formula

$$\dot{Q}''_{\text{fuel}} \otimes \dot{S}_c = \dot{Q}''_{\text{fuel}}\left(1 - \exp\left(-t/\tau_C\right)\right) \tag{57}$$

A similar effect is expected for a combustible material that behaves as Equation (47) with the result

$$\dot{Q}''_{\text{m,cone}} = \dot{Q}''_{\text{m}} \otimes \dot{S}_c = \dot{Q}''_{\text{m,ig}}\left(\frac{\exp\left(-\omega_m t\right) - \exp\left(-t/\tau_c\right)}{1 - \omega_m \tau_c}\right) \tag{58}$$

The total heat release flux is the integral of Equation (58) as

$$\text{THR} = \int_0^\infty \dot{Q}''_{\text{m,cone}} dt = \int_0^\infty \dot{Q}''_{\text{m}} dt = \dot{Q}''_{\text{m,ig}} / \omega_m \tag{59}$$

and is substituted into Equation (58). At the zero slope of Equation (58), the time of maximum HRR is

$$t_{\text{peak}} = \frac{\tau_c \ln\left(\omega_m \tau_c\right)}{\omega_m \tau_c - 1}$$

which when substituted into Equation (58) results in

$$\begin{aligned} \text{PHRR} &= \dot{Q}''_{\text{m,cone}}\left(t_{\text{peak}}\right) \\ &= \frac{\text{THR}\,\omega_m}{1 - \omega_m \tau_c}\left(\left(\omega_m \tau_c\right)^{\left(\omega_m \tau_c / \left(1 - \omega_m \tau_c\right)\right)} \right. \\ &\qquad \left. - \left(\omega_m \tau_c\right)^{\left(1/\left(1 - \omega_m \tau_c\right)\right)}\right) \end{aligned} \tag{60}$$

Materials with high ratio of PHRR/THR, such as the FRT polyurethane foam, could have its true peak heat release double that of the measured PHRR. One advantage of using THR is that it represents mostly the total volatiles available in a given thickness of a material and is relatively unaffected by the edge and backing conditions of the specimen in the cone calorimeter. Recall the gypsum board (as a backing material in the room tests) serves to absorb heat losses that otherwise would be a significant cause of a second peak HRR as observed in cone calorimeter tests. As a further validation, Equation (58) was able to reproduce the ramp behavior of HRR immediately following ignition for most materials tested in the cone calorimeter. Indeed, the accumulation of volatiles above the material just prior to ignition would give rise to a spike in the heat of combustion at ignition but tends to be smeared by the time constant of the sampling gas analysis system.

In the section on the cone calorimeter data, the PHRR and THR are shown approximately as linear functions of the cone flux, and their values are listed in Table 3. To determine the appropriate cone flux level for use in the fire growth model, we consider the data from Rhodes (1994) in which a small-diameter fluxmeter was inserted through a PMMA sample (which has emissivity of unity) exposed to 50 kW/m^2. At this flux level, the PMMA flame is more than 20 cm high; this led Rhodes to calculate the flame emissivity to have the value 0.09, which we adopt for our data. However, we differ slightly as to the convective heat transfer from the flame to the specimen. For this we use the convective heat transfer coefficient calibrated for the horizontal position of specimen as Equation (7). Another factor to consider is that the viewfactor from the cone heater to a small-diameter fluxmeter is very nearly unity, whereas that to the specimen with dimensions of 100 by 100 mm has the value 0.9679 (Janssens 1991). Under these conditions Rhodes measured with the fluxmeter a value 77 kW/m^2. Using our assumptions, we obtained a flame temperature of 1,154 K, which corresponds to a flame radiative flux of 9 kW/m^2 and a convective flux of 18 kW/m^2 on the fluxmeter. However, the net flux on the PMMA must be adjusted for the reduction in the cone heater viewfactor and for the setting of surface temperature to about 600 K for pyrolyzing PMMA instead of 298 K for the fluxmeter. This means the flame flux is reduced and reradiation from the surface is increased such that the net heat flux comes out at 62 kW/m^2, a reduction of 15 kW/m^2 from that measured with the fluxmeter and an increase of 12 kW/m^2 from that of the cone heater setting.

We can expect a similar situation with respect to net flux on the pyrolyzing wall materials heated by the propane burner in the room test. Thus 55 kW/m^2 measured with a fluxmeter on the wall would give a net flux of 44.5 kW/m^2 for the PMMA material at pyrolyzing temperatures (recall $T_f = 1{,}173$ K, $\varepsilon_f = 0.395$, and $h_c = 0.0165$ kW/m^2 K for the propane burner). The cone heater would have had to be set at 33 kW/m^2 in order to produce a net flux of 44.5 kW/m^2 on the pyrolyzing PMMA specimen in the cone calorimeter, and thus achieve also the same level of heat release flux expected in the room test. Although the PMMA has been used as an example, other materials gave somewhat similar but varying results for the required cone flux levels. The important result is that a cone heater flux required to provide the correct levels of HRR is much less than that measured with fluxmeters in the wall or that required for wall ignition. Therefore a fire growth model based on the use of only a single flux level in the cone calorimeter is not viable, unless one has access to a sophisticated CFD pyrolysis model.

Because the measurements of HRR for the room tests are based on the oxygen consumption method similar to the

cone calorimeter, the consideration of gas flow trains affecting the time response of HRR also applies. Although nitrogen gas and span gas are used to calibrate the steady-state levels of signals from the gas analyzers, they are also used to directly determine the time response of the gas flow analysis system. Using a formula like Equation (33), the gas profiles responding to step changes in the calibration gases for oxygen, carbon dioxide, and carbon monoxide are most consistent with the time constant, $\tau_g = 10$ s. For the case when the propane burner is under the hood for the 100/300 kW calibration, a low-pass digital filter with a time constant of 10 s is applied to the mass flow rate signal from the electronic mass flow device and the output is then multiplied by the heat of combustion of propane. The resulting HRR is found to be in close agreement with the HRR from the oxygen consumption even during step changes in the burner output. However, for the case when the burner is placed in the corner of the test room, the mixing of combustion products in the upper gas layer adds an effective time constant to the gas concentrations escaping out of the doorway to the hood. Putting the propane burner through the same 100/300 kW calibration sequence as under the hood, we measured the room time constant as $\tau_{room} = 18$ s by application of a second low-pass digital filter to the filtered HRR and comparing with the HRR from the oxygen consumption method. If a fire growth model does not incorporate a submodel for the gas mixing in the upper hot gas layer, then double low-pass filters with time constants of 10 and 18 s should be applied to the model predictions in order to compare with our room test results. The analytical equivalent for the analytical fire growth model is the double application of the Duhamel's integral as

$$\dot{Q}_{\text{test}} = \dot{Q}_t \otimes \dot{S}_{\text{g}} \otimes \dot{S}_{\text{room}} \tag{61}$$

as a modification to Equation (56). Simplicity to the model is still maintained when the following generic evaluation is performed for Equation (61):

$$\exp\left(s_i t^*\right) \otimes \dot{S}_1 \otimes \dot{S}_2 = \left(\frac{\tau_1 \exp\left(-t^*/\tau_1\right)}{(\tau_2 - \tau_1)(1 + s_i \tau_1)} + \frac{\tau_2 \exp\left(-t^*/\tau_2\right)}{(\tau_1 - \tau_2)(1 + s_i \tau_2)} + \frac{\exp\left(s_i t^*\right)}{(1 + s_i \tau_1)(1 + s_i \tau_2)} \right) \tag{62}$$

Upward Fire Growth Parameterization

This completes the model solution method, and the coefficients a, b, and c will now be determined to complete the analytical fire growth model. For the case of upward flame spread, recall that the flame height was assumed to be a nonlinear function of HRR and pyrolysis area, which was then linearized. The correlation from experimental data (Tran and Janssens 1993) of visible flame height is

$$y_{\text{f}} = y_0 + 0.0433\left(\frac{\dot{Q}_t}{2w}\right)^{2/3} \tag{63}$$

Because the arc length of the pyrolysis front is $2w$, Equation (63) is rearranged as the flame area,

$$A_{\text{f}} = 2w\left(y_{\text{f}} - y_0\right) = 0.0433(2w)^{1/3}\dot{Q}_t^{2/3} \tag{64}$$

In the linearization of Equation (64), a good reference point is the transition from upward to lateral flame spread, which is the flame height, $y_{\text{fu}} - y_0 = 2.4 - 0.3 = 2.1$ m. Substitution into Equation (64) shows that the HRR at the reference point can be related as $\dot{Q}_{t\text{u}} = 161 A_{\text{fu}}$. The linear approximation to Equation (64) is then

$$A_{\text{f}} = A_{\text{fu}} + \frac{dA_{\text{f}}}{d\dot{Q}_t}\left(\dot{Q}_t - \dot{Q}_{t\text{u}}\right) = \left(1 - 161\frac{dA_{\text{f}}}{d\dot{Q}_t}\right)A_{\text{fu}} + \frac{dA_{\text{f}}}{d\dot{Q}_t}\dot{Q}_t \tag{65}$$

At first it seems the derivative of the flame area should also be evaluated at the reference point. However, the flame area would be much too large at lower values of HRR, particularly at 40 kW for the ASTM burner and 100 kW for the ISO burner. With only a 23% increase in the derivative at the reference point the formula for the flame area for use in the model becomes

$$A_{\text{f}} = \frac{A_{\text{fu}}}{5.6} + \frac{\dot{Q}_t}{196} \tag{66}$$

In the case of the ASTM burner, where HRR is 40 kW and width of burner is 0.3 m, the computed flame area impinged on the wall is 0.429 m^2. This converts to a flame length of 0.715 m, compared with 0.71 m obtained with Equation (64). Likewise, for the case of the ISO burner, where HRR is 100 kW and width of burner is 0.17 m, the computed flame area is 0.638 m^2. This converts to a flame length of 1.88 m, compared with 1.91 m obtained with Equation (64). With these approximations it would be possible to examine the effects of changes in the burner dimensions or output to a limited extent. Returning finally to the discussion concerning the flame characteristic length, the coefficients a, b, and c can now be easily determined by noting that

$$\begin{aligned} 2w\delta_{\text{f}} &\equiv \frac{2w\left(y_{\text{f}} - y_0\right) - 2w\left(y_{\text{p}} - y_0\right)}{c_{\text{f}}} \equiv \frac{A_{\text{f}} - A_{\text{p}}}{c_{\text{f}}} \\ &\equiv \frac{A_{\text{fu}}}{5.6c_{\text{f}}} + \frac{\dot{Q}_t}{196c_{\text{f}}} - \frac{A_{\text{p}}}{c_{\text{f}}} = a + c\dot{Q}_t + bA_{\text{p}} \end{aligned} \tag{67}$$

Inspection of Equation (55) shows that the initial ignition area can be set to zero because a positive value for the coefficient a will ensure a solid growth in the pyrolysis area. Recall that the parameter c_{f} was allowed to have a range between 1.2 and 1.4, for which we found the optimum value to be 1.3. It was found this overall set of model constants predicted quite well the upward flame spread for all the materials tested, without the need for additional empiricism or functions.

Downward Fire Growth Parameterization

Before discussing our problems with predicting lateral flame spread, the model for during downward flame spread turns out to be relatively simple. The simple concept is that the radiative flux profile developed at the flame front is due to the viewfactor of radiation from the bottom surface of the smoky and flaming upper gas layer to a narrow strip ahead of the flame front. As an approximation, assume that the radiating surface is infinite in the direction parallel to the flame edge. Then the viewfactor to a narrow strip ahead of the flame edge from a perpendicularly finitely wide sheet of width ℓ is

$$F_{dx-\ell} = \frac{1}{2}\left(1 - \frac{1}{\left(1+(\ell/y)^2\right)^{1/2}}\right) \approx \frac{1}{2}\exp(-y/\ell) \qquad (68)$$

Noting the similarity with Equation (36), it is obvious to identify $\ell = \delta_f$ for the downward flame spread geometry. Noting that the length of the flame edge is the length of the room, the coefficient a is merely the area of the radiating sheet for downward flame spread along one wall. Because there are three walls with downward flame spreading, we make the identification for the coefficients as

$$a = 3A_{roof}/c_f, \quad b = -a/A_{max}, \quad c = 0 \qquad (69)$$

The coefficient b is defined to allow for damping of fire growth because all the material becomes involved. Finally, the material time constant is not changed, because there is not a better estimate for the imposed heat flux at the flame front for downward flame spreading. Indeed, the results show the model's good agreement with experiment during this fourth stage of downwardly rapid flame spread to the event of flashover.

Empirical Relationships to Predict Lateral Flame Spread

The reason for a special section on lateral flame spread is the considerable difficulty in developing the submodels needed to determine the transition to and out of lateral flame spread as well as in determining the coefficients of the fire growth model. Indeed, once the flame extends considerably on the ceiling, the correlation Equation (67) represents an extrapolation from the experimental data. There is also the factor of a small lateral flame spreading along with the upward flame spread, resulting in a V-shaped pyrolysis region on the wall. This is partly a reason for adopting Equation (45) for the rate of pyrolysis area as the controlling equation for fire growth. Eventually, at some critical time of fire growth, the HRR will change direction as a result of upward flame spreading being exhausted. This appears to occur when the pyrolysis area reaches a critical level given by

$$A_{p,cr} = 1.7A_{fu} \qquad (70)$$

This is equivalent to a critical lateral spread of the pyrolysis region at the ceiling with an extension length slightly greater than the width of the burner. Our video recordings of fire growth appear to be consistent with this observation, although the transition to only a lateral flame spread is difficult to detect visually. At the critical time it is expected the nature of flame extension on the ceiling will change the coefficients a, b, and c, which will require a solution restart. The simplest change is to modify the parameter c_f, which is the ratio of flame extension length over the imposed flux profile characteristic length. To further simplify evaluation of these constants, we considered only the materials that flashed over during the 100-kW output of the burner. This left us with 11 materials, none of which had FRT. Six of these 11 materials correlated well with the value $c_f = 15$ and are the materials with a constant or decreasing HRR during the lateral flame spread phase. The pyrolysis area continuously increases while the HRR is decreasing (see tests 3, 5, 9, 12, 14, and 16 in the Part 1 report). Because of the order of magnitude increase in the value of c_f as compared to its upward flame spread value, it is supposed the dominant process is lateral flame spread in opposed flow, as in the LIFT apparatus. For the remaining five materials, it was also necessary to go back to Equation (65) and change the derivative to a different constant, as $dA_f / d\dot{Q}_t = 0.011$ m²/kW. This is also the value consistent with experimental data obtained for flame spread with assisting flow (Gandhi and others 1997), such as that in the Steiner tunnel (ASTM E 84). The c_f parameter in this case correlated best with the value 5. These five materials correspond to tests 10, 11, 13, 17, and 18, and all of them had continuously rising HRR to flashover. To provide for a clear demarcation into two groups of lateral flame spread, the product of time to ignition and total heat release flux is used to define a switching function as

$$F_{sw} = \frac{1}{1 + 1.1671\times10^6 \times \left(t_{ig}\times \mathrm{THR}\right)^{-20}} \qquad (71)$$

so it can be used in the following functions:

$$c_f = 5F_{sw} + 15(1 - F_{sw}) \qquad (72)$$

$$\frac{dA_f}{d\dot{Q}_t} = 0.011F_{sw} + 0.0051(1 - F_{sw}) \qquad (73)$$

Thus materials in the first group with low enough values of time to ignition or total heat release flux will have a relatively slow lateral flame spreading and result in a high value of time to flashover as compared to materials in the second group. It seems contradictory that as ignition time is decreased, the time to flashover will increase. To clarify this we note that within a group, a decrease in the time to ignition will also decrease the time to flashover. It is in the ability to go from a group of materials associated with fast flame spread to a group associated with slow flame spread

that a decrease in time to ignition would achieve a higher time to flashover. Thus the multiple functionalities found for the time to ignition data would create a problem with using simple correlations for time to flashover that use the ignitability parameters. Because of our desire to avoid multiple roles for the time to ignition data, alternative forms of the switching function that do not include the time to ignition variable did not succeed. Progress on this problem will be considerable if experiments to better characterize the lateral/ceiling flame spread behavior are done.

To complete the model, the criteria for the transition to downward flame spread at time t_3 is needed so that the fire growth solution can be restarted with the new coefficients corresponding to downward flame spread. Using the pyrolysis area or any other single parameter generally did not succeed as candidate criteria. However, an empirical relationship was found to relate the time at the transition of lateral to downward flame spread t_3 as function of time, HRR, and pyrolysis area at the transition points 2 (upward to lateral) and 3 (lateral to downward) as

$$t_3 = 1.5t_2 + \frac{\dfrac{A_{p3}}{0.00431\dot{Q}_{t3}} - 1}{\dfrac{A_{p2}}{\dot{Q}_{t2}}\left(1 + \left|\dfrac{A_{p3}}{0.0154\dot{Q}_{t3}} - 1\right|^{2.54}\right)} \tag{74}$$

With this function it was possible to primarily focus on the fire growth characteristics. On the other hand, there is the situation where the time of transition to the fourth phase (downward flame spread) will increase and decrease in different regimes depending on the ratio of pyrolysis area over HRR. The multiple functionalities developed for various parameters in the fire growth model are not really satisfactory. Perhaps a more explicit dependence on the development of the upper gas layer in affecting lateral and downward flame spread in conjunction with experimentation will be sufficient to improve the analytical model. For the case of the materials with FRT, there are only three tests in which it is not really possible to develop empirical relationships. Thus they are modeled on a case-by-case basis with a view toward demonstrating features of the model.

Comparison to HRR for FPL Room Tests

The HRR plots shown in the first report on a test-by-test basis are replotted together in Figures 62 to 64. It is noted that all four plywoods and the OSB tend to have low time to ignition and high PHRR to account for a rapid initial increase in HRR, but for which a low value of THR will not support a rapid lateral flame spread. The oak veneer plywood has an especially high value of PHRR that accounts for the initial rapid increase in HRR as compared to all other materials. It is noted the flashover event with the plywood materials can occur relatively suddenly after a latent period of slow lateral

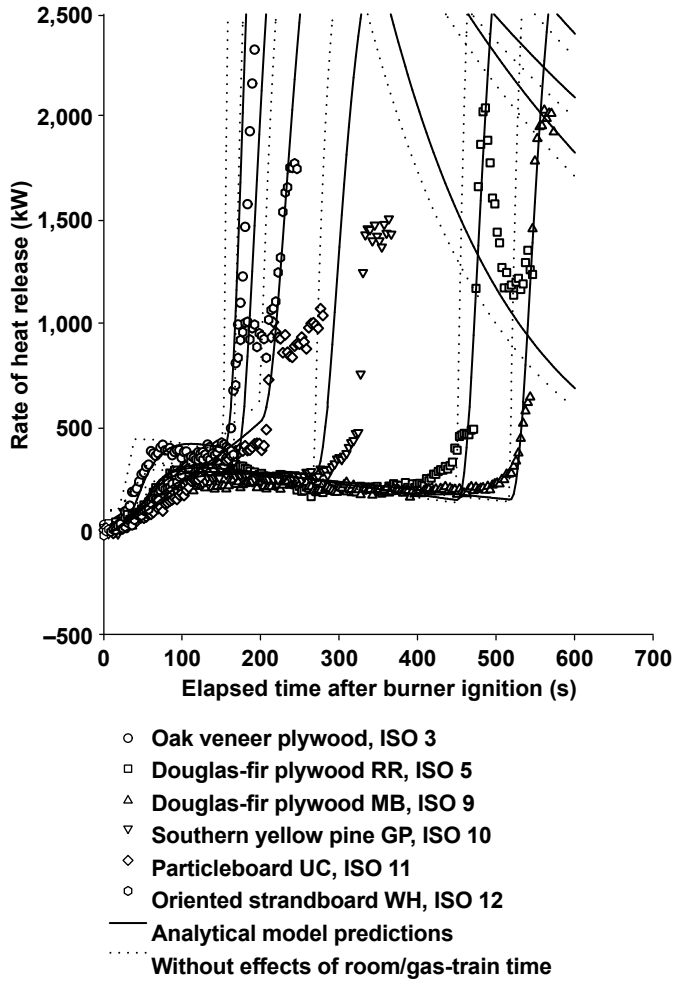

Figure 62. Model predictions for test nos. 3, 5, 9, 10, 11, and 12.

flame spread or even of the fire appearing to die down. The wood composites and the Southern Pine flooring lumber in both Figures 62 and 63 appear to have rapid lateral flame spreading as their HRRs continue increasing. These materials have relatively high values for THR and time to ignition to place them in the group with rapid lateral flame spread. Yet because of the higher time to ignitions as compared to other materials, the initial rise of HRR is relatively slower. But with high values of THR, a larger flame relative to pyrolysis area can be supported during lateral flame spread and thus lead to continuing increasing HRR.

In the case of materials with FRT, their relatively lower values of PHRR and THR will not give much increase in HRR during the 100-kW level of the burner. However, the effect of increasing the burner to 300 kW after a latent heating period of 10 min at the 100-kW level is to cause fairly rapid ignition of additional areas. In Figure 64, the additional ignited area sufficient to reach the HRR levels observed is 2.9 m^2, which also is applicable to the gypsum board.

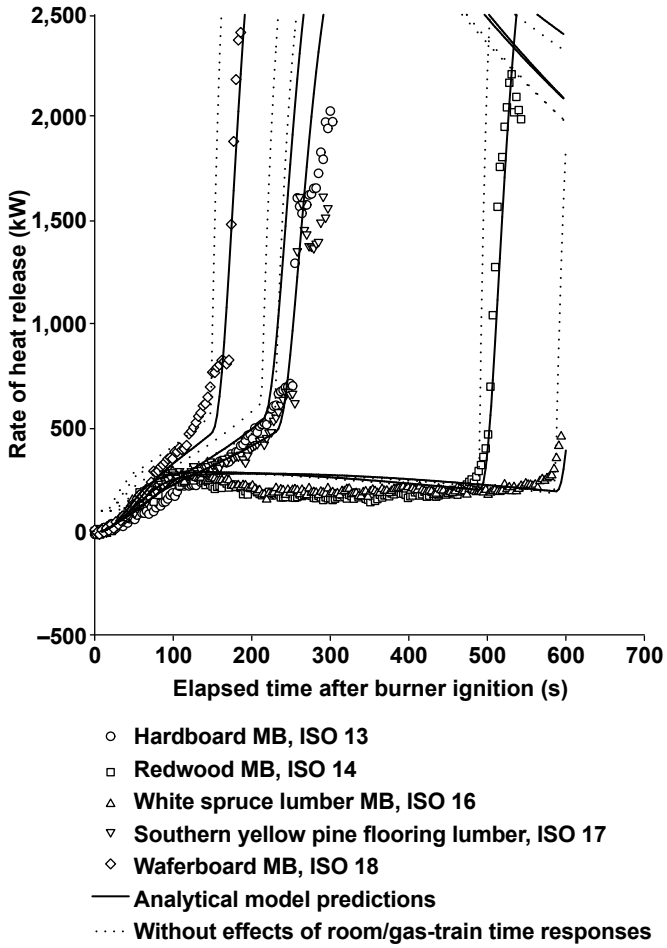

Figure 63. Model predictions for test nos. 13, 14, 16, 17, and 18.

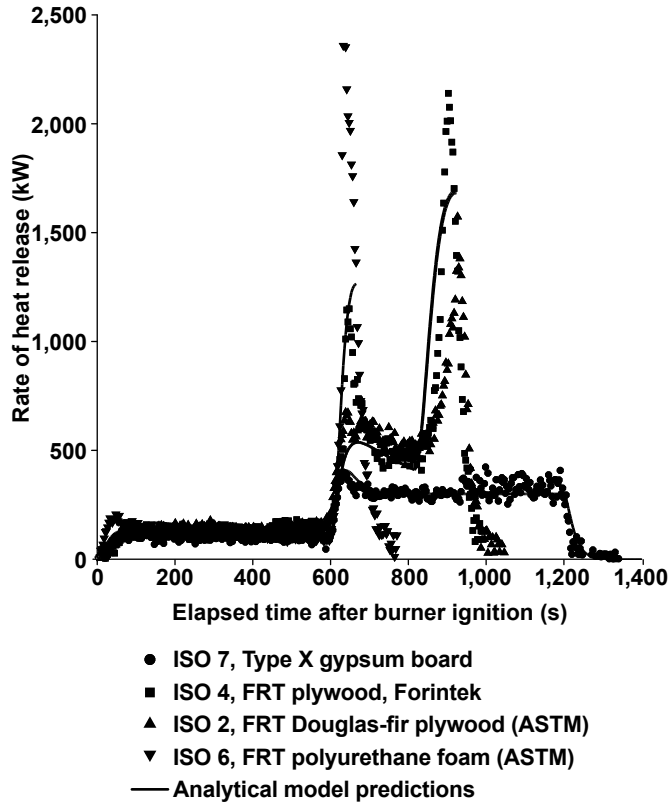

Figure 64. HRR predictions for materials with FRT during burner's 300-kW stage.

The reason the HRR is not predicted to immediately reach high values is the ramping of the HRR profile caused by time responses of the gas flow train. In each case the HRR will peak and decay to the point of transition to downward flame spread, except that the gypsum board does not make the transition to downward flame spread. On a case-by-case basis we defined the transition time t_3 so that the model can take it the rest of the way with the simple analysis of downward flame spread.

Model Sensitivity to Fire Growth Properties

Various fire growth properties can be studied with the analytical model. Perhaps the most important one is defining the value of HRR at the point of flashover and its sensitivity to the time responses of the gas flow train. Figures 62 and 63 show the dashed curves predicted by the model that represents true HRR, $\dot{Q}_t$, rather than the "measured" HRR, $\dot{Q}_{\text{test}}$ (see Eq. (61)). In the first report, we determined that a HRR of 600 kW correlates best with the flashover event for flames out of the door or for the floor flux to be 20 kW/m^2. Using the criterion of 600 kW to use with "measured" HRR, $\dot{Q}_{\text{test}}$, we derived the times to flashover for the 11 materials without FRT. This is shown in Table 16 and their comparison with experimental TFO is shown in Figure 65.

Selecting 90- and 110-kW levels instead of the usual 100-kW level checked the model sensitivity to burner output. For the group of materials identified as HRR accelerants, the 10% increase in burner output resulted in around a 5% decrease in the time to flashover. On the other hand, for the group of materials identified as HRR decelerants, the 10% increase in burner output instead resulted in around a 4% increase in the time to flashover. This seemingly contradictory prediction for the time to flashover might be an artifact of the empirical formula, Equation (74). In any case, the model is predicting that the burner need not be set at 100 kW very accurately because it has a relatively minor effect on time to flashover.

If the time responses of the gas flow train suddenly vanish during a test, the expected HRR at the derived flashover times range from 1,500 to 3,500 kW, depending on the test. Because it is not possible to eliminate gas mixing in the upper gas layer of the room, suppose just the time constant for gas sampling system suddenly vanishes. The expected HRR at the derived flashover times then range from 740 to 1,210 kW, depending on the test. Thus a HRR of 1,000 kW

Table 16—HRR at time to flashover for different room and gas time constants on materials without FRT

Material	Test no.	Experimental flashover time at 600 kW (s)	Model flashover time at 600 kW t_{flash} (s)	Room and gas time constants vanished HRR (kW)	Gas time constant vanished only HRR (kW)
Oak veneer plywood	3	165	162	3,508	1,168
Douglas Fir plywood (ASTM)	5	474	466	2,711	1,131
Douglas Fir plywood (MB)	9	543	534	2,623	1,191
Southern Pine plywood	10	327	285	2,154	1,045
Particleboard	11	210	207	1,536	768
Oriented strandboard	12	168	179	2,787	1,207
Hardboard	13	228	221	1,683	839
Redwood lumber	14	507	505	2,574	1,092
White spruce lumber	16	606	600	1,863	739
Southern Pine boards	17	240	241	1,580	790
Waferboard	18	144	157	1,911	806

to correspond to the flashover event may find agreement with a highly developed model of fire growth but would still be in disagreement with the room test data in various laboratories. Each laboratory would even disagree on the level of HRR at flashover and not realize that the problem is due to their differing time constants of the gas sampling systems. Finally, the analytical model predicts that 10 s is the average time interval for the HRR to go from 600 kW to 1 MW. This is comparable to that experimentally obtained in the Part 1 report in the section on the time to flashover criteria. Thus, to ensure that HRR = 1 MW is accurately computed by the oxygen consumption method for our laboratory, we should wait at least 10 s before terminating the test after observing the flame out of the door. Early in our testing program we did not realize this, and as a result in almost all cases the pulling of the fan to the highest level coincides with the 1-MW level.

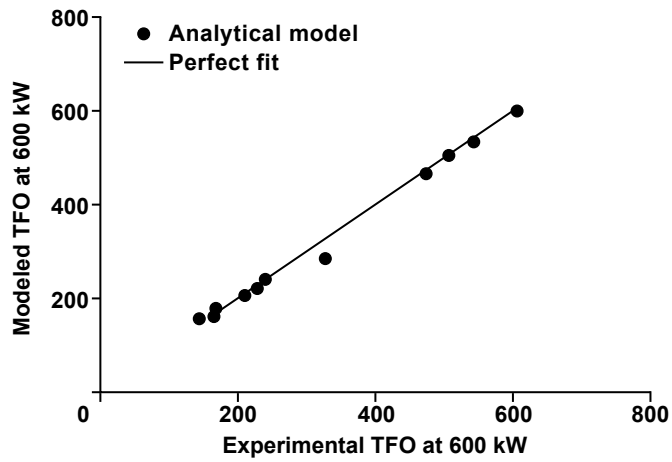

Figure 65. Analytical model predictions for TFO at 600 kW.

Simplified Correlations of the Small-Scale and Full-Scale Tests

Several authors reported on correlating the small-scale test results with the ISO 9705 (ISO 1993a) test results for wall and ceiling lined (Karlson 1993; Östman and Nussbaum 1989; Östman and Tsantaridis, 1994; Dietenberger 2002) by simple correlating equations. The advantages of these correlations are that they are easy to use and usually only one small-scale instrument is needed to obtain the required parameters. The disadvantages of these correlations are that the results are valid only for the full-scale configuration against which the small-scale data were validated and the correlating equations lack theoretical aspects of the full-scale fire. The early models used the idea that flame propagation rate (rate of change in pyrolysis area) is proportional to the total HRR (in kW rather than in kW/m^2) and inversely proportional to TTI or t_{ig}. The total HRR was in turn the sum of the burner output and the material HRR over the pyrolysis area. By assuming no sudden or gradual material burnout, one could show by analytic integration that the acceleration parameter of flame spread (as well as pyrolysis area and HRR) is controlled by the ratio of peak HRR over TTI. Brabrauskas (in Grand and Wilke 2000) used this ratio to show a linear correlation to the inverse of time to flashover in room/corner tests with the ceiling lined. A slight variation is to consider ratio of peak HRR over the time-to-peak HRR, which is preferred in the European market (see Hees and Axelsson 2001). However, this simple ratio was found to correlate poorly with the flame spread index (FSI) as defined in ASTM E 84. Quintiere (1993) included a sudden material burnout feature in their simple wind-aided flame spread analysis and derived the acceleration parameter in the flame spread solution to correlate with time to flashover in the database considered above by Babrauskas. Dillon and others (2001) provided a further modification by considering the exponentially decaying HRR profile. They used the corresponding exponential decay factor to replace the burnout time variable in the acceleration parameter to compare with time to flashover in the room/corner test as

specified in NFPA 265 or NFPA 286. We applied these different definitions of the acceleration parameter for predicting FSI or time to flashover for our data, and obtained poor results, particularly for gypsum board and FRT rigid polyurethane foam. In this paper, some simple correlation of the cone calorimeter data with time to flashover measured in the room/corner test is suggested.

Guided Statistical Approach

The fire growth models rely heavily on certain cone calorimeter test parameters, and these parameters used for the correlation are time to ignition, t_{ig}, total heat release (THR), and heat release rate (HRR). For values of time to ignition, we used those corresponding to irradiance of 25 kW/m^2 because at the lowest irradiance, the greatest differences of t_{ig} were measured for different materials. We note that at irradiance of 65 kW/m^2, the ignition times were quite small for most materials (around 10 s) so that differences in thermal properties of materials had little effect on t_{ig}. The average HRR was chosen, rather than the peak value measured in the cone calorimeter, because of its better consistency between test results of SDVU and FPL cone calorimeters. Indeed, the correlation coefficient of the average HRR as the linear function of irradiance was higher than that for the peak values for most cases. Therefore the average value of HRR measured at irradiance 50 kW/m^2 was chosen for the correlation with the flashover time. Total heat release from material represents total energy of the material available in a fire. This parameter also defines the burnout time in the full-scale test by dividing THR by the average HRR. For most materials tested in the full-scale test, the burning time was longer than time to flashover. However, the burning time for the FRT rigid polyurethane foam was quite small, which affected the flashover time. Therefore, the total heat released during cone calorimeter test was also included into the correlation expressed as

$$t_{FO} = b\left(t_{ig}^{p}\right) + c\left(\mathrm{THR}^{q}\right) + d\left(\mathrm{HRR}^{r}\right) \qquad (75)$$

where

t_{FO} is time to flashover, defined as 1 MW HHR (s),

t_{ig} time to ignition at irradiance 25 kW/m^2 (s),

THR average total heat released (MJ/m^2), and

HRR average HRR at irradiance 50 kW/m^2 (kW/m^2).

The best correlation was obtained for the following coefficients to Equation (75):

$b = 15{,}453$
$c = -0.0238$
$d = -466$
$p = 0.06$
$q = 2.0$
$r = 0.25$

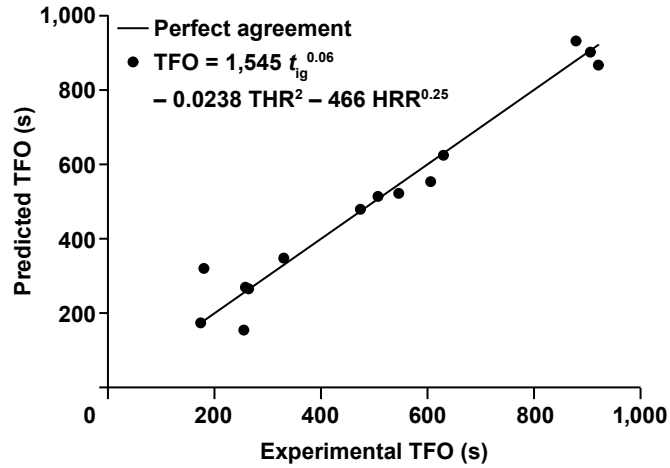

Figure 66. Correlation of time to flashover for statistical based approach.

Figure 66 compares calculated and experimentally measured flashover times. The data points represent the values calculated with Equation (75), and the line corresponds to perfect agreement. As mentioned earlier, Equation (75) represents a simple correlation of the reaction to fire parameters as measured in the cone calorimeter to the defined full-scale room fire scenario. It does not include any effects, such as the deformation of materials, neither in the small- nor full-scale test, and the calculation results are not valid for any other burner program than the one that was used for these tests. Therefore, we excluded or adjusted some materials for the correlation. In the case of oak veneer plywood, delamination occurred shortly after start of the full-scale test that "prematurely" shortened the flashover time. Next, the Type X gypsum board did not flashover, so it could not be used in the correlation. As for the FRT Southern Pine plywood, the burner program differed from the other tests. However, it appears to agree with the correlation if we artificially add 300 s during the 100-kW burner output to correct for the burner program error. In Table 17, input values to Equation (75) and its resulting calculated flashover times are listed. It can be seen from this table and Figure 61 that the three groups of materials, identified in the full-scale test are clearly differentiated. That is, we have composite materials with accelerating HRR in full-scale test, untreated wood materials with the constant HRR until prior to flashover in full-scale test, and FRT wood and FRT polyurethane foam products with flashover occurring in the second part of the test under increased ignition burner output. The correlation coefficient R^2 obtained from the Equation (75) was 0.96.

Acceleration Parameter Approach

There are various deficient aspects of the guided statistical approach. First, it lacks the understanding of how each measured parameter of the cone calorimeter contributes to fire growth. According to both fire growth models described in this paper, the time to ignition measured at irradiance of

Table 17—Input parameters to Equation (75) and comparison of flashover times

Material	Test no.	TFO experiment (s)	TFO model (s)	t_{ig} (s) at 25 kW/m^2	THR (MJ/m^2)	HRR average (kW/m^2)
Waferboard	18	174	173.9	116.5	104.3	147
OSB	12	180	320.3	138	83.2	136
Hardboard	13	255	154.4	116.5	88.7	183
Southern Pine board	17	258	269.5	198	117.4	114.5
Particleboard	11	264	265.3	175	111.4	121
Southern Pine plywood	10	330	347.8	197.5	82.6	143
Douglas Fir plywood ASTM	5	474	479.0	142	58.6	113
Redwood lumber	14	507	513.6	250.5	101.4	80
Douglas Fir plywood	9	546	521.8	178	67.2	101.5
White spruce lumber	16	606	553.3	250.5	92.8	80
FRT rigid PU foam	6	630	624.3	6.333	9.35	31
FRT Douglas Fir plywood	2	879	931.4	621	32.9	63.5
FRT Plywood (Forintek)	4	906	901.2	423.3	30.9	60
FRT Southern Pine plywood	8	921[a]	866.4	514.5	41.0	68.5
Beech lumber, 0% MAP	—	NA	348.8	473.3	109.8	139
Beech lumber, 0.7% MAP	—	NA	432.3	654.5	106.1	132
Beech lumber, 1.4% MAP	—	NA	455.8	88.75	71.35	92.5
Beech lumber, 2.8% MAP	—	NA	818.3	787	65.45	78
Beech lumber, 5.1% MAP	—	NA	862.5	1,054.5	65.8	77

[a]300 s added to measured total flashover (TFO).

25 kW/m^2 is hardly relevant. Next, our material database also includes a Type X gypsum board and an FRT rigid polyurethane foam that have short burning times, such that 5- or 10-min averaged HRR data would not fairly evaluate these materials. Using the THR data to compensate for these short burning time materials moves one further away from the understanding of fire growth. If at all possible, a single cone calorimeter test at an optimum irradiance is desired to provide all needed information, while understanding of the fire growth remains intact.

Therefore, it is critical to make the best possible use of the ignition conditions. This makes the heat flux of 50 kW/m^2 a favored choice for irradiance because the time to ignition is not too fast for manual observation, whereas the combustible volatiles are relatively easy to ignite with the spark plug, particularly for many FRT wood materials. In addition, it is the flux level that is most correlated with the 100- and 300-kW propane flame from a corner burner in terms of time to ignition of the wall sample. A data acquisition time interval of 1 s was found sufficient to effectively capture peak HRR. The time constants of oxygen gas analyzers were measured around 9 s and used in an analytical model of HRR profile by convoluting the gas analysis system response with an exponentially decaying "true" HRR profile. This analytical convolution function was fitted to HRR profile data to estimate true peak HRR (Dietenberger and Grexa 1999). The added advantage of modeling materials with an exponentially decaying HRR profile during the duration of a fire test (typically 600 s or less) is that analytical prediction of flame spread is possible in some fire growth scenarios that include material burnouts. Because of the time constant of 9 s for the gas analyzers, the "smoothed" HRR profile would need to be deconvolved to obtain a true HRR profile of the material. Not only that, one should also remove the HRR due to glowing combustion because the burner's flames in full-scale tests prevents oxidation of the char surface. One is left with a "corrected" HRR profile that approximates an exponential decay function, with somewhat increased peak HRR and a lowered flaming THR compared with the original measured HRR profile. One might even suggest that the original HRR profile obtained at 50 kW/m^2 approximates the "corrected" HRR profile corresponding to 35 kW/m^2, thus avoiding the corrections to the HRR profile needed for fire growth modeling. The presence of FRT in wood or intumescent coating on wood leads to a reduction in the first peak HRR. In extreme cases, one should treat the "modeled" HRR profile as relatively flat during the test duration.

We note that the materials in our database behave as thermally thick materials at fluxes of 50 kW/m^2, which means the formula for material time constant is proportional to the time to ignition (TTI) as in (see Eq. (20))

$$\tau_{\mathrm{m}} = k\rho C_{\mathrm{p}}\left(\frac{T_{\mathrm{ig}} - T_{\mathrm{m}}}{\dot{q}''_{\mathrm{w}} - \dot{q}''_{\mathrm{ig}}}\right)^2 \approx (4/\pi)\mathrm{TTI} \tag{76}$$

For materials that are thermally thin, the time constant is equal to TTI except when the backing board commonly used for full-scale test affects the thermal response time. The material HRR decay parameter is related to the THR of a completely charred, 12.5-mm-thick sample by the equation

$$\frac{\dot{Q}''_{\mathrm{m,ig}}}{\omega_{\mathrm{m}}} = \int_0^{\infty} \dot{Q}''_{\mathrm{m,ig}} \exp(-\omega_{\mathrm{m}} t) dt \approx (12.5/\delta_{\mathrm{m}}) \int_0^{\infty} \dot{Q}''_{\mathrm{m,cone}} dt = \mathrm{THR}(12.5/\delta_{\mathrm{m}}) \tag{77}$$

Most materials were around 12.5 mm thick so that one would not have a problem with incomplete charring of the specimen in the cone calorimeter. The combustibility parameter that these equations have considerable sensitivity to is peak HRR, which also can increase significantly with imposed heat flux. Combining this effect with the problems associated with measuring peak HRR in the cone calorimeter indicates that serious attention should be given to ensuring the reliability of the profile near the peak HRR. Further simplification can be achieved if our attention is focused on the neutral zone between the accelerative and damped fire growth in the analytical fire spread model. This occurs when the roots calculated from Equation (53) are relatively close to zero. Close examination of Equation (56) for total HRR shows that for small values of roots and at small times, the direction of fire growth is dominated by the sum of the roots and multiplied by the material time constant. This defines the fire growth acceleration parameter as

$$\beta_{\mathrm{growth}} = (s_1 + s_2)\tau_{\mathrm{m}} = b + c\dot{Q}''_{\mathrm{m,ig}} - \omega_{\mathrm{m}}\tau_{\mathrm{m}} \tag{78}$$

where the time constant is obtained with Equation (76) and the decay constant is obtained with Equation (77). The growth acceleration parameter is therefore a well-defined function of peak-HRR, THR, and time-to-ignition as evaluated at 50 kW/m^2. The neutral point is the acceleration parameter at zero, or $\beta_{\mathrm{growth}} = 0$. Calculating the acceleration parameter to some positive value will indicate a degree of fire growth acceleration above that of a steady growth. Likewise, a negative value will give a degree of damping to the fire growth after ignition. Therefore it is expected that the time to flashover decreases as the acceleration parameter increases.

In the case of the room/corner test, TFO (based on 20 kW/m^2 critical floor flux) versus growth acceleration parameter is shown as montonically decreasing for most materials in Figure 67 for the materials on walls only scenario (Dietenberger and White 2002). It seems that materials with high smoke development need a severe adjustment to the acceleration parameter to account for the accelerating potential of high thermal radiation due to the heavy smoky ceiling layer upon the downward flame spreading. Our previous paper on smoke correlations (Dietenberger and Grexa 2000) suggests using the peak SEA at cone heater fluxes higher than 30 kW/m^2 on horizontal samples for correlating with smoke production in the room/corner tests. So in the case of Figure 67, the acceleration parameter was adjusted by adding the term

$$\beta_{\mathrm{smoke}} = \mathrm{SEA}_{\mathrm{peak}} / 3{,}000 \tag{79}$$

to Equation (78) to provide a more effective acceleration parameter. That is, the value 3,000 in Equation (79) was empirically derived to cause a collapse of the data to a single curve that is fitted by the solid lines in Figure 67. By considering smoke, the anomalous performance behavior of the FR polyurethane rigid foam in various testing scenarios is explained (Dietenberger and White 2002). The good

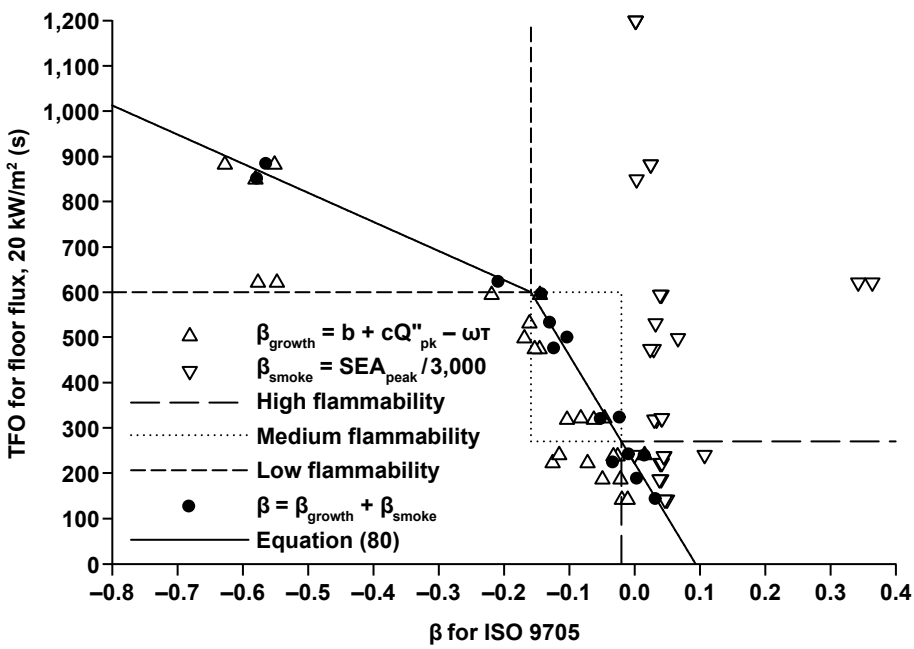

Figure 67. Time to flashover correlation using acceleration parameter.

Table 18—Input to Equation (80) and comparison of flashover times

Material	Test no.	TFO at 20 kW/m^2 (s)	TFO predict (s)	Thick (mm)	T_{ig} (s)	PHRR (kW/m^2)	THR (MJ/m^2)	Peak SEA (m^2/s)
Waferboard	18	141	143	13	21.4	208	101	145
OSB	12	186	211	11.5	23.3	204	91	119
Hardboard	13	222	299	7	27.6	189	93	119
Particleboard	11	237	183	12.8	31.4	211	102	136
Southern Pine board	17	240	241	19	21.4	181	143	323
Southern Pine plywood	10	321	274	11	19.1	197	65	126
Douglas Fir plywood (ASTM)	5	474	513	11.8	17.6	173	67	81
Redwood lumber	14	498	465	19	18.9	171	95	200
Douglas Fir plywood	9	531	528	12	16.6	168	74	97
White spruce lumber	16	594	559	17.3	17.0	165	89	122
FRT rigid PU foam	6	621	631	23	2.69	89.9	4.0	1,061
FRT Douglas Fir plywood	2	849	869	12.5	34.2	72	34	10
FRT Southern Pine plywood	8	882[a]	860	11.3	62.5	88	39	75
Type X gypsum board	1	NFO[b]	NFO	16	48	118	2.79	6

[a]300 s added to measured total flashover (TFO).
[b]NFO indicates no flashover.

correlation ($r^2 = 0.98$) for TFO for walls only scenario as a function of effective acceleration parameter in Figure 67 is given by the simple empirical equation

$$t_{\mathrm{FO-floor}} = 600 + a\left(\beta_{600} - \beta_{\mathrm{growth}} - \beta_{\mathrm{smoke}}\right) \qquad (80)$$

where $t_{\mathrm{FO\text{-}floor}}$ is time to flashover defined as 20 kW/m^2 floor flux, $\beta_{600} = -0.158$ is the acceleration parameter identified with TFO of 600 s, and

$$a = 644 \quad \text{for} \quad \beta_{600} \geq \beta_{\mathrm{growth}} + \beta_{\mathrm{smoke}}$$

$$a = 2383 \quad \text{for} \quad \beta_{600} \leq \beta_{\mathrm{growth}} + \beta_{\mathrm{smoke}}$$

are parameter values for the two burner regimes.

Only four empirical parameters were required for this correlation for the walls only scenarios and indicated the effectiveness of using a simple correction due to smoke production, an option not previously known in other publications. Even in the case where the ceiling material is included, the effect of smoke production was found to be applicable (Dietenberger and White 2002).

It is noted that four regions of room flammability characteristics can be identified, as shown in Figure 67. The high flammability, identified with TFO less than 270 s or $\beta \geq -0.02$, is characterized by continuous fire growth, often in an accelerative fashion. The medium flammability, with TFO greater than 270 s and less than 600 s, or $-0.158 \leq \beta \leq -0.02$, is characterized by an initial upward fire growth, a pause in lateral flame spread, and finally the condition is reached for rapid downward flame spread on the walls. This medium flammability regime is non-existent for the scenario in which the test materials are on both the wall and the ceiling. The low flammability, with TFO greater than 600 s and less than 1,200 s, or $-1.09 \leq \beta \leq -0.158$, is characterized by rapid ignition of the wall area underneath the 300 kW burner flames, a pause in lateral flame spread, and ending with a rapid downward flame spread on the walls. The negligible flammability, described as no TFO or $\beta \leq -1.09$, result in combustion of test materials directly underneath the 300 kW burner flame only, as with the Type X gypsum board.

Table 18 lists the materials that are grouped into these four regions of flammability. Thus, high flammability products are waferboard, OSB, hardboard, particle board, and Southern Pine board; medium flammability products are Southern Pine plywood, both Douglas Fir plywoods, redwood lumber, and white spruce lumber; low flammability products are FRT rigid PU foam, FRT Douglas Fir plywood, and FRT Southern Pine plywood; and Type X gypsum board has negligible flammability. One notes that any one of the five variables for the correlation of Equation (80), thickness, time to ignition, peak HRR, THR, and peak SEA, do not in themselves provide a good indication of material behavior in these four regions of flammability, as measured as time to flashover of ISO 9705 (ISO 1993a) or, in the case of ASTM E 84, as flame spread index. Using an advanced analytical fire growth model suggested by the use of an acceleration parameter that is not derivable from simpler models but which was effective in organizing materials according to their flammability (except for hardboard product, which may benefit from further cone calorimeter testing to better define typical values). Furthermore, cone calorimeter tests at just a single irradiance value of 50 kW/m^2 provide directly the data needed to correlate with the time to flashover. That is, no intermediate analysis is required, such as determining materials properties of surface ignition temperature, thermal inertia, heat of pyrolysis, HRR profiles, and so on, as they are implicitly provided for in Equations (76) and (77). Finally, less empiricism was involved in deriving Equation (80) in comparison to previous correlations to predict TFOs.

Conclusion

The versatility of the cone calorimeter was demonstrated for our tested building materials for its three main uses:

(1) comparison of materials and determining material and pyrolysis properties, (2) applications to fire growth modeling, and (3) correlations for building code applications. Although considerable results were achieved, various questions still remain unresolved and were identified for future research. Indeed, one must be cautious in interpreting and using combustibility parameters, particularly TTI, peak HRR, and peak SEA.

The fire properties measured in the cone calorimeter are still quite useful for wood-based materials, including those that have fire-retardant treatment. That is, we can derive from the ignition versus irradiance data the reasonable values for ignition temperature, thermal inertia, and thermal diffusivity using an appropriate heat conduction theory. Then by measuring the THR and MLR after piloted ignition, we derived effective heats of combustion and pyrolysis. Often in the case of a charring wood pyrolysis, it is better to consider HRR and MLR as a function of time that results in a relatively constant heat of combustion along with a changing heat of pyrolysis, or with just an exponentially decreasing HRR with time during a full-scale test. This affects the selection of or limits the usefulness of theoretical fire growth models. Further detailed analysis of the averaged mass flow measurements of O_2, CO, CO_2, soot, and fuel resulted in describing the empirical formula for the wood volatile composition for use in CFD fire models. It was found that materials tested with the gypsum backing, as is done in the full-scale tests, have combustion properties most in agreement between small-scale and full-scale tests. However, it is cautioned that the over ventilation and idealized conditions in the cone calorimeter test produced concentrations of CO and soot (relative to oxygen consumption concentrations) much less than those observed in the full-scale room tests.

The results of varying the fire-retardant MAP impregnated in the beech wood showed that main effect of FRTs is to drastically reduce the heat of combustion (and thus also the HRR and THR). However, this seemed to be counteracted by reductions in time to ignition and ignition temperature (see effects on the time to flashover in Table 17), presumably due to smoldering at low temperatures of wood degradation. By the time the uptake of MAP reached 40% in the beech wood, the ignition time and ignition temperature were restored to at or beyond the level of untreated samples, and the effective heat of combustion became as low as 6.4 MJ/kg. These factors would certainly increase the time to flashover to a large estimated value of 863 s, as compared to that estimated for untreated beech of 349 s.

As a starting point for fire growth modeling, we evaluated and modified Quintiere's numerical model that had been previously used to successfully simulate fire behavior in the case of both wall and ceiling lined. By merely removing the lined ceiling in the model, we revealed the model's failure in modeling the lateral flame spread and the downward wall flame spread just prior to flashover. An empirical formula was developed for the source function controlling the lateral flame spread, but it still could not distinguish materials in the medium and high flammability regions. Therefore, we constructed a detailed analytical fire growth model, which consisted of four stages of fire growth of wall ignition, upward flame spread, lateral flame spread, and downward flame spread, taking into account time responses of the ignition burner, burn room gas mixing, and instruments gas mixing. Without using empirical functions, the analytical model successfully predicted the HRR as a function of time for the wall ignition, upward flame spread, and downward flame spread. However, the lateral flame spread modeling required a high level of empiricism to predict the HRR profile leading up to flashover. Despite the level of empiricism used in the analytical model, the analytical fire growth model as presented for spreadsheet applications was used to obtain a physical understanding of fire growth processes at full-scale, indicate sensitivities to different combustibility parameters, and provide the theoretical basis as to the use of the acceleration parameter for classifying materials.

The correlation based on acceleration parameter, Equation (80), seems preferred over that of the considered fire growth models or of statistical approach correlations for predicting time of flashover for the wall-only protocol of ISO 9705 (ISO 1993a) room/corner test for various reasons. That is, the fire growth models can (1) be cumbersome to use, (2) require time-consuming derivation of basic fire properties to predict the HRR profiles, (3) require multiple cone calorimeter tests to properly define the fire properties, or (4) be burdened with empiricisms in the model in order to predict the fire growth that includes the unusual features of lateral flame spread. The statistical approach correlations provide little or no indication for transitioning the fire growth behavior, specifically into high, medium, low, and negligible flammability that is provided with Equation (80) in Figure 67. Also, Equation (80) merely uses the cone calorimeter global properties of TTI, PHRR, THR, and peak SEA measured at a single irradiance of 50 kW/m^2 to predict quite well the time to flashover. It is noted that additional tests of wall linings of materials in the low and negligible flammability regions, as well as with variations of smoke levels, are needed to further confirm the correlation. In consideration of various identified problems in cone calorimeter measurements, analysis, and modeling, it was still possible to organize combustibility properties, which are measured solely in the cone calorimeter, that are suitable for both wood and plastics and relative to performances in both the Steiner tunnel and the room/corner tests (Dietenberger and White 2002). More materials that are non-wood in origin should be tested to help confirm the generality that is implied with the acceleration parameter correlation approach with a smoke term correction.

Nomenclature

A	Area, m^2
a, b, and c	Fire growth coefficients, Equation (67)
B	Biot number, Equation (12)
$C\rho$	Heat capacity (J/Kg)
EHC	Effective heat of combustion (MJ/kg)
Fo	Fourier number, Equation (13)
H	Heaviside function
ΔH	Heat of combustion, (MJ/kg)
h	Heat transfer coefficient, (kW/Km^2)
HRR	Heat release rate (kW/m^2)
k	Thermal conductivity, (kW/Km)
L	Heat of pyrolysis vaporization, (MJ/kg)
$\dot{m}$	Mass flow rate (g/s)
MLR	Mass loss rate (g/sm^2)
P	Pressure (mbar)
$\dot{Q}$	Heat release rate (kW)
$\dot{q}''$	Heat flux (kW/m^2)
r_O	Stoichometric oxygen mass consumption fraction of fuel mass
S	Any measurement signal
s_i	Singularities of transform, Equation (53)
SEA	Smoke extinction area (m^2/kg)
t	Time (s)
T	Temperature (Celsius)
V_i	Volume of zone i (m^3)
w	Burner width (m)
x	Surface distance—lateral direction (m)
y	Surface distance—upward direction (m)
Y_l	Species product mass per fuel mass
z	Surface distance—downward direction (m)
β_l	Species product mass per oxygen depletion mass
δ	Feature dimension (m)
ε	Emissivity or integrating variable
ω	Exponential decay coefficient (1/s)
ρ	Material density (kg/m^3)
ρ_i	Air density of zone i (kg/m^3)
σ	Boltsmann radiation constant (kW/m^2T^4)
τ	Time constant (s)
ϕ	Flame heating parameter for lateral flame spread in LIFT (kW^2/m^3)

Subscripts

a	Ambient conditions
b	Ignition burner fuel—propane
c	Convective condition
CO	Carbon monoxide
CO_2	Carbon dioxide
f	Material fuel mixture, $C_XH_YO_Z$
g	Gaseous environment
H_2O	Water vapor
ig	Ignition condition
m	Material property or condition
O_2	Oxygen gas
p	Pyrolyzing condition
r	Response value
s	Smoke—soot, or surface condition, depending on use
st	Stiochiometric condition
t	True value
THC	Total hydrocarbons, CHW
w	Wall of the room, or wood material
W	Number of hydrogen atoms in the THC's empirical formula
X	Number of carbon atoms in empirical fuel
Y	Number of hydrogen atoms in empirical fuel
Z	Number of oxygen atoms in empirical fuel

Literature Cited

ASHRAE. 2001. ASHRAE Fundamentals Handbook, 2001. Chapter 25 – Thermal and water vapor Transmission data, Table 4, p. 25.6

Atreya, A, 1998. Ignition of Fires. Phil. Trans. R. Soc. Lond. A, Vol. 356, p. 2787-2813

Babrauskas, V. 1992. Heat of combustion and potential heat. In: Babrauskas, V.; Grayson, E.S.P., eds. Heat release in fires. London: 207–223.

Beitel, J. 1994. Interlaboratory test program—proposed ASTM standard method for room fire test of wall and ceiling materials and assemblies. Project Report PCN: 33–000012–31. Philadelphia: ASTM Institute for Standards Research.

Boroson, M.L.; Howard, J.B.; Longwell, J.P.; Peters, W.A. 1989. Product yields and kinetics from the vapor phase cracking of wood pyrolysis tars. AIChE Journal. (35)1: 120–128.

Brenden, J.J. 1973. An apparatus developed to measure the rate of heat release from building materials. Res. Pap. FPL 217. Madison, WI: U.S. Department of Agriculture, Forest Service, Forest Products Laboratory.

Brenden, J.J. 1974. Rate of heat release from wood-base building materials exposed to fire. Res. Pap. FPL 230. Madison, WI: U.S. Department of Agriculture, Forest Service, Forest Products Laboratory.

Brenden, J.J. 1975. Wood-base building materials: rate of heat release. Journal of Fire and Flammability.(6): 274–293.

Brenden, J.J. 1977. Measurements of heat release rates on wood products and an assembly. Res. Pap. FPL 281. Madison, WI: U.S. Department of Agriculture, Forest Service, Forest Products Laboratory.

Browne, F.L.; Tang, W.K. 1962. Thermogravimetric and different analysis of wood treated with salts. Fire Resource Abstract Review. 4(1962): 76.

Dietenberger, M.A. 1991. Piloted ignition and flame spread on composite solid fuels in extreme environments. Dayton, OH: University of Dayton. Ph.D. dissertation.

Dietenberger, M.A. 1995. Protocol for ignitability, lateral flame spread, and heat release rate using lift apparatus. In: Nelson, G.L., ed. Fire and polymers II. Materials and tests for hazard prevention: Proceedings of 208th national meeting of the American Chemical Society; 1994 August. 435–449. Chapter 29 http://www.fpl.fs.fed.us/documnts/pdf1995/diete95c.pdf. [Accessed 10/28/10].

Dietenberger, M. 1996. Ignitability analysis using the cone calorimeter and LIFT apparatus. Proceedings of international conference on fire safety; Vol. 22. Product Safety Corporation: 189–197.

Dietenberger, M. 1999. Effect of backing board on the heat release rate of wood. Proceedings of international conference on fire safety; Vol. 28. Columbus, OH. July 1999. Sissonville, WV. Product Safety Corporation: 62–73.

Dietenberger, M. 2002. Update for combustion properties of wood components. Fire and Materials Journal. (26): 255–267. Also in: Proceedings of fire and materials conference 2001. San Francisco, CA: 159–171.

Dietenberger, M.; Grexa, O. 1999. Analytical model of flame spread in full-scale room/corner tests (IS0 9705). In: Proceedings of the 6th international conference and exhibition of fire and materials; 1999 February 22–23; San Antonio, TX. London, United Kingdom: Interscience Communications Ltd.: 211–222.

Dietenberger, M.A.; Grexa, O. 2000. Correlation of smoke development in room tests with cone calorimeter data for wood products. Proceedings of 4th international scientific conference on wood and fire safety. May 14–19. Slovak Republic: The High Tatras, Hotel Patria, Strbske Pleso. 45–56 pp.

Dietenberger, M.A.; White, R.H. 2002. Reaction-to-fire testing and modeling for wood products. Twelfth annual BCC conference on flame retardancy. May 2001. Stamford, CT: 54–69. http://www.fpl.fs.fed.us/documnts/pdf2001/diete01b.pdf. [Accessed 10/28/10].

Dietenberger, M.A.; Grexa, O.; White, R.H.; Sweet, M.; Janssens, M. 1995. Room/corner tests of wall linings with 100/300 kW burner. Proceedings of fire and materials 4th international conference. Washington; 15–16 November. 53–62.

Dietenberger, M.A.; White, R.H.; Grexa, O.; Janssens, M. 1996. Room/corner tests of wall linings with 100/300 kW burner. In: Annual conference on fire research: book of abstracts. 1996 October 28–31. NISTIR 5904: 95–96. Gaithersburg, MD: U.S. Department of Commerce, National Institute of Standards and Technology, Building and Fire Research Laboratory.

Dillon, S.E.; Janssens, M.L.; Hirschler, M.M. 2001. Using the cone calorimeter as a screening tool for the NFPA 265 and NFPA 286 room test procedures. In: Fire and materials 2001, 7th international conference; 2001 January 22–24. Fisherman's Wharf, San Francisco, CA. London: Interscience Communications Ltd.: 527–539.

Drews, M.J.; Barker, R.H. 1974. Pyrolisis and combustion cellulose. Journal of Fire Flammability 5(1974): 116.

Gandhi, P.D.; Caudill, L.; Hoover, J.; Chapin, T. 1997. Determination of fire exposure heat flux in cable fire tests. In: Hasemi, Y., ed. Fire safety science—Proceedings of the fifth International symposium. Melbourne, Australia: World Congress Centre.1997 March 3–7. International Association for fire safety science: 141–151.

Grand, A.F.; Wilke, C.A., eds. 2000. Fire retardancy of polymeric materials. New York: Marcel Dekker, Inc.

Green, A. 1995. A simple mathematical model for the Brandschacht test. SP Report; Vol. 45.

Grexa, O.; Janssens, M.; White, R. 1995. Analysis of cone calorimeter data for modelling of the room/corner test on wall linings. Fourth fire and materials conference. London: Interscience Communications: 63–71.

Grexa O.; Janssens M.; White, R.; Dietenberger, M. 1996. Fundamental thermophysical properties of materials derived from the cone calorimeter measurements. Proceedings of wood and fire safety, 3rd international scientific conference. Slovokia: High Tatras. 1996 May 6–9. 139–147. Zvolen: Technical University in Zvolen, Faculty of Wood Technology.

Grexa, O.; Dietenberger, M.A.; White, R.H. 2012. Reaction-to-fire of wood products and other building materials: part I: room/corner tests. Madison, WI: U.S. Department of Agriculture, Forest Service, Forest Products Laboratory.

Hasemi, Y.; Tokunaga, T. 1984. Some experimental aspects of turbulent diffusion flames and buoyant plumes form fire sources against a wall and in a corner of walls. Combustion Science and Technology. Vol. 40: 1–17.

Hasemi, Y.; Yoshida, M.; Yasui, N.; Parker, W.J. 1997. Upward flame spread along a vertical solid for transient local heat release rate. In: Proceedings of Fire Safety Science Symposium, 1997.

Hees, P.V.; Axelsson, J. 2001. Mathematical modelling of fire development in cable installations., In: Fire and materials 2001. 7th international conference; 2001 January 22–24; Fisherman's Wharf, San Francisco, CA. London: Interscience Communications Ltd.: 23–37.

ISO. 1993a. Fire tests—full scale room test for surface products (ISO 9705): 1993 (E). Geneva, Switzerland: International Organization for Standardization.

ISO. 1993b. Fire tests—reaction to fire—part 1: rate of heat release from building products (cone calorimeter method) ISO 5660-1: 1993 (E). Geneva, Switzerland: International Organization for Standardization.

Janssens, M.L. 1991. Fundamental thermophysical characteristics of wood and their role in enclosure fire growth. Washington, DC: National Fire Protection Association. Ph.D. dissertation.

Janssens, M. 1993. Improved method of analysis for the LIFT apparatus—part 1: ignition. In: Proceedings of the second fire and materials conference. Arlington, VA. 1993 September 23–24. London: Interscience Communications Ltd.: 37–46.

Janssens, M.; Parker, W. 1992. Oxygen consumption calorimetry. In: Babrauskas, V.; Grayson, S.J., eds. Chapter 3 of heat release in fires.London: Elsevier Applied Science. pp 3159.

Janssens, M.; Tran, H.C. 1992. Data reduction of room tests for zone model validation. Journal of Fire Sciences. 10: 528–555.

Janssens, M.; Grexa, O.; Dietenberger, M.; White, R. 1995. Predictions of ISO 9705 room/corner test using a simple model. Proceedings of fire and materials 4th international conference. Washington: 15–16 November 1995. London: Interscience Communications Ltd.: 73–83.

Johnson, D.G.,1995. Combustion Properties of Plastics, J.Applied Fire Science, Vol. 4(3), p.185-201

Karlson, B. 1993. A mathematical model for calculating heat release rate in the room corner test. Fire Safety Journal. 20(1993): 93–113.

Karlsson, B.; Magnusson, S.E. 1991. Combustible wall lining materials: numerical simulations of room fire growth and the outline of a reliability based classification procedure. In: Cox, G.; Langford, B., eds. Fire safety science, proceedings of the 3rd international symposium. London: Elsevier Applied Science.

Keylwerth, R.; Christoph, N. 1963. Grundlegende Untersuchungen uber die Thermische Zersetzung und Entzundung von Holz. Mitteilungen der Deutschen Gesellschaft fur Holzforschung. 50(1963): 125–137.

Kokkala, M.A. 1993. Sensitivity of the room/corner test to variations in the test system and product properties. Fire and Materials. 17: 217–224.

Kokkala, M.; Heinila, M. 1991. Flame height, temperature, and heat flux measurements on a flame in an open corner of walls. Project 5 of the EURIFIC fire research programme.

Kosik, M.; Reiser, V. Dolezal, J. Mihalik, P. 1977. Anorganic salts asfire-retardants for wood –part II. Drevarsky vyskum. 3(1977): 175–183.

Kulkarni, A.K.; Brehob, E.; Manohar, S.; Nair, R. 1994. Turbulent upward flame spread on a vertical wall under external radiation. NIST–GCR–94–638. Washington, DC.

McCaffrey, B.J.; Quintiere, J.G.; Harkleroad, M.F. 1981. Estimating room temperatures and the likelihood of flashover using fire test data correlations. Fire Technology. 17: 98–119.

Östman, B.A.-L.; Nussbaum, R.M. 1989. Correlation between small-scale rate of heat release and full-scale room flashover for surface linings. In: Fire safety science—Proceedings of the second international symposium (1988). New York: Hemisphere Publishing: 823–832.

Östman, B.A.-L.; Tsantaridis, L.D. 1994. Correlation between cone calorimeter data and time to flashover in the room fire test. Fire and Materials. 18: 205–209.

Parker, W.M. 1988. Prediction of the heat release rate of wood. Washington, DC: George Washington University, School of Engineering and Applied Science. Ph.D. dissertation.

Quintiere, J.G. 1993. A simulation model for fire growth on materials subject to a room-corner test. Fire Safety Journal. 20(1993): 313–339.

Rhodes, B.T. 1994. Burning rate and flame heat flux for PMMA in the cone calorimeter. NIST–GCR–95–664. Washington, DC.

Saito, K.; Quintiere, J.G.; Williams, F.A. 1985. Upward turbulent flame spread. Proceedings of the 1st international symposium on fire safety science. Gaithersburg, MD.

Schartel, B.; Hull, T.R. 2007. Development of fire-retarded materials—Interpretation of cone calorimeter data. Fire and Materials. 31: 327–354.

Shafizadeh, F. 1968. Pyrolysis and combustion of cellulosic materials. Advanced Carbohydrate Chemistry. 23(1968): 919.

TenWolde, A.; McNatt, J.D.; Krahn, L. 1988. Thermal properties of wood and wood panel products for use in buildings. ORNL DOE/USDA–2 1697/1. Washington, DC: 26.

Tran, H.C. 1988. Rates of heat and smoke release of wood in an Ohio State University calorimeter. Fire and Materials. (12): 143–151.

Tran, H.C. 1990. Modifications to an Ohio State University apparatus and comparison with cone calorimeter results. Proceedings, AIAA/ASME thermophysics and heat transfer conference. The Society of Mechanical Engineers. HTD-Vol. 141: 131–139.

Tran, H.C. 1992. Experimental data on wood materials. In: Babrauskas, V.; Grayson, S.J., eds. Heat release in fires. New York: Elsevier Applied Sciences. Chapter 11. Part b.

Tran, H.; Janssens, M. 1989. Room fire test for fire growth modeling—A sensitivity study. Journal of Fire Sciences. 7: 217–136.

Tran, H.C.; Janssens, M.L. 1991. Wall and corner fire tests on selected wood products. Journal of Fire Science. 9: 106–124.

Tran, H.; Janssens, M. 1993. Modeling the burner source used in the ASTM room fire test. Journal of Fire Protection Engineering. 5: 53–66.

Tran, H.C.; White, R.H. 1992. Burning rate of solid wood measured in a heat release rate calorimeter. Fire and Materials. 16: 197–206.

Ward, F. 1974. Flame resistant cell. Materials. J. Soc. Dyer. Colour. 71(1955): 569.

Wesson, H.R.; Welker, J.R.; Sliepcevich. 1971. The piloted ignition of wood by thermal radiation. Combustion and Flame. (16): 303–310.

White, R.H.; Dietenberger, M.A.; Tran, H.; Grexa, O.; Richardson, L.; Sumathipala, K.;Janssens, M. 1999. Comparison of test protocols for the standard room/corner test. Fire and Materials Journal. (23): 139–146.

Wickstrom, U.; Goransson, U. 1992. Full-scale/bench-scale correlations of wall and ceiling linings. Fire and Materials. (16): 15–22.

Williamson, R.B.; Revenaugh, A.; Mowrer, F.W. 1991. Ignition sources in room fire tests and some Implications for flame spread evaluation. Proceedings of the 3rd international symposium of fire safety science. 657–666.

Yan, Z.; Holmstedt, G. 1996. CFD and experimental studies of room fire growth on wall lining materials. Fire Safety Journal. (27): 201–238.